Characterization of a titanium coaxial condenser

L Vermooten

orcid.org/ 0000-0002-9487-0431

Dissertation accepted in fulfilment of the requirements for the degree Master of Engineering in Mechanical Engineering at the North-West University

Supervisor: Prof M. van Eldik
Co-Supervisor: Dr P.v.Z. Venter

Graduation: October 2020
Student number: 24251577

ACKNOWLEDGEMENTS

"I can do all things through Christ who gives me strength." (Philippians 4:13)

To my parents, thank you for all your love, guidance, support, and the opportunity you gave me to study and finishing my degree. I appreciate everything and will always love you.

To Prof Martin van Eldik and Dr Philip Venter, thank you for your quality guidance, advice, and patience during this study. I learned a lot from you both and appreciate all the hard work.

Thank you M-Tech Industrial for providing me with the necessary equipment and assistance during the test set-up phase. Thank you for also providing me with financial support during this study.

Thank you to Michael McIntyre and Pieter Oberholzer for your humour and supporting roles throughout this study.

Last but certainly not least, thank you to Lauren Snyman for your support, patience, and love during the past two years. I appreciate you endlessly.

ABSTRACT

Title: Characterization of a titanium coaxial condenser

Author: Lemmer Vermooten

Supervisor: Prof M. van Eldik

Co-supervisor: Dr P.v.Z. Venter

School: School of Mechanical Engineering

Degree: Master of Engineering

In South Africa a leading engineering company, focusing on energy engineering services and products to the mining industry, developed a mobile refrigeration unit known as the air-cooling unit (ACU) MKII. The ACU MKII uses a stainless-steel tube-in-tube condenser, which in some cases has a higher than anticipated corrosion rate due to impurities in the mine supply water used as heat sink. A solution to this problem is the use of titanium for the inner tube due to its corrosion resistance. Advancements in manufacturing techniques have resulted in titanium being used in coaxial coils.

The coaxial configuration with its pure counterflow characteristics results in an enhanced heat transfer compared to smooth tube heat exchangers while the physical compactness of the coaxial coil is beneficial. However, limited performance data, such as heat transfer and pressure drop characteristics, exists for these titanium coaxial heat exchangers.

To better understand the applicability of a titanium coaxial condenser in the ACU MKII, a need exists to develop a thermal-fluid simulation model to predict the coil's convection heat transfer and pressure drop for R-407C refrigerant inside the annuli and water through the inner tube. The simulation is based on a modelling approach in literature that was developed for copper coaxial condensers employing enhancement factors for the complex geometry.

Enhancement factors are incorporated into published correlations to improve the accuracy of the titanium coaxial condenser predictions of convection heat transfers and pressure drops. The allowance for enhancement factors in the simulation model are made to account for any differences between a standard helical coil and the coaxial tube annulus. Experimental data were gathered from a test-bench and incorporated to calculate the enhancement factors through comparison between simulated and measured values. The resulting heat transfer and friction (pressure drop) enhancement factors were 0.5288 and 5.1534 respectively.

Simulated heat transfer and pressured drop values, using no enhancement factor in the simulation model, were compared to the measured values and produced an average difference of 5.23% and 90.42% respectively. The average differences for the log mean temperature difference (LMTD) was 11.57%. After implementing the above-mentioned average enhancement factors in the simulation model, the average differences between the simulated and measured heat transfer and pressure drop were 5.79% and 32.62% respectively. The average LMTD differences was 6.83%.

Keywords: Titanium coaxial coil; Condensation; Heat pump; R-407C; Thermal-fluid simulation model.

TABLE OF CONTENTS

NOMENCLATURE

A	:	Area	[m^2]
Cp	:	Specific heat	[J/kg.K]
D	:	Diameter	[m]
e	:	Flute depth	[m]
e^*	:	Non-dimensional flute depth	
e_f	:	Friction enhancement factor	
e_{f_w}	:	Water friction enhancement factor	
e_h	:	Heat transfer enhancement factor	
e_r	:	Absolute surface roughness	[m]
f	:	Friction factor	
$f_{helical}$	:	Helical coil friction factor	
$f_{straight}$	:	Straight tube friction factor	
G	:	Mass flux	[kg/m^2s]
h	:	Specific enthalpy	[J/kg]
h	:	Heat transfer coefficient	[W/m^2K]
k	:	Thermal conductivity	[W/m.K]
L	:	Length	[m]
$\dot{m}$	:	Mass flow rate	[kg/s]

N	:	Number of flute starts	
Nu	:	Nusselt number	
ΔP	:	Pressure drop	[kPa]
P	:	Pressure	[kPa]
p	:	Flute pitch	[m]
Pr	:	Prandtl number	
pr	:	Pressure ratio	
p^*	:	Non-dimensional flute pitch	
q	:	Heat transfer rate	[W]
Re	:	Reynolds number	
s	:	Specific entropy	[J/kg.K]
ΔT_{lm}	:	Logarithmic mean temperature difference	[°C]
T	:	Temperature	[°C]
t	:	Wall thickness	[m]
U	:	Overall heat transfer coefficient	[W/m^{2}K]
u	:	Velocity	[m/s]
V	:	Volume	[m^3]
x	:	Quality	

Subscripts

avg	:	Average value

$Bubble$	:	Bubble point temperature
c	:	Cold
cal	:	Calculated value
Dew	:	Dew point temperature
e	:	Experimental value
h	:	Hydraulic
i	:	Inlet
ii	:	Inner-inner
io	:	Inner-outer
l	:	liquid
lm	:	Logarithmic mean
o	:	Outlet
oi	:	Outer-inner
r	:	Refrigerant
$R-407C$	:	The refrigerant, R-407C
$Rousseau$	:	Rousseau-factor
R_s	:	Refrigerant single-phase
SP	:	Single-phase
t	:	Theoretical value
TP	:	Two-phase

v	:	Vapour	
vi	:	Volume-based inside	
vo	:	Volume-based outside	
w	:	Water	

Greek symbols

ε	:	Effectiveness	
μ	:	Viscosity	[Ns/m^2]
ρ	:	Density	[kg/m^3]
θ	:	Helix angle	[°]
θ^*	:	Non-dimensional helix angle	

LIST OF FIGURES

LIST OF TABLES

CHAPTER 1

INTRODUCTION

1.1 Background

South Africa's deep underground mining operations can be a hazardous environment, considering all the dust present, as well as occasional inadequate air circulation and soaring ambient temperatures (Anderson & De Souza, 2017). It is of utmost importance to properly ventilate and cool working areas in deep underground mines to relieve heat stress on personnel and mining equipment. Heat management in underground mines is becoming more of a challenge as mines are exploring deeper levels. Consequently, heat stress on mine workers and equipment is becoming a larger focal point in the mining industry. One of the most important aspects to consider is the health and safety of the mining personnel working in these harsh conditions. A person will experience heat stroke when their body's internal temperature rises above 40 °C (Anderson & De Souza, 2017).

Most mines rely on a surface fridge plant for chilled water that is pumped underground. In remote underground areas localised cooling, also known as spot cooling, is utilized to ensure suitable ambient conditions for the mine workers. In order to make spot cooling possible, mainly two technologies, i.e. chilled water cars (CCs) and mobile refrigeration units are being used to provide suitable working temperatures in line with the wet bulb globe temperature (WBGT) heat stress criteria (Potgieter et al, 2015). The WBGT is generally used to measure heat stress where regularly updated WGBT charts display the accepted temperatures for a specific area. The acceptable WGBT numbers are dependent (among other factors) on the average metabolic rate (workload) of the mine worker, on the worker's state of acclimation and clothing as well on the air movement present in the worker's location (Kroemer Elbert et al, 2018).

In South Africa, a leading engineering company focusing on energy engineering services and products to the mining industry developed two types of modular and mobile refrigeration plants (MRPs) also known as the ACU (Air Cooling Unit) for use in deep underground mines (M-Tech Industrial, 2015). The first ACU developed is known as the MKI which delivers nominal 100 kW of cooling, and the second known as the MKII delivers between 250 kW and 300 kW cooling depending on the environment and operating circumstances (M-Tech Industrial, 2015).

These ACUs were specifically designed for effective localised cooling of underground working areas with the advantage of being moved with relative ease to new working areas as the mining operations expand. The vapour compression heat pump system of the ACU uses water as heat sink on the condenser side, which makes the product unique in the market. The efficiency of this system is comparable to a conventional surface refrigeration system (Rankin & van Eldik, 2011)

As opposed to cooling cars (CCs) the ACU is not dependent on chilled water and operates effectively with mine service water up to 40°C (Potgieter & van Eldik, 2017). Potgieter and van Eldik (2017) reported that the ACU is more energy efficient than a traditional CC since it uses less water, and therefore, reduces the total required power input to cool deep underground mines.

The current tube-in-tube condenser of the ACU MKII is designed for water operating pressures of up to 20 000 kPa to cover a wide range of applications. The condenser coil mainly consists of high-pressure stainless-steel piping for the water side and an outer carbon steel pipe for the refrigerant side. Designing the condenser for this wide range of applications resulted in the condenser having a complex pipe configuration.

In recent times the quality of the mine supply water, flowing through the inner stainless-steel tube, has deteriorated resulting in increased corrosion causing the heat exchanger to fail much quicker than expected. This results in the ACU losing its refrigerant charge and therefore a shutdown in its operations. Due to the complexity of the coil the position of the leak cannot easily be detected and repaired and the entire ACU unit must be brought from deep underground to the surface

where a coil replacement must be done. This takes a substantial amount of time to correct and can result in an income loss for the mine. The need therefore exists to develop a more practical condenser that has a higher corrosion resistance, improved space efficiency (more compact) but which is also designed for a lower maximum water operating pressure of 2 500 kPa. The water pressure will be spread among a series of coaxial coil heat exchangers joined either in series or parallel, thus lowering the maximum water operating pressure for each individual coil.

A technology successfully used in the water heating heat pump industry is the coaxial tube-in-tube condenser, also known as a fluted tube (Rousseau et al, 2003). These coils are compact with a high efficiency due to the enhanced heat transfer surface area and counter-flow configuration. Until recently these coils were only manufactured with copper inner tubes which has a limited use in mining conditions due to the inadequate quality of the mine supply water.

In recent times technology has advanced to the extend where the coaxial condensers can be manufactured using a titanium inner tube (Extek, 2015). Titanium is more suitable for underground applications as it is a more corrosive resistant material than copper, but with a lower thermal conductivity. The titanium coaxial coil should be able to operate for extended periods in the corrosive nature of the mine supply water.

1.2 Problem statement

The heat transfer and pressure drop characteristics of the titanium coaxial condenser needs to be understood before being used in the design of an ACU condenser pack. There exists no information in literature where existing correlations can be used to accurately predict the heat transfer and pressure drop through a titanium coaxial condenser.

1.3 Purpose of the study

The purpose of this study is to develop a thermal-fluid simulation model of a condensing refrigerant-to-water titanium coaxial coil. This model will be used to test

the accuracy of existing coaxial coil heat transfer and pressure drop correlations found in literature against that of experimentally obtained results.

1.4 Scope of the study

The study will comprise a thermal-fluid model developed in the software Engineering Equation Solver (EES), to predict the heat transfer and pressure drop of a titanium coaxial refrigerant-to-water condenser. To develop this thermal-fluid simulation, the following are required:

- Different correlations, found in literature, to predict the heat transfer and pressure drop of a coaxial coil need to be investigated.
- Experimental data of a titanium coaxial condenser using the zeotropic refrigerant mixture, R-407C, is needed to assist in the development of a thermal-fluid simulation model. A heat pump test setup will be used where a sample titanium coaxial coil are incorporated for water heating. The titanium condenser coil will be tested over a wide range of operating conditions, measuring both the inlet and outlet pressures and temperatures, as well as the mass flows of the refrigerant and water.
- The experimental data will be used to verify the accuracy of the simulation model. A sample calculation listed in Appendix B was made to ensure the correlations used in the simulation model are implemented correctly. The heat transfer and pressure drop correlations may be slightly adjusted with an enhancement factor to deliver the best possible heat transfer and pressure drop prediction. The use of an enhancement factor will be discussed later in this study.

CHAPTER 2

LITERATURE SURVEY

2.1 Introduction

In the previous chapter the background, problem statement, purpose of the study as well as the scope of the study were discussed.

In this chapter a summary of previous work done on enhanced tubes and coaxial coils as well as on previous methods used to predict the heat transfer and pressure drop characteristics is given. General and background theory existing in literature as well as heat transfer and pressure drop correlations regarding coaxial coils will be investigated.

2.2 Coaxial coils

2.2.1 General overview

Heat exchangers are widely used in various fields and form an integral part of countless refrigeration and heat pump systems. Numerous methods have been developed as well as been applied to heat exchangers to improve their overall performance. A passive technique forms part of one of the more important enhancement techniques to heat exchangers (Vijayaragham et al, 1994).

Passive schemes incorporate techniques such as surface extensions, inlet vortex generators, devices influencing a swirl flow profile and roughened artificially surfaces. A coaxial coil is an example of a passive technique to enhance the heat transfer capability of the heat exchanger. Wessels (2007:22) states that due to the coaxial coil's surface geometry the boundary layer is disrupted by the swirl at the tube surface. The convective heat transfer is thus enhanced due to the swirl flow inside the coaxial coil (Wessels, 2007).

The type of heat exchanger used in this study is a refrigerant-to-water titanium coaxial coil condenser with water flowing inside the inner tube in counter-flow with the zeotropic refrigerant mixture, R-407C, in the twisted annulus. The geometry along with the water and refrigerant flow paths within the coaxial coil are illustrated in Figure 2-1.

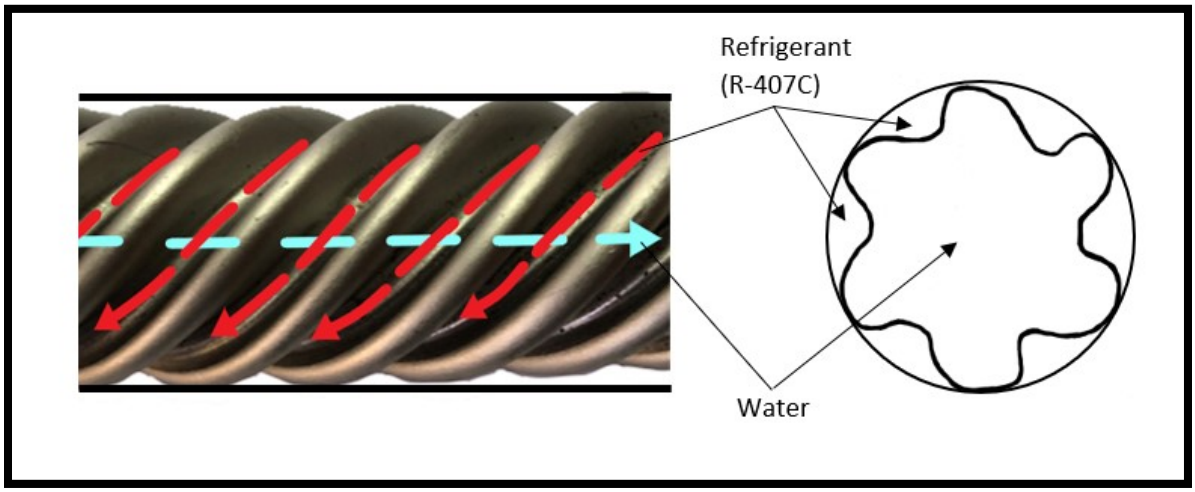

Figure 2-1: Coaxial coil heat exchanger.

Coaxial coil condensers can enhance the flow conditions on both sides of the transfer area causing the coil to produce higher convection heat transfer coefficients opposed to straight smooth tube heat exchangers. van Eldik (1998:38) states that micro-circulation on the water side allows for an increase in the convective heat coefficient without causing a substantial increase in the water pressure drop when compared to straight tube heat exchangers.

van Eldik (1998:38) continues to state that in the annulus of the coaxial coil, the convection heat transfer coefficients of the refrigerant are increased in both the single- and two-phase regions. In the single-phase liquid region, the refrigerant, similar to the water side, also undergoes a degree of micro-circulation, mostly at the outlet side of the coil, causing hot refrigerant liquid to replace cold refrigerant liquid at the outer surface of the inner tube. For the two-phase region, surface tension causes the refrigerant condensate to draw towards the outer sides of the coaxial channels, causing the remaining hot refrigerant gas to stay in contact with

the inner heat transfer area. With the enhanced convection heat transfer coefficients, a minor increase in pressure drop is sacrificed (van Eldik, 1998).

2.2.2 Background overview and correlation investigation

Numerous correlations to predict the heat transfer and pressure drop of fluids and refrigerants with the use of enhanced tubes, such as coaxial coils, are found in literature. This section will investigate the relevant correlations.

Traviss et al. (1971:6-7) investigated the high vapour velocity inside a tube analytically. The condensate flow was determined by applying the Von Karman universal velocity distribution. The Lockhart-Martinelli method was used to determine the pressure drops where the momentum and heat transfer analogy was used to calculate the convection heat transfer coefficients. By applying non-dimensional heat transfer and order of magnitude equations a simple formulation was introduced for the local convection heat transfer coefficient. Experimental data was compared to the analysis and the results were used to create a general design equation used to predict the forced convection condensation.

A simple dimensionless correlation to predict the heat transfer coefficients experiencing film condensation inside pipes was developed by Shah (1979:548). The author used the Dittus-Boelter equation combined with a correlation in terms of the quality to predict the two-phase flow region. The correlation is verified by comparing it to experimental data comprising of 474 data points. The mean deviation for all the data points analysed was 15.4%. This result was considered acceptable for practical design purposes.

Shah (1981:1086-1105) researched all the available information and literature regarding the prediction of heat transfer experiencing film condensation in tubes and annuli. The author concentrated his research on the fluids used in refrigeration and air-conditioning. The author also covered important issues such as condensation of high and low velocity vapours, the effects of oil, non-condensable and superheat as well as the effects of interfacial phase change resistance and

return bends. The author concluded that no efficiently verified method existed for predicting the heat transfer coefficients for high velocity superheated vapour.

Christensen & Srinivasan (1990:1) as well as Christensen & Garimella (1990:1) have done research on spirally fluted, also known as coaxial tubes, and enhanced tubes using a confined crossflow configuration. The first part of the study focused on the flow inside the fluted tube while the second part investigated the flow through the annulus side. The study consisted of fourteen different inner fluted tubes which were tested with three different smooth outer tubes. This study mainly focused on the friction enhancements influenced by the geometry of the fluted tube. The study investigated the friction and heat transfer within three different flow regimes inside the spirally fluted tubes, these flow regimes comprised of laminar, turbulent and transition flow.

Christensen & Srinivasan (1990:1) and Christensen & Garimella (1990:1) discovered that the Nusselt numbers and the friction factors were functions of the complex fluted tube geometry, which includes the pitch, flute depth as well as the helix angle. The details of these fluted tube geometry features will be discussed in the following chapter. The authors correlated the friction factors as a function of the Reynolds number as well as the non-dimensional geometrical parameters.

Sami & Schnolate (1992:137) conducted research on two-phase flow boiling of a ternary refrigerant mixtures for internally enhanced surfaces, such as fluted tubes. A simulation model was developed to predict the heat transfer and pressure drop characteristics of the ternary refrigerants, R-22/R-114 and R-22/R-152a. The model showed a deviation for both the heat transfer and pressure drop to be ±20% and ±15% respectively for both ternary refrigerants.

A heat exchanger design manual was specifically developed for fluted tubes by Christensen et al. (1993:1). This manual includes confined crossflow and tube-in-tube geometries and is based on the research done by Christensen & Srinivasan (1990:1) and Christensen & Garimella (1990:1). The manual provides the reader with step-by-step instructions, along with the necessary governing equations, on how to design and simulate a compact heat exchanger.

Das (1993:972) used six helical coils to generalise a correlation for accurately predicting the friction factor. These six helical coils were all made from rough transparent PVC pipes and experimental data was obtained for water in a turbulent flow regime. The acceptable confidence interval of the correlation developed for the friction factor was 95%.

Sami et al. (1994:755,756) conducted an experimental study of boiling zeotropic refrigerant mixtures in two-phase flow for horizontal enhanced surface tubing. The focus of this study is to predict the boiling heat transfer characteristics. The authors used flow key parameters to develop correlations to predict the boiling heat transfer coefficient and pressure drop. For these correlations, the mean deviation of the predicted heat transfer is 20% and 30% for the pressure drop.

MacBain et al. (1997:65) examined the characteristics of the heat transfer and pressure drop inside a deep horizontal spirally fluted tube. The authors compared the results of this fluted tube heat exchanger to that of a smooth tube heat exchanger and found that for the refrigerant, R12, the heat transfer was 50 – 170 greater than that of the smooth tube, however the pressure drop was 6 – 20 times higher inside the fluted tube. The authors repeated the experiment for the refrigerant, R134a, and reported a heat transfer increase of 40 – 150% and a pressure drop increase of 11 – 19 times compared to the smooth tube heat exchanger.

Wang et al. (2000:993) introduced a carbon steel spirally fluted tube and aimed to replace the existing copper smooth tube heat exchangers used in a powerplant's high pressure preheaters, due to the corrosion of the copper smooth tubes caused by the feedwater containing ammoniac. While experimental results of the carbon steel spirally fluted tube showed that the total heat transfer was 10 – 17% higher than that of a carbon steel smooth tube heat exchanger, it yielded about the same overall heat transfer as a copper smooth tube heat exchanger. The authors concluded that it is feasible to replace a copper smooth tube heat exchanger with the carbon steel spirally fluted tube when using the refrigerants R22, R-407C and R-134a.

Rousseau et al. (2003:232) developed a thermal-fluid simulation to describe the characteristics of the heat transfer and pressure drop correlations of a refrigerant-to-water copper fluted tube condenser using the refrigerant, R22. The author's formulation of the thermal-fluid model was based on the work done by Christensen et al. (1993) and Das (1993) for the annulus side. The refrigerant and water properties can be evaluated for any number of sections of the pipe length due to the model enabling the surface area to be divided into any number of pipe length sections. This enables the model to predict the convection heat transfer coefficients and pressure drop of heat exchanger cycles employing zeotropic refrigerant mixtures. Heat transfer and friction correlations were predicted by using empirical equations existing in literature for the waterside.

Rousseau et al. (2003:232) continue to state that no correlations in literature are available to predict the heat transfer and friction characteristics accurately on the refrigerant side. Therefore, the authors used the approach where enhancement ratios based on correlations available for helical coils along with smooth tube correlations are used combined with enhancement factors based on empirical data for copper fluted tube condensers. The results from independent tests of two commercial fluted tubes were used to validate the simulation model. The authors compared the measured and simulated results where they reported an average difference of 7.27% for the measured and simulated pressure drop as well as an average difference of 4.41% for the log mean temperature difference (LMTD).

van Eldik & Wessels (2013:2379) used the existing model developed by Rousseau et al. (2003) and investigated the applicability of the model for R-407C condensation inside the fluted tube annuli. Experimental data from a test facility was obtained to evaluate the model. Using the existing model, the average differences between the simulated results and experimental data for the pressure drop were 48% and 56% for the log means temperature difference (LMTD). Based on these accuracies the authors decided to develop new enhancement factors, resulting in an average difference for simulated and experimental results of 9.5% in the pressure drops and 3.3% for the LMTD.

Huang et al. (2014:11) developed a generalized finite volume model capable of predicting single-phase and two-phase flow for a coaxial heat exchanger with a fluted or smooth inner tube. This model is capable of tracking the phase change points over the length of the tube with the subdivision and segment insertion (moving boundary within the segment) concepts incorporated in the model. The authors proposed modifications to existing fluted surface two-phase heat transfer and pressure drop correlations by applying empirical two-phase flow multipliers onto existing single-phase correlations of a fluted tube. The modified correlations and model are validated against the experimental data of a brine-to-refrigerant evaporator and condenser operating in a heat pump application.

Huang et al. (2014:21) compared the simulated results and experimental data and found that the simulated results for the heat transfer and pressure drop for the condenser varies ±5% of the experimental data. The evaporator heat transfer simulation data varies ±5% of the experimental data while the simulated pressure drop differs ±10% of the experimental data.

Ndiaye (2017:413) tested a refrigerant-to-water helically coiled double tube with corrugations in the inner tube to develop a transient model of the coil. A superposition principle is adopted to deal with a lack of a suitable heat transfer and friction factor correlation. The author also applied the finite volume method to numerically solve the governing equations.

Ndiaye (2017:419) used experimental data for both steady-state and transient conditions from a commercial 10.5 kW water-to-air heat pump unit. The refrigerant-to-water heat exchanger with refrigerant, R-22, used in the unit is a tube-in-tube coil which are partly spiral, partly helical and is modelled as a helical coil. The deviation between the simulated and measured refrigerant pressure drop for steady-state conditions are 45% for the heating mode and -34% for the cooling mode. The enthalpy differences are both less than 1% for both the cooling and heating modes.

2.3 Approach temperature

In a heat exchanger, neither the hot stream temperature can be cooled below the cold stream temperature nor can the cold stream temperature be heated to a temperature higher than the supply temperature of the hot stream. The hot stream of the heat exchanger can only be cooled to a temperature defined by the temperature approach (Sahdev, 2010).

Sahdev (2010) states that the temperature approach is defined as the minimum allowable temperature difference ($\Delta T_{\min}$) between the hot and cold streams of the heat exchanger. The temperature level where the minimum temperature difference is observed in the heat exchanger is known as the pinch point of the heat exchanger. The overall heat transfer coefficient (U) as well as the geometry of the heat exchanger determines the magnitude of the approach temperature.

Sahdev (2010) further states that in the design of a heat exchanger, the approach temperature must be chosen carefully as the $\Delta T_{\min}$ value influences both the capital and energy costs. For a given heat transfer value (q), if a small $\Delta T_{\min}$ value is chosen, the area requirements of the heat exchanger increase. If a high $\Delta T_{\min}$ value is chosen, the heat recovery in the heat exchanger decreases causing the demand for external utilities to increase. The initial selection of the approach temperature value for shell and tube heat exchangers are typically at best in the range of 3 – 5°C (Sahdev, 2010).

2.4 Counter-flow configuration

A counter-flow configuration is normally used to obtain the maximum heat transfer in the coaxial coil condenser due to the possibility to obtain water outlet temperatures exceeding the condensing temperature (Rousseau et al., 2003:233-234). According to Thulukkanam (2013:54-56), this phenomenon is known as a temperature cross. This property of a counter-flow configuration used in a coaxial condenser is illustrated in Figure 2-2. The hot outlet water temperature (Tw_4) is warmer than the refrigerant condensing temperature (between Tr_2 and Tr_3) due to

the superheated gas exchanging heat to the water. The superheated gas is at a higher temperature than the condensing temperature.

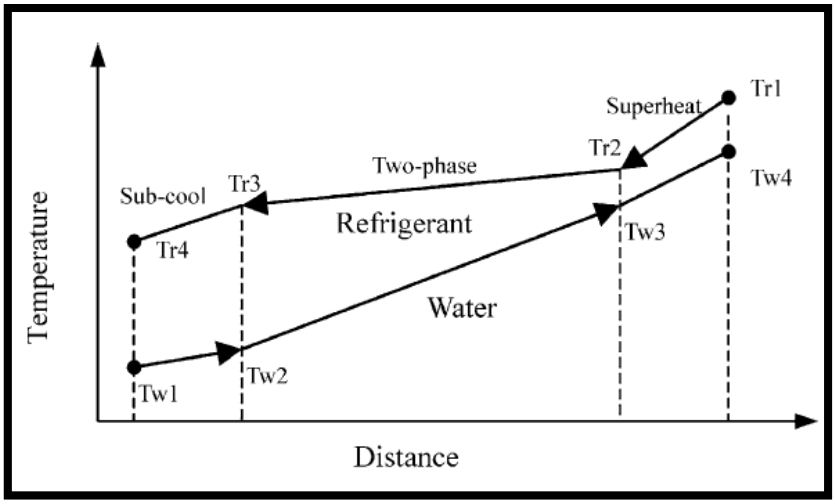

Figure 2-2: Temperature distribution through a coaxial condenser (Rousseau et al. 2003).

In a counter-flow configuration of a coaxial condenser, the water normally flows in the inside of the tube with the refrigerant flowing in the outer annulus as illustrated in Figure 2-1. A representation of a counter-flow configuration inside a titanium coaxial condenser can be seen in Figure 2-3.

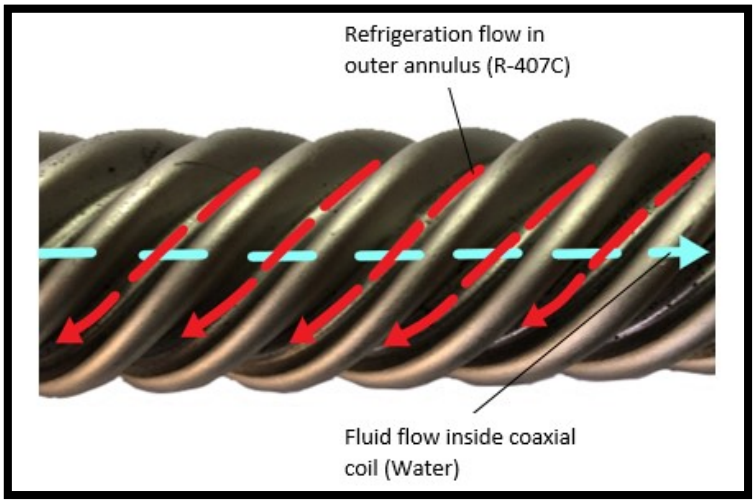

Figure 2-3: Counter-flow representation inside a titanium coaxial coil.

2.5 Summary

After reviewing all the available literature, it was decided that this study will generally focus on the model developed by Rousseau et al. (2003:232) which predicts the heat transfer and pressure drop of a refrigerant-to-water copper fluted tube condenser with the refrigerant R22.

The titanium coaxial condenser simulation model in this study will utilize the following information contained in the literature review:

- Coaxial coil geometry → The non-dimensional correlations developed by Christensen & Srinivasan (1990:1) and Christensen & Garimella (1990:1).
- Friction factor → The correlations developed by Christensen & Srinivasan (1990:1) and Christensen & Garimella (1990:1) based on the Reynolds number and non-dimensional geometry of the fluted tube.
- The water convection heat transfer coefficient → The correlations developed by Christensen & Srinivasan (1990:1) based on the Reynolds number and non-dimensional geometry of the fluted tube.
- The two-phase convection heat transfer coefficient in the annulus → The method implemented by Shah (1979:548).
- The single-phase convection heat transfer coefficient in the annulus → The model developed by Christensen & Garimella (1990:1) where their model incorporates the friction factor correlation developed by Christensen & Srinivasan (1990:1).
- The refrigerant single-phase pressure drop → The method developed by Das (1993:972).
- The refrigerant two-phase pressure drop → The correlation based on the friction factor correlation by Christensen & Srinivasan (1990:1) combined with the correlation for straight tube two-phase pressure drop put forward by Traviss et al. (1971:13).

The techniques mentioned above, which are also used in the model of Rousseau et al. (2003:232), will be discussed in Chapter 3 for implementation into the titanium coaxial condenser simulation model.

CHAPTER 3

THEORETICAL BACKGROUND AND SIMULATION

3.1 Introduction

In the previous chapter, a summary of previous work and methods to predict the heat transfer and pressure drop of enhanced tubes and coaxial coils were given. Theory existing in literature and heat transfer as well as pressure drop correlations regarding coaxial coils was explored.

In this chapter, information regarding concentric tube and coaxial coil heat exchangers will be discussed concerning the simulation model of the refrigerant-to-water titanium coaxial condenser. From this information, a simulation routine containing the necessary correlations to predict the heat transfer and pressure drop of a titanium coaxial condenser will be discussed. A method to determine the uncertainty and percentage error in measured and simulated data will also be explored following the simulation routine discussion.

In the literature chapter, coaxial coil heat exchangers are mentioned as fluted tubes, spirally fluted tubes, corrugated helical coils etc., this study will refer to these tubes as coaxial coils.

3.2 Heat exchanger heat transfer analysis methods

3.2.1 Energy balance equation

For any heat exchanger design procedure, the first law of thermodynamics must be satisfied. The overall energy balance for any two-fluid heat exchanger is given by Thulukkanam (2013:41) as:

$$\dot{m}_h \cdot C_{p,h}(T_{h,i} - T_{h,o}) = \dot{m}_c \cdot C_{p,c}(T_{c,o} - T_{c,i}) \tag{3.1}$$

where

$\dot{m}$ [kg/s] = the mass flow of the fluid.

C_p [J/kg.K] = the specific heat of the fluid.

T [K] = the temperature of the fluid.

The subscripts h and c refer to the hot and cold fluids, whereas the subscripts i and o designate the fluid inlet and outlet conditions. Under the usual idealizations made for the basic design theory of heat exchangers, the above mentioned equation satisfies the "macro" energy balance. (Thulukkanam, 2013).

3.2.2 Heat transfer

Assuming there is negligible heat transfer between the heat exchanger and its surroundings, as well as negligible potential and kinetic energy changes, the heat transfer for two fluid streams, for any flow arrangement, is given by Thulukkanam (2013:41) as:

$$q = \dot{m} \cdot C_p (T - T) \tag{3.2}$$

According to Bergman et al. (2011:711), the energy balance equation mentioned above can also be expressed as:

$$\dot{m}_h (h_{h,i} - h_{h,o}) = \dot{m}_c (h_{c,o} - h_{c,i}) \tag{3.3}$$

where

h [kJ/kg] = the enthalpy of the fluid.

Thus, Equation (3.2) can be expressed as:

$$q = \dot{m}(h - h) \tag{3.4}$$

3.3 Concentric tube heat exchanger

The basic principles needed to formulate a thermal-fluid simulation model of a concentric tube heat exchanger needs to be understood before attempting to follow with a coaxial heat exchanger model.

3.3.1 Concentric tube geometry

A concentric tube heat exchanger consists of an inner tube inside an outer tube with a fluid flowing in the inner tube and another fluid flowing outside and around the inner tube concealed inside the outer tube, this area is also known as the annulus. The two fluids has a temperature difference to allow heat transfer to occur. The inner tube is usually manufactured from a good heat conducting material, such as copper, to allow efficient conductive heat transfer between the two fluids through the inner tube. The outer tube consists of a lower heat conducting material to minimise the heat loss to the surrounding environment, an insulating material conceals the outer tube to further minimise this effect.

The direction of the flow for each fluid is dependent on which flow configuration is chosen for the heat exchanger, in this study the counter-flow configuration will be used as reviewed for coaxial coils in the literature chapter.

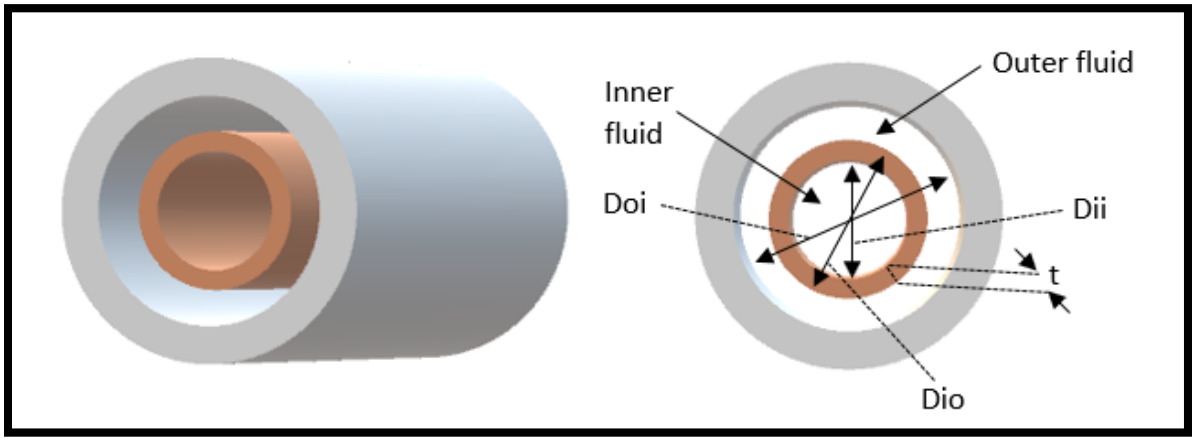

Figure 3-1: Illustration of the geometry for a concentric tube heat exchanger.

Figure 3-1 represents an illustration of the geometry for a concentric tube heat exchanger with a fluid flowing in the inner pipe and another fluid flowing in the

outer pipe in the opposite direction. Assume efficient insulation on the outer pipe to prevent heat loss to the surrounding environment. The concentric tube heat exchanger is defined by the following parameters:

- The inner diameter of the inner tube (D_{ii}) [m].
- The outer diameter of the inner tube (D_{io}) [m].
- The thickness (t) of the inner tube [m].
- The inner diameter of the outer tube (D_{oi}) [m].

3.3.2 Heat transfer

The purpose for formulating a thermal-fluid simulation model of a concentric tube heat exchanger is to ultimately determine the amount of heat transfer occurring inside this heat exchanger. This section describes the process needed to determine the heat transfer of the heat exchanger.

The heat transfer area of the two tubes are calculated using equations from Bergman et al. (2011:710). The heat transfer area of the inner tube is calculated as:

$$A_i = \pi \cdot D_{ii} \cdot L \tag{3.5}$$

where

A_i [m^2] = heat transfer area of the inner fluid.

L [m] = total length of the heat exchanger.

The heat transfer area of the outer tube is calculated as:

$$A_o = \pi \cdot D_{io} \cdot L \tag{3.6}$$

where

A_o [m^2] = heat transfer area of the outer fluid.

D_{io} [m] = the outer diameter of the inner tube, calculated by adding the inner tube wall thickness (t) twice to the inner diameter of the inner tube as:

$$D_{io} = D_{ii} + 2 \cdot t \tag{3.7}$$

To obtain the total heat transfer between the two fluids inside the heat exchanger tubes, the convection heat transfer coefficient of both fluids needs to be determined. Convection heat transfer is defined as the heat transfer occurring between a moving fluid and a solid, in this case the forced convection heat transfer is between the inner/outer flowing fluid and the inner solid tube. The appropriate rate equation of convection heat transfer is described by Newton's law of cooling from Bergman et al. (2011:8) as:

$$q'' = h(T_s - T_\infty) \tag{3.8}$$

where

q'' [W/m^2] = the convective heat flux.

h [W/m^{2}K] = the convection heat transfer coefficient.

T_s [K] = surface temperature of the solid component.

T_∞ [K] = bulk fluid temperature.

This coefficient is dependent on the conditions in the boundary layer, which are influenced by surface geometry, the nature of the fluid motion, and an assortment of transport and fluid thermodynamic properties (Bergman, et al., 2011).

It is important to determine the type of flow present inside a heat exchanger when calculating the convection heat transfer coefficient of a specific fluid. The fluid flow inside a heat exchanger is mainly either laminar or turbulent flow. Laminar flow is described as an orderly flow where every particle of fluid flows along one smooth path as where turbulent flow is an unorderly flow with particles moving back and forth between flow layers creating whirlpool-like patterns.

Bergman et al. (2011:390) states that the transition from laminar to turbulent flow is due to triggering mechanisms such as small disturbances. These disturbances may be induced by surface roughness, minute surface vibrations or fluctuations in the free stream. Bergman et al. (2011:390) continues to state that the onset of turbulent flow depends on whether the triggering mechanisms are enlarged or reduced in the direction of the fluid flow, which in turn will ultimately depend on a dimensionless grouping of parameters called the Reynolds number.

The Reynolds number represents the ratio of the inertia to viscous forces (Bergman, et al., 2011). For a small Reynolds number, the inertia forces are insignificant compared to the viscous forces, thus the forces are dissipated and the flow remains laminar. However, for a large Reynolds number, the inertia forces can be enough to amplify the triggering mechanisms where a transition to turbulent flow occurs (Bergman, et al., 2011).

The Reynolds number for both fluids in the concentric tube heat exchanger are determined with the method used by Christensen & Srinivasan (1990:39) as:

$$Re = \frac{\rho.u.D}{\mu} \tag{3.9}$$

where

Re = Reynolds number.

ρ [kg/m^3] = fluid density.

μ [Ns/m^2] = fluid viscosity.

u [m/s] = fluid velocity.

D [m] = the diameter of the tube, where D_{ii} is used to calculate the Reynolds number for the inner fluid and D_h for the outer fluid.

The hydraulic diameter is calculated as:

$$D_h = D_{oi} - D_{io} \tag{3.10}$$

where

D_h [m] = the hydraulic diameter.

The Nusselt number in heat exchanger calculations is a dimensionless parameter used to describe the ratio of the thermal energy convected to the fluid with the thermal energy conducted within the fluid. Bergman et al. (2011:401) states that the Nusselt number is equal to the dimensionless temperature gradient at the surface where it provides a measure of the convection heat transfer occurring at this surface. The Dittus-Boelter equation stated by Bergman et al. (2011:544) is used to determine the Nusselt number for a concentric tube heat exchanger with turbulent flow as:

$$Nu = 0.023 Re^{0.8} . Pr^{n} \tag{3.11}$$

where

Nu = Nusselt number.

Re = Reynolds number.

Pr = Prandtl number.

n = 0.3 for the fluid being cooled and n = 0.4 for the fluid being heated.

According to Bergman et al. (2011:407) the Prandtl number is defined as the ratio of the kinematic viscosity. The Prandtl number is also referred to as the momentum diffusivity to the thermal diffusivity. Thus, the Prandtl number is a fluid property and provides a measure of the relative effectiveness of momentum and energy transport by diffusion in the velocity and thermal boundary layers, respectively (Bergman, et al., 2011).

The Prandtl number for both fluids are calculated as:

$$Pr = \frac{Cp.\mu}{k} \tag{3.12}$$

where

μ [Ns/m^2] = the viscosity of the fluid.

k [W/m.K] = the thermal conductivity of the fluid.

Cp [J/kg.K] = the specific heat of the fluid.

Specific heat is defined as the amount of heat energy needed to uniformly raise the temperature of a body per unit of mass (Helmenstine, 2019). Thus, for example, the specific heat of water, as used in this study, is the amount of energy needed in joules (J) to raise the temperature of one kilogram (kg) of water by one Kelvin (K).

The local Nusselt number equation for a concentric tube heat exchanger as used by Bergman et al. (2011:422) is as follows:

$$Nu_D = \frac{h \cdot D}{k} \tag{3.13}$$

where

h [W/m^{2}K] = the convection heat transfer coefficient of the fluid.

D [m] = diameter of the tube, use D_{ii} to calculate the Nusselt number of the inner fluid and D_h for the outer fluid.

k [W/m.K] = thermal conductivity of the fluid within the heat exchanger.

Determining the Nusselt number with Equation (3.11), Equation (3.13) can be used to determine the convection heat transfer coefficient as:

$$h = Nu_D \cdot \frac{k}{D} \tag{3.14}$$

where

D [m] = diameter of the tube, use D_{ii} to calculate the convection heat transfer coefficient of the inner fluid and D_h for the outer fluid.

The heat transfer of the concentric tube heat exchanger is determined by satisfying the energy balance equation mentioned earlier.

3.3.3 LMTD method

In this study, a counter-flow configuration is used to obtain the maximum heat transfer in the coaxial condenser as reviewed in the literature chapter. According to Bergman et al. (2011:714) the total heat transfer of a counter-flow heat exchanger can be calculated with the use of a log mean temperature difference (LMTD) in the form of:

$$q = UA \cdot \Delta T_{lm} \tag{3.15}$$

where

q [W] = total heat transfer of the heat exchanger.

UA [W/m^{2}K] = the overall heat transfer coefficient.

ΔT_{lm} [°C] = the log mean temperature difference (LMTD).

The overall heat transfer coefficient (U) based on the heat transfer area (A) for a concentric tube heat exchanger is calculated as follows:

$$\frac{1}{UA} = \frac{1}{h_i.\pi.D_{ii}.L} + \frac{\ln\left(D_{io}/D_{ii}\right)}{2\pi.k.L} + \frac{1}{h_o.\pi.D_{io}.L} \tag{3.16}$$

where

h_i [W/m^{2}K] = The inner fluid convection heat transfer coefficient in the inner tube.

h_o [W/m^{2}K] = The outer fluid convection heat transfer coefficient in the outer tube.

k [W/m.K] = The thermal conductivity of the inner tube.

The LMTD for the counter-flow configuration is calculated as:

$$\Delta T_{lm} = \frac{\Delta T_1 - \Delta T_2}{\ln\left(\Delta T_1 / \Delta T_2\right)} \tag{3.17}$$

where

ΔT_1 [°C] = $T_{h,in} - T_{c,out}$

ΔT_2 [°C] = $T_{h,out} - T_{c,in}$

All the relevant theory necessary to successfully formulate a thermal-fluid simulation model of a concentric tube heat exchanger has been presented in this chapter. The next section will discuss the geometry and correlations necessary to formulate a thermal-fluid simulation model of a coaxial condenser.

3.4 Coaxial coil heat exchanger

Several methods have been applied to heat exchangers to enhance the heat transfer process. The coaxial coil is one technique used where swirl is introduced in the bulk flow in the inside and annulus side of the tube due to the surface geometry. These coaxial tubes enhances heat transfer without causing a great increase in the friction factor of the coil (Srinivasan & Christensen, 1992). To formulate an effective thermal-fluid model of a titanium coaxial condenser, the complex characteristics of this heat exchanger needs to be investigated.

3.4.1 Specifications of the coaxial coil

3.4.1.1 Coaxial coil geometry

Figure 3-2 represents the geometry of the titanium coaxial coil heat exchanger and indicates the important geometry needed to formulate the simulation model.

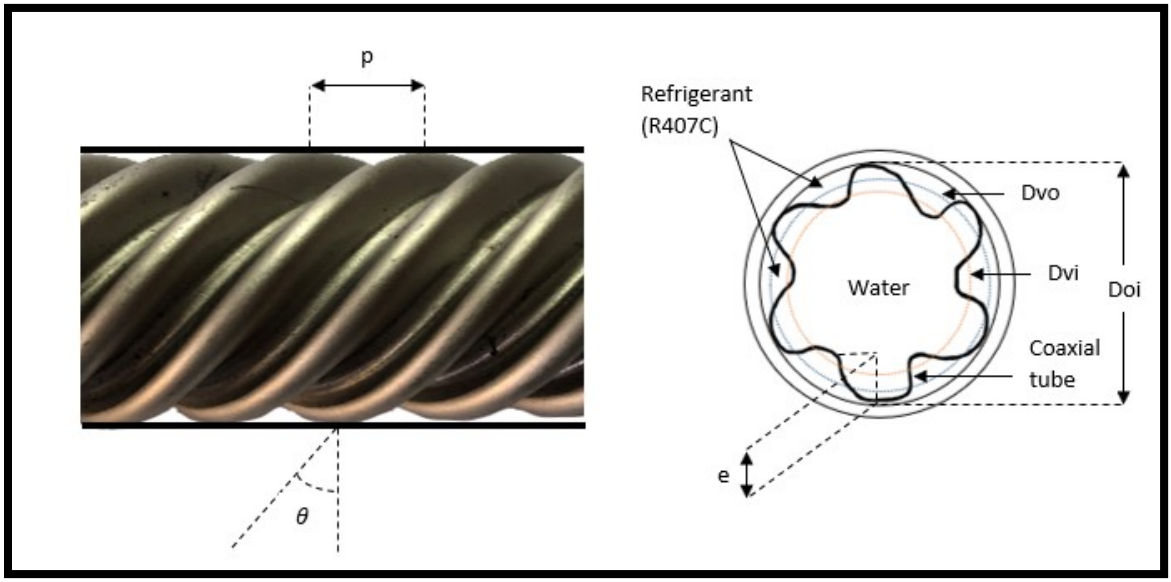

Figure 3-2: Illustration of the titanium coaxial coil dimensions.

The geometry of the coaxial coil is defined by the following parameters as indicated on Figure 3-2:

- Volume-based inside diameter (D_{vi}) [m]
- Volume-based outside diameter (D_{vo}) [m]
- Pitch (p) [m]
- Flute depth (e) [m], and the
- Helix angle (θ) [°].

The coaxial coil has a complex geometry with no circular cross section. The volume-based inside diameter is used in this study where it represents an approximate

cross-sectional flow area of the inner tube. Thus, the volume-based inside diameter is calculated with the method used by Christensen & Srinivasan (1990:37) as:

$$D_{vi} = \sqrt{\frac{4.V}{\pi.L}} \tag{3.18}$$

where

D_{vi} [m] = volume-based inside diameter.

V [m^3] = the volume inside the tube.

L [m] = Length of the coaxial tube.

The volume-based outside diameter (D_{vo}) is determined in a similar manner as in which the outside diameter of the inner tube (D_{io}) was calculated for the concentric tube heat exchanger discussed earlier. The volume-based outside diameter (D_{vo}) is calculated by adding the tube wall thickness, t, twice to the volume-based inside diameter (D_{vi}) as:

$$D_{vo} = D_{vi} + 2 \cdot t \tag{3.19}$$

where

D_{vo} [m] = volume-based outside diameter.

t [m] = coaxial tube wall thickness.

Christensen & Srinivasan (1990:58-61) presented an equation containing non-dimensional parameters to determine the Nusselt number of the fluid flowing inside the coaxial tube. The non-dimensional parameters found in this equation are determined from the coaxial geometry as seen in Figure 3-2 and are as follows:

The first non-dimensional parameter is the non-dimensional flute depth (e^*):

$$e^* = \frac{e}{D_{vi}} \tag{3.20}$$

where

e [m] = the flute depth, which is defined as a measured depth of any flute.

The second non-dimensional parameter is the non-dimensional flute pitch (p^*):

$$p^* = \frac{p}{D_{vi}} \tag{3.21}$$

where

p [m] = the flute pitch, which is defined as the axial distance among any end-to-end flutes.

And the third non-dimensional parameter is the non-dimensional helix angle (θ^*). First, the helix angle needs to be understood before the non-dimensional helix angle can be determined.

The helix angle of the coaxial coil is an important factor as this determines the swirl flow as well as the velocity of the gas or liquid which will flow through the inner coaxial tube and annulus. The helix angle is effectively the angle of the flow in the flute of the coaxial coil in terms of the centre axis as seen on Figure 3-3.

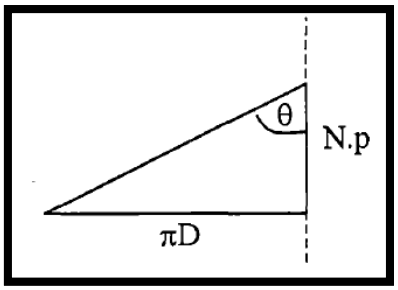

Figure 3-3: Helix angle demonstration (van Eldik, 1998).

The helix angle is thus determined by stating: If the flow has moved a distance πD perpendicular to the axis along the centre on the inner tube, it has also moved along the axis a distance of $N.p$. The helix angle is formulated as follows:

$$\theta = \arctan\left(\frac{\pi D_{vo}}{N.p}\right) \tag{3.22}$$

where

D_{vo} [m] represents the diameter (D) in Figure 3-3.

N = the number of flute starts as shown in Figure 3-4.

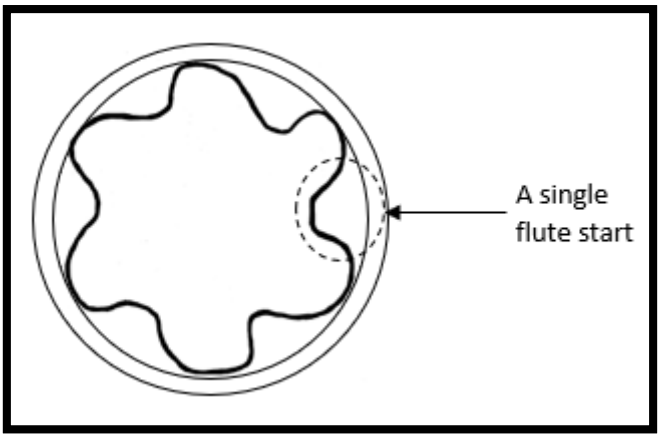

Figure 3-4: Coaxial coil flute starts (N).

The titanium coaxial coil used in this study has six flute starts as seen in Figure 3-4.

The non-dimensional helix angle can now be calculated as a ratio relative to perpendicular flow:

$$\theta^* = \frac{\theta}{90°} \tag{3.23}$$

Equation (3.18) to Equation (3.23) are implemented in the model to determine the geometry of the coaxial coil with the known pitch (p) and flute depth (e). The convection heat transfer coefficients and pressure drop will be determined in the next section using the above-mentioned geometry.

3.5 Heat transfer and pressure drop prediction

3.5.1 The single-phase region

This section describes the convection heat transfer coefficient as well as the pressure drop of the water and the single-phase refrigerant. The single-phase of

the refrigerant refers to the phase the refrigerant experiences inside the coaxial coil annulus, being either a liquid or a gas. The refrigerant used in this study is the zeotropic refrigerant mixture, R-407C.

3.5.1.1 Convection heat transfer coefficient of water inside the inner coaxial tube

This section will provide information on how to calculate the single-phase convective heat transfer coefficient of the water flowing inside the coaxial tube.

The velocity of the water can be computed by employing the equation used by Christensen et al. (1993:9) as:

$$u_w = \frac{4 \cdot \dot{m}_w}{\pi \cdot \rho_w \cdot (D_{vi})^2} \tag{3.24}$$

where

u_w [m/s] = the velocity of the water.

$\dot{m}_w$ [kg/s] = the mass flow rate of the water.

ρ_w [kg/m^3] = the water density.

D_{vi} [m] = the volume-based inside diameter of the inner coaxial tube.

The Reynolds number of the water flowing inside the coaxial tube can be computed by employing Equation (3.9) and substituting the concentric tube diameter with the volume-based inside diameter.

The correlation of Christensen & Srinivasan (1990:61) is used to determine the Nusselt number of the water flowing inside the coaxial tube. The Nusselt number of the water (Nu_w) is a function of the water Reynolds number (Re_w) and is explained below.

For $Re_w \leq 5000$, Equation (3.25 a) is used:

$$Nu_w = 0.014 Re_w^{0.842} . \left(e^*\right)^{-0.067} . \left(p^*\right)^{-0.293} . \left(\theta^*\right)^{-0.705} . Pr_w^{0.4} \quad \text{(3.25 a)}$$

For $Re_w > 5000$, Equation (3.25 b) is used:

$$Nu_w = 0.064 Re_w^{0.773} . \left(e^*\right)^{-0.242} . \left(p^*\right)^{-0.108} . \left(\theta^*\right)^{0.599} . Pr_w^{0.4} \quad \text{(3.25 b)}$$

where

Pr_w = the Prandtl number of the water flowing inside the coaxial tube which is computed by employing Equation (3.12).

Equation (3.13) can also be used to determine the Nusselt number of the water flowing inside the coaxial tube replacing the concentric tube diameter with D_{vi}. Thus, the convection heat transfer coefficient of the water flowing inside the coaxial tube is calculated using Equation (3.14).

3.5.1.2 Convection single-phase refrigerant heat transfer coefficient in the annulus

This section will provide information on how to predict the single-phase convective heat transfer coefficient of the refrigerant, R-407C, flowing in the annulus of the coaxial condenser.

Firstly, to predict the refrigerant convection heat transfer coefficient in a coaxial condenser, the convection heat transfer coefficient of the refrigerant inside a straight concentric tube heat exchanger of similar size needs to be determined. Thereafter, the convective heat transfer coefficient of the refrigerant is converted from the straight concentric tube heat exchanger to the coaxial condenser with the use of a heat transfer enhancement factor and ratio, where:

e_h = Heat transfer enhancement factor

r_h = Heat transfer enhancement ratio.

The heat transfer enhancement factor (e_h) is applied to account for the differences in the annulus of the coaxial coil compared to helical coil heat exchangers as well as other deviations from the assumptions originally made from the friction heat transfer analogy (Rousseau, et al., 2003).

The value of e_h was computed by comparing the results of the coaxial condenser simulation model to the experimental data obtained in the experimental set-up (Chapter 4). An optimisation routine was formulated and linked to the simulation model where it was used to obtain a single e_h value resulting in the best fit between the simulated and experimental heat transfer values.

The heat transfer enhancement ratio (r_h) is equal to the friction enhancement ratio (r_f) used in the single- and two-phase refrigerant pressure drop calculations. The friction enhancement ratio (r_f) is better known as the ratio of the effective friction factors when comparing straight and helical coils (Rousseau, et al., 2003). Wessels (2007:32) states that according to the Chilton-Colburn analogy the heat transfer enhancement ratio (r_h) is around the same as the friction enhancement ratio (r_f) for simple geometries, therefore we can assume:

$$r_f = r_h$$

The friction enhancement factor (r_f) will be further discussed in section 3.5.1.3.2 of this chapter.

The velocity of the single-phase refrigerant can be computed by employing Equation (3.26) used by Christensen et al. (1993:14). All the subscripts labelled " R_S " refers to the refrigerant thermodynamic properties in the single-phase:

$$u_{R_S} = \frac{\dot{m}_r}{\rho_{R_S} \cdot A_{cr}} \tag{3.26}$$

where

$\dot{m}_r$ [kg/s] = the refrigerant mass flow rate.

ρ_{R_S} [kg/m^3] = the single-phase refrigerant density.

A_{cr} [m^2] = the cross-sectional area of the annulus which is calculated by employing Equation (3.27) as used by Christensen et al. (1993:14):

$$A_{cr} = \pi \frac{(D_{oi}^{\ 2} - D_{vo}^{\ 2})}{4} \tag{3.27}$$

where

D_{oi} [m] = The inner diameter of the outer steel tube of the coaxial coil.

The single-phase refrigerant Reynolds number inside the annulus is determined with Equation (3.9) by replacing the concentric diameter with the hydraulic diameter determined with Equation (3.28) as:

$$D_h = D_{oi} - D_{vo} \tag{3.28}$$

The single-phase refrigerant Prandtl number is computed by employing Equation (3.12).

The Dittus-Boelter equation stated by Bergman et al. (2011:544) is initially used to determine the Nusselt number for straight concentric tube heat exchangers ($Nu_{straight}$):

$$Nu_{straight} = 0.023 Re_{R_S}^{\ 0.8} . Pr_{R_S}^{\ 0.3} \tag{3.29}$$

where

Pr_{R_S} = The Prandtl number of the single-phase refrigerant.

The Nusselt number for the helical tube ($Nu_{helical}$) is determined by converting the Nusselt number for straight tubes ($Nu_{straight}$) with the use of the heat transfer enhancement factor and ratio as:

$$Nu_{helical} = e_h . r_h . Nu_{straight} \tag{3.30}$$

The single-phase convection heat transfer coefficient in the annulus of the coaxial condenser is determined as:

$$h_{SP} = \frac{Nu_{helical}.k_{R_S}}{D_h} \tag{3.31}$$

where

h_{SP} [W/m^{2}K] = the refrigerant single-phase convection heat transfer coefficient inside the annulus of the coaxial condenser.

3.5.1.3 Single-phase pressure drop

The following section describes the pressure drop of the water flowing inside the coaxial condenser as well as the pressure drop of the refrigerant, R-407C, flowing in the annulus while in a single-phase stage, either being a superheated gas or a sub-cooled liquid.

3.5.1.3.1 Pressure drop inside the coaxial tube

The water pressure drop in the coaxial tube is determined with a correlation containing a friction factor (f). This friction factor (f) is a function of the fluid flowing inside the coaxial tube, the Reynolds number as well as the geometry of the coaxial tube. Christensen et al. (1993) used the Darcy-Weisbach friction factor to determine the pressure drop inside a coaxial tube.

The water velocity (u_w) and the volume-based inside diameter (D_{vi}) is used to determine the water Reynolds number (Re_w). The friction factor (f) is a function of the water Reynolds number (Re_w).

If $\mathrm{Re}_w \leq 1500$, Equation (3.32 a) is used:

$$f = 0.554\left(\frac{64}{\mathrm{Re}_w - 45}\right).\left(e^*\right)^{0.384}.\left(p^*\right)^{-1.454+2.083e^*}.\left(\theta^*\right)^{-2.426} \tag{3.32 a}$$

If $\mathrm{Re}_w > 1500$, Equation (3.32 b) is used:

$$f = 1.209\left(\mathrm{Re}_w\right)^{-0.261}.\left(e^*\right)^{1.26-0.05p^*}.\left(p^*\right)^{-1.66+2.033e^*}.\left(\theta^*\right)^{-2.699+3.67e^*} \quad (3.32\ b)$$

Once the friction factor is determined, the total water pressure drop is calculated by employing the correlation used by Christensen et al. (1993:11) with a water friction enhancement factor as:

$$\Delta P_w = e_{f_w}.\rho_w.u_w{}^2.\frac{f.L}{2D_{vi}} \quad (3.33)$$

where

ρ_w [kg/m^3] = the density of the water flowing inside the coaxial tube.

e_{f_w} = the water friction enhancement factor.

This water friction enhancement factor is used to account for any differences between straight concentric tube and coaxial coil heat exchangers. The water friction enhancement factor was calculated on the same method as the heat transfer enhancement factor where a single e_{f_w} value is obtained resulting in the best fit between the simulated and experimental water pressure drop values.

3.5.1.3.2 Pressure drop in the annulus

A friction enhancement ratio (r_f) is used in the pressure drop correlation to determine the single-phase refrigerant pressure drop inside the annulus of the coaxial condenser as discussed earlier in this chapter.

This friction enhancement ratio (r_f) is calculated as follows:

$$r_f = \frac{f_{helical}}{f_{straight}} \quad (3.34)$$

where

$f_{straight}$ = the friction factor for straight concentric tube heat exchangers.

$f_{helical}$ = the friction factor for helical coil heat exchangers.

The friction factor for straight concentric tube heat exchangers ($f_{straight}$) is calculated with the use of the correlation determined by Swamee & Jain (1976) for a standard single-phase condition:

$$f_{straight} = \frac{0.25}{\left\{\log\left[\frac{\mathrm{e_r}}{3.7\times \mathrm{D_h}} + \left(\frac{5.74}{Re_{R_S}^{\ 0.9}}\right)\right]\right\}^2} \tag{3.35}$$

where

e_r [m] = the surface finish (absolute roughness) of the coaxial tube material.

The friction factor for helical coil heat exchangers ($f_{helical}$) is calculated with the use of the correlation formulated by Das (1993) for a standard single-phase condition:

$$f_{helical} = 4\left[0.079 Re_{R_S}^{\ -0.25} + 0.0075\left(\frac{\mathrm{D_h}}{\mathrm{d_{coil}}}\right)^{0.5} + 17.5782 Re_{R_S}^{\ -0.3137}.\left(\frac{\mathrm{D_h}}{\mathrm{d_{coil}}}\right)^{0.3621}.\left(\frac{\mathrm{e_r}}{\mathrm{D_h}}\right)^{0.6885}\right] \tag{3.36}$$

where

d_{coil} = the helical friction parameter which is calculated as follows:

$$d_{coil} = \frac{D_h}{sin\theta} \tag{3.37}$$

The single-phase pressure drop in the annulus of a straight concentric tube heat exchanger is calculated by employing the correlation used by Christensen et al. (1993:15) as:

$$\Delta P_{straight} = \rho_{R_S}.u_{R_S}^{\ 2}.\frac{f_{straight}.L}{2D_h} \tag{3.38}$$

where

ρ_{R_S} [kg/m^3] = the density of the single-phase refrigerant in the annulus.

u_{R_S} [m/s] = the velocity of the single-phase refrigerant in the annulus.

The total pressure drop for the single-phase refrigerant in the annulus of the coaxial condenser is calculated by converting the concentric tube pressure drop, calculated with Equation (3.38), with the friction enhancement factor and ratio as:

$$\Delta P_{SP} = e_f . r_f . \Delta P_{straight} \tag{3.39}$$

where

ΔP_{SP} [kPa] = the pressure drop of the single-phase refrigerant in the annulus of the coaxial condenser.

e_f = the friction enhancement factor.

r_f = the friction enhancement ratio.

The friction enhancement factor (e_f) is determined by comparing experimental data with simulated results from the simulation model. The experimental data is obtained from a test set-up where a titanium coaxial condenser is tested in various operating conditions. The testing of the titanium coaxial condenser will be discussed in Chapter 4. An optimisation routine was formulated and linked to the simulation model where it was used to obtain a single e_f value resulting in the best fit between the simulated and experimental pressure drop values.

3.5.2 The two-phase region

This section describes the convection heat transfer coefficient as well as the pressure drop of the refrigerant, R-407C, in the two-phase region. Two-phase refers to the refrigerant being a saturated gas or liquid.

3.5.2.1 Two-phase heat transfer coefficient

Shah (1979:548) introduced a method to compute the two-phase refrigerant convection heat transfer coefficient for straight concentric tube heat exchangers (Equation (3.49)). This method includes the convection heat transfer coefficient of

the refrigerant in a liquid phase as a parameter. This coefficient can be determined by substituting Equation (3.14) with the Nusselt number in the single-phase refrigerant Dittus-Boelter equation (Equation (3.29)) as:

$$h_l = 0.023 Re_l^{0.8} . Pr_l^{0.3} \cdot \frac{k_l}{D_h} \tag{3.40}$$

where all the subscripts labelled "l" refers to the refrigerant thermodynamic properties in a liquid phase.

The two-phase convection heat transfer coefficient of the refrigerant in straight concentric tube heat exchangers is calculated by implementing the method of Shah (1979:548). Here the average refrigerant quality, x_{avg}, represents the specific section of the annulus being analysed. The two-phase convection heat transfer coefficient is determined as follows:

$$h_{tp} = h_l \left[\left(1 - x_{avg}\right)^{0.8} + \frac{3.8 x_{avg}^{0.76} \left(1 - x_{avg}\right)^{0.04}}{pr^{0.38}} \right] \tag{3.41}$$

where

h_l [W/m^{2}K] = the convection heat transfer coefficient of the refrigerant in a liquid phase computed by employing Equation (3.40).

pr = The pressure ratio between the local static pressure and critical pressure of the refrigerant R-407C. This pressure ratio is calculated as follows:

$$pr = \frac{P_{Local}}{P_{Critical}} \tag{3.42}$$

The two-phase convection heat transfer coefficient of the refrigerant in the annulus of the coaxial condenser is calculated by implementing the heat transfer enhancement factor and ratio as:

$$h_{TP} = e_h . r_h . h_{tp} \tag{3.43}$$

Note that a single heat transfer enhancement factor (e_h) for the prediction of the refrigerant convection heat transfer coefficient is used for both the single- and two-phase regions. Furthermore, the heat transfer enhancement ratio (r_h) employed in the two-phase region (Equation (3.43)) differs from the enhancement ratio used in the single-phase region. The Chilton-Colburn analogy described in section 3.5.1.2 also applies to the two-phase region where:

$$r_f = r_h$$

The computation method of the friction enhancement ratio (r_f) used in the two-phase region will be discussed in section 3.5.2.2.

3.5.2.2 Two-phase pressure drop

Traviss et al. (1971:13) describes the pressure drop for a straight concentric tube heat exchanger in the two-phase region. The pressure drop is subject to the quality of the refrigerant (x) and is calculated as:

$$\Delta P_{straight} = 0.09 Re_v^{-0.2} \cdot x^{1.8} \left[1 + 2.85 \left(\mu_x^{-0.1} \left(\frac{1-x}{x} \right)^{0.9} \cdot \rho_x^{0.5} \right)^{0.523} \right]^2 \cdot \left(\frac{G_{R407C}^{\ 2}}{\rho_v \times D_h} \right) \quad (3.44)$$

where

$\Delta P_{straight}$ [kPa] = the pressure drop of the two-phase refrigerant in a concentric tube heat exchanger.

G_{R407C} [kg/m^{2}s] = The refrigerant mass flux.

Re_v = the Reynolds number based on the thermodynamic properties of the refrigerant in a vapour phase.

μ_x = the two-phase refrigerant viscosity ratio.

ρ_x = the two-phase refrigerant density ratio.

The mass flux of the refrigerant is determined as:

$$G_{R407C} = \frac{\dot{m}_r}{A_{cr}} \tag{3.45}$$

where

$\dot{m}_r$ [kg/s] = The mass flow rate of the refrigerant.

A_{cr} [m] = The annulus cross-sectional area, calculated with Equation (3.27).

The refrigerant viscosity and density ratios are determined with Equations (3.46) and (3.47) respectively, as used by Traviss et al. (1971:13). The subscript "v" refers to the refrigerant thermodynamic properties in a vapour phase and "l" in a liquid phase.

$$\mu_x = \frac{\mu_v}{\mu_l} \tag{3.46}$$

$$\rho_x = \frac{\rho_v}{\rho_l} \tag{3.47}$$

The friction enhancement ratio (r_f) used in the two-phase region is calculated with Equation (3.42) as used in the single-phase region, section 3.5.1.3.2. However, the parameters $f_{straight}$ and $f_{helical}$ are computed in a different manner.

The friction factor for straight concentric tube heat exchangers ($f_{straight}$) is calculated with the use of the correlation formulated by Swamee & Jain (1976) and implemented for a two-phase condition as:

$$f_{straight} = \frac{0.25}{\left\{\log\left[\frac{\mathrm{e_r}}{3.7\times \mathrm{D_h}} + \left(\frac{5.74}{Re_x^{\,0.9}}\right)\right]\right\}^2} \tag{3.48}$$

where

Re_x = the two-phase refrigerant Reynolds number.

Re_x is calculated by employing Equation (3.49) as:

$$Re_x = Re_l + \mu_x \cdot \left(\frac{1}{\rho_x}\right)^{0.5} \cdot Re_v \tag{3.49}$$

The friction factor for helical coil heat exchangers ($f_{helical}$) is calculated with the use of the correlation formulated by Das (1993) implemented for a two-phase condition:

$$f_{helical} = 4\left[0.079Re_v^{-0.25} + 0.0075\left(\frac{\mathrm{D_h}}{\mathrm{d_{coil}}}\right)^{0.5} + 17.5782Re_v^{-0.3137}.\left(\frac{\mathrm{D_h}}{\mathrm{d_{coil}}}\right)^{0.3621}.\left(\frac{\mathrm{e_r}}{\mathrm{D_h}}\right)^{0.6885}\right] \tag{3.50}$$

The equation used in the single-phase region (Equation (3.39)) is also applied in the two-phase region to determine the total pressure drop of the two-phase refrigerant in the annulus of the coaxial condenser:

$$\Delta P_{TP} = e_f.r_f.\Delta P_{straight} \tag{3.51}$$

where

ΔP_{TP} [kPa] = the two-phase refrigerant pressure drop in the annulus of the coaxial condenser.

Note that a single friction enhancement factor for the prediction of the refrigerant pressure drop is used for both the single- and two-phase regions.

The total pressure drop of the refrigerant inside the annulus of the coaxial condenser is calculated as:

$$\Delta P_r = \Delta P_{SP} + \Delta P_{TP} \tag{3.52}$$

where

ΔP_r [kPa] = the total refrigerant pressure drop.

ΔP_{SP} [kPa] = the single-phase refrigerant pressure drop.

ΔP_{TP} [kPa] = the two-phase refrigerant pressure drop.

3.5.3 Coaxial condenser heat transfer equations

The need exists in this study to obtain experimental data of a titanium coaxial condenser in order to accurately predict the total heat transfer and pressure drop of the heat exchanger. The titanium coaxial condenser uses water as heat sink flowing in the inner tube while the zeotropic refrigerant, R-407C, flows in the outer annulus.

The titanium coaxial condenser uses a counter-flow configuration to maximize the heat transfer of the condenser. To achieve an accurate simulation model the following experimental data needs to be obtained:

- Inlet water and refrigerant temperature and pressure.
- Outlet water and refrigerant temperature and pressure.
- Water mass flow rate.

The experimental heat transfer of the water was calculated by employing Equation (3.4). In this study, the refrigerant mass flow rate is calculated with the assumption of 100% heat transfer efficiency between the water and refrigerant by using Equation (3.4).

This approach is followed due to the difficulty in accurately measuring the refrigerant mass flow rate with unavoidable two-phase flow entering the refrigerant mass flow measuring system which is calibrated to only measure the mass flow rate of the single-phase liquid of the refrigerant. This results in inaccuracies in the experimental refrigerant mass flow rate data.

Consequently, the refrigerant mass flow rate is calculated by employing Equation (3.4) with the experimental refrigerant inlet and outlet enthalpy values obtained

from R-407C thermodynamic property tables using the above-mentioned experimental data as:

$$q_w = \dot{m}_r.\left(h_{r_i} - h_{r_o}\right) \tag{3.53}$$

where

q_w [W] = heat transfer of the water.

$\dot{m}_r$ [kg/s] = mass flow rate of the refrigerant R-407C.

h_{r_i} [J/kg] = inlet enthalpy of the refrigerant R-407C.

h_{r_o} [J/kg] = outlet enthalpy of the refrigerant R-407C.

The experimental heat transfer of the refrigerant is calculated by employing Equation (3.4) once more. The test set-up used in this study to obtain the experimental data will be discussed in Chapter 4.

3.5.4 Coaxial condenser - LMTD method

Calculating the heat transfer of the coaxial condenser by employing Equation (3.17), the overall heat transfer coefficient in Equation (3.18) needs to be adjusted for coaxial heat exchangers as:

$$\frac{1}{UA} = \frac{1}{h_w.\pi.D_{vi}.L} + \frac{\ln\left(D_{vo}/D_{vi}\right)}{2\pi.k_{Ti}.L} + \frac{1}{h_r.\pi.D_{vo}.L} \tag{3.54}$$

where

h_w [W/m^{2}K] = The water convection heat transfer coefficient in the coaxial tube determined with Equation (3.14).

h_r [W/m^{2}K] = The refrigerant convection heat transfer coefficient in the annulus determined either with Equation (3.31) when in single-phase or with Equation (3.43) when in two-phase.

k_{Ti} [W/m.K] = The thermal conductivity of the titanium coaxial tube determined with water temperature.

The LMTD for the coaxial condenser using a counter-flow configuration is calculated with Equation (3.19) with the values of ΔT_1 as:

$T_{h,in}$ [°C] = Refrigerant temperature entering the condenser.

$T_{c,out}$ [°C] = Water temperature exiting the condenser.

and ΔT_2 as:

$T_{h,out}$ [°C] = Refrigerant temperature exiting the condenser.

$T_{c,in}$ [°C] = Water temperature entering the condenser.

3.6 Simulation of a titanium coaxial condenser

This section consists of implementing the equations and correlations of the different heat exchangers discussed above into a simulation routine to formulate a thermal-fluid simulation model of a titanium coaxial condenser. The objective of the simulation model is to predict the heat transfer and pressure drop of a titanium coaxial condenser operating over a wide variety of operating conditions. Experimental data was gathered through a test set-up which will be discussed in Chapter 4. The experimental data was used to prove the validity of the simulation model and to obtain the necessary enhancement factors specifically for a titanium coaxial condenser.

When a simulation is conducted on a heat exchanger, appropriate inputs are needed to predict the required outputs. These inputs are the inlet conditions to the heat exchanger such as the temperatures and pressures which needs to be specified before the required outlet temperatures and pressures can be simulated.

Furthermore, for each defined point in the heat exchanger, applicable thermodynamic boundary conditions are employed to uncover the thermodynamic properties needed at that point, such as the fluid or gas density (ρ), specific heat (Cp), viscosity (μ), conductivity (k), enthalpy (h), entropy (s) and quality (x). Using simulation, these uncovered properties are used to determine the necessary thermodynamic properties at each discrete interval of the heat exchanger.

During the simulation process, the non-dimensional parameters such as the Reynolds number, Prandtl number and the Nusselt number needs to be determined at each of these discrete points by applying knowledge of the underlying thermodynamic properties. An important factor is the convection heat transfer coefficient as this needs to be computed in order to calculate the heat transfer between the two fluids in the heat exchanger. This coefficient can only be calculated after the computation of the Nusselt number using a suitable empirical correlation.

An accurately determined Nusselt number leads to an accurate prediction of the convection heat transfer coefficient, which further results in an accurate simulation of the heat transfer occurring inside the heat exchanger. For the coaxial condenser, the Dittus-Boelter correlation may be employed to predict the Nusselt number for the water side (Nu_w). The Dittus-Boelter correlation is also used to predict the Nusselt number for the single-phase refrigerant in straight concentric tube heat exchangers ($Nu_{straight}$) which forms part of the coaxial condenser simulation calculations.

The coaxial condenser was divided into smaller, equal in length, increments and the thermodynamic properties at each inlet and outlet for every discrete point were computed. There exists a refrigerant two-phase condition in the annulus of the condenser. Thus, the condenser were divided into the following decided increments represented in Figure 3-5, where the superheated region of the condenser were divided into three increments, the two-phase region into five increments and the sub-cooled region into two increments to simplify the simulation process.

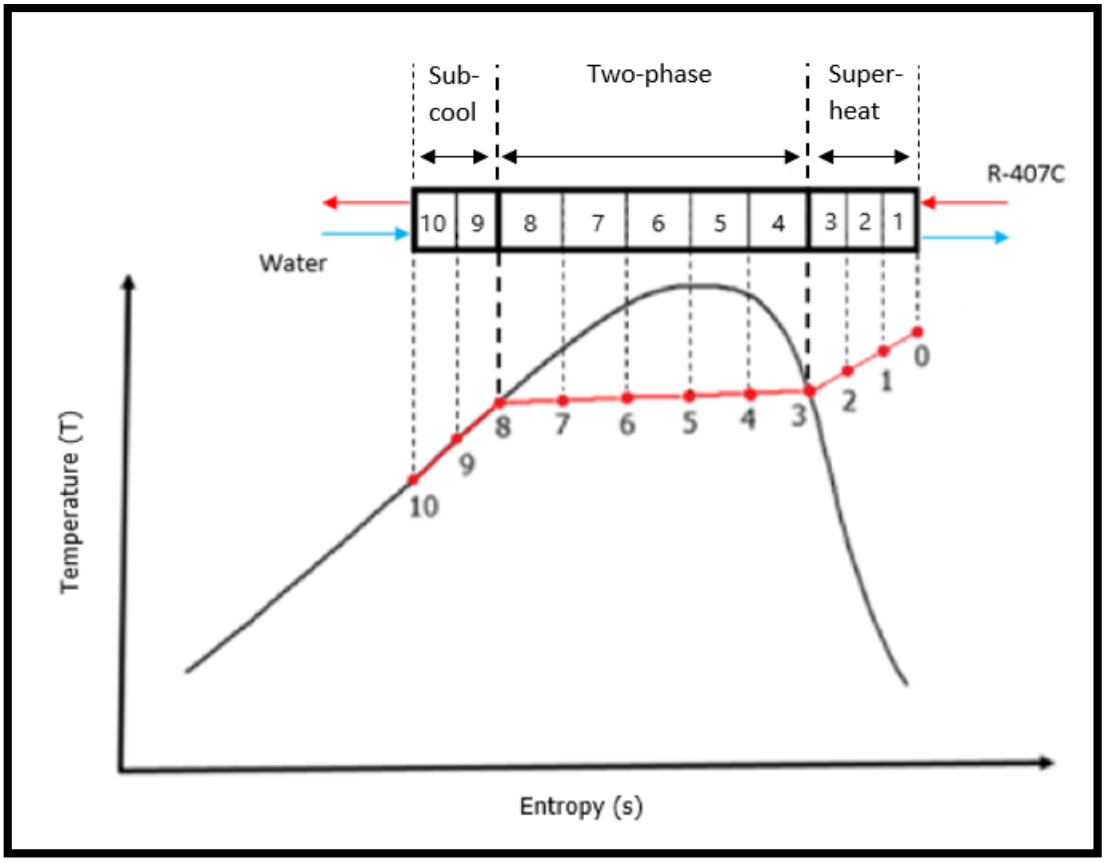

Figure 3-5: R-407C Temperature-Entropy diagram.

Note that the inlet conditions to an increment are the outlet conditions of the previous neighbouring increment in the direction of the fluid flow. In this simulation model, it was assumed that the flow was fully developed and that no heat loss occurred to the surrounding environment at any point of the heat exchanger during the simulation process. Thus, there was no need to use the outside diameter of the outer mild steel pipe of the coaxial condenser as a parameter in this simulation due to the assumption that the condenser is perfectly insulated from the environment and that no heat loss will occur.

The titanium coaxial coil used in this study is the model ET020ST manufactured by Extek (Extek, 2015). The supplier did not provide enough dimensions needed to formulate a simulation model. However, after the testing of the coaxial coil was concluded in the test set-up (Chapter 4), the titanium coil was deconstructed to gain access inside the heat exchanger to measure the required dimensions. These

measured dimensions are summarised in Table 3-1. Note that the absolute surface roughness (e_r) of titanium was given by BP group (2006).

Table 3-1: Titanium coaxial coil specifications.

Parameter	**Measurement**
Volume (V)	0.00219 m^3
Coaxial tube thickness (t)	0.0007 m
Length of titanium coaxial coil (L)	5.07 m
Flute pitch (p)	0.013334 m
Flute depth (e)	0.00506 m
Flute starts (N)	6
Inside diameter of the outer steel tube (D_{oi})	0.033318 m
Absolute surface roughness of titanium (e_r)	0.0000457 m

Since all the relevant dimensions are specified, the volume-based inside and outside diameters could be calculated by employing Equations (3.18 – 19). Thereafter, the non-dimensional parameters such as the non-dimensional flute depth (e^*), non-dimensional flute pitch (p^*) and the non-dimensional helix angle (θ^*) as well as the helix angle (θ) were computed using Equations (3.20 – 23).

The next few sections will discuss the convection heat transfer coefficient, total heat transfer as well as the total pressure drop simulation calculations of the water and refrigerant sides since all the geometrical parameters were computed.

3.6.1 Water convection heat transfer coefficient simulation

This section will describe the simulation routine to predict the convection heat transfer coefficient of the water flowing inside the inner coaxial tube.

Figure 3-6 illustrates a flow diagram of the simulation routine to compute the water convection heat transfer coefficient of the titanium coaxial condenser discussed in this section.

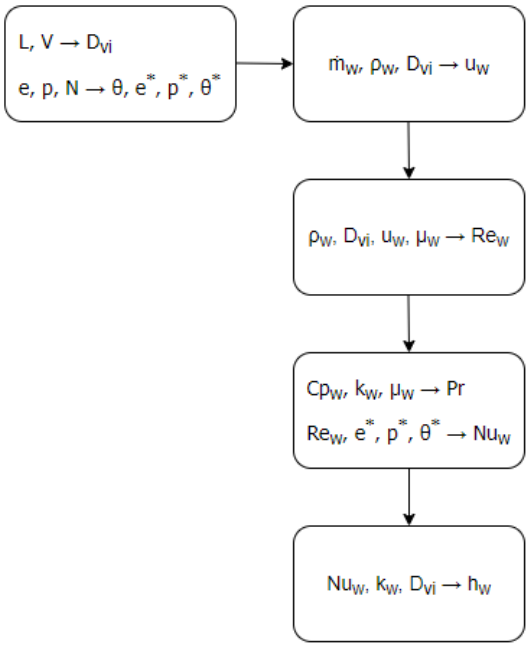

Figure 3-6: Flow chart of the water convection heat transfer coefficient simulation routine.

From Equation (3.24) it follows that the velocity of the water at any point of the heat exchanger can be computed if the water mass flow rate and density are known at that point. With the computation of the water velocity, density, viscosity and volume-based inside diameter, the water Reynolds number were computed by employing Equation (3.9).

From Equation (3.13), it follows that the water Prandtl number can be computed at any point of the heat exchanger if the values of the water specific heat, viscosity and the thermal conductivity of the water at that point are known. After the computation of the water Reynolds and Prandtl number, either Equation (3.25 a) or

(3.25 b) are employed, depending on the magnitude of the Reynolds number, to compute the Nusselt number of the water.

After the computation of the water Nusselt number, Equation (3.14) is employed to calculate the convection heat transfer coefficient of the water (h_w).

3.6.2 R-407C convection heat transfer coefficient simulation

3.6.2.1 Single-phase convection heat transfer coefficient

This section will describe the simulation routine to predict the convection heat transfer coefficient of the single-phase refrigerant flowing inside the annulus of the coaxial condenser.

Figure 3-7 illustrates a flow diagram of the simulation routine to compute the single-phase convection heat transfer coefficient of the titanium coaxial condenser discussed in this section.

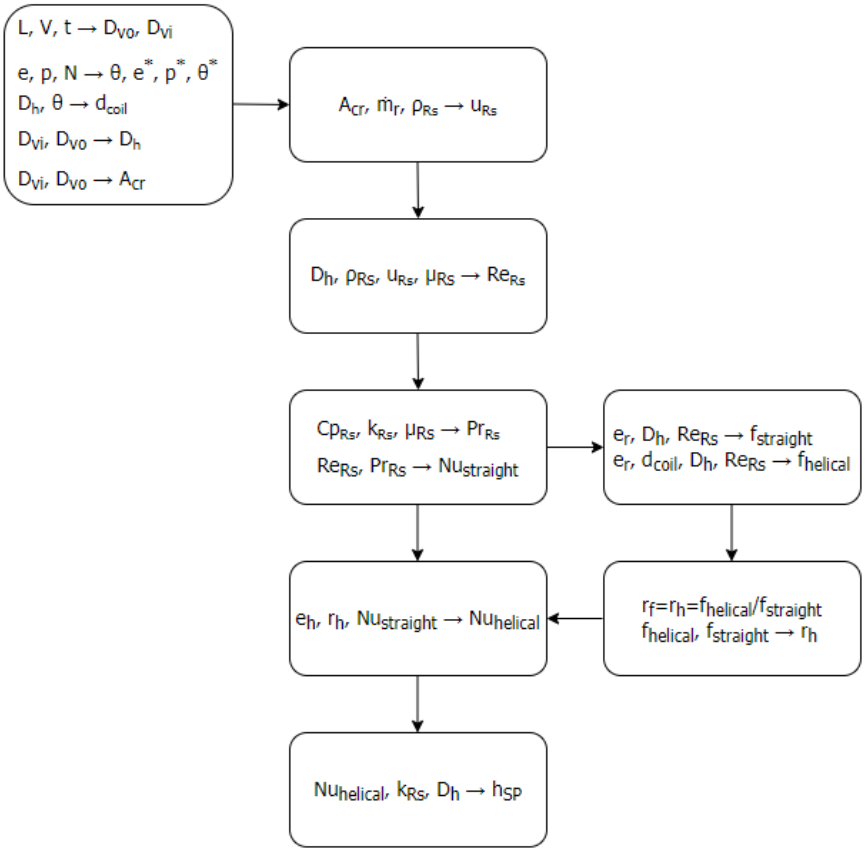

Figure 3-7: Flow chart of the R-407C single-phase convection heat transfer coefficient simulation routine.

By calculating the cross-sectional area of the annulus (A_{cr}) with Equation (3.27), the velocity of the refrigerant was computed by employing Equation (3.26) and knowing the refrigerant mass flow rate and the single-phase density. After computing the hydraulic diameter using Equation (3.28) and knowing the single-phase refrigerant density, velocity and viscosity, the single-phase refrigerant Reynolds number was computed by employing Equation (3.9).

Knowing the single-phase refrigerant thermodynamic properties, such as the specific heat, viscosity and thermal conductivity, the Prandtl number was computed by using Equation (3.12). Once the Reynolds and Prandtl numbers are computed, the single-phase refrigerant Nusselt number inside a straight concentric tube heat exchanger of similar size was determined with Equation (3.29). The single-phase refrigerant Nusselt number for the coaxial condenser was computed by employing Equation (3.30) with the use of the heat transfer enhancement factor (e_h) and ratio (r_h).

The reason to firstly determine the Nusselt number for a straight concentric tube heat exchanger and the computation method of e_h were discussed in section 3.5.1.2 of this chapter. The heat transfer enhancement ratio (r_h) is equal to the friction enhancement ratio (r_f) as mentioned in section 3.5.1.2. Therefore, r_h was calculated by employing Equation (3.34) after calculating $f_{straight}$ and $f_{helical}$.

The parameter, $f_{straight}$, is defined as the friction factor for straight concentric tube heat exchangers. Here, $f_{straight}$ is a function of the absolute surface roughness (e_r) of titanium, the hydraulic diameter and the single-phase refrigerant Reynolds number. By knowing e_r (Table 3-1) and using the computed hydraulic diameter and single-phase refrigerant Reynolds number, $f_{straight}$ was computed by employing Equation (3.35), a correlation put forth by Swamee & Jain (1976).

The parameter, $f_{helical}$, is known as the friction factor for helical coil heat exchangers. It follows that $f_{helical}$ is a function of the absolute surface roughness (e_r) of titanium,

the hydraulic diameter, the single-phase refrigerant Reynolds number and a helical friction parameter known as d_{coil} which was calculated by employing Equation (3.37). By using all these computed parameters, $f_{helical}$ was computed by employing Equation (3.36), a correlation formulated by Das (1993). Note that a small change in the absolute surface roughness (e_r) value causes a substantial increase or decrease in the enhancement factor values used in both the heat transfer and pressure drop correlations.

The convection heat transfer coefficient of the single-phase refrigerant (h_{SP}) was computed with Equation (3.31) after the computation of the single-phase refrigerant Nusselt number for the coaxial condenser.

3.6.2.2 Two-phase convection heat transfer coefficient

This section will describe the simulation routine to predict the convection heat transfer coefficient of the two-phase refrigerant flowing inside the annulus of the coaxial condenser.

Figure 3-8 illustrates a flow diagram of the simulation routine to compute the two-phase convection heat transfer coefficient of the titanium coaxial condenser discussed in this section.

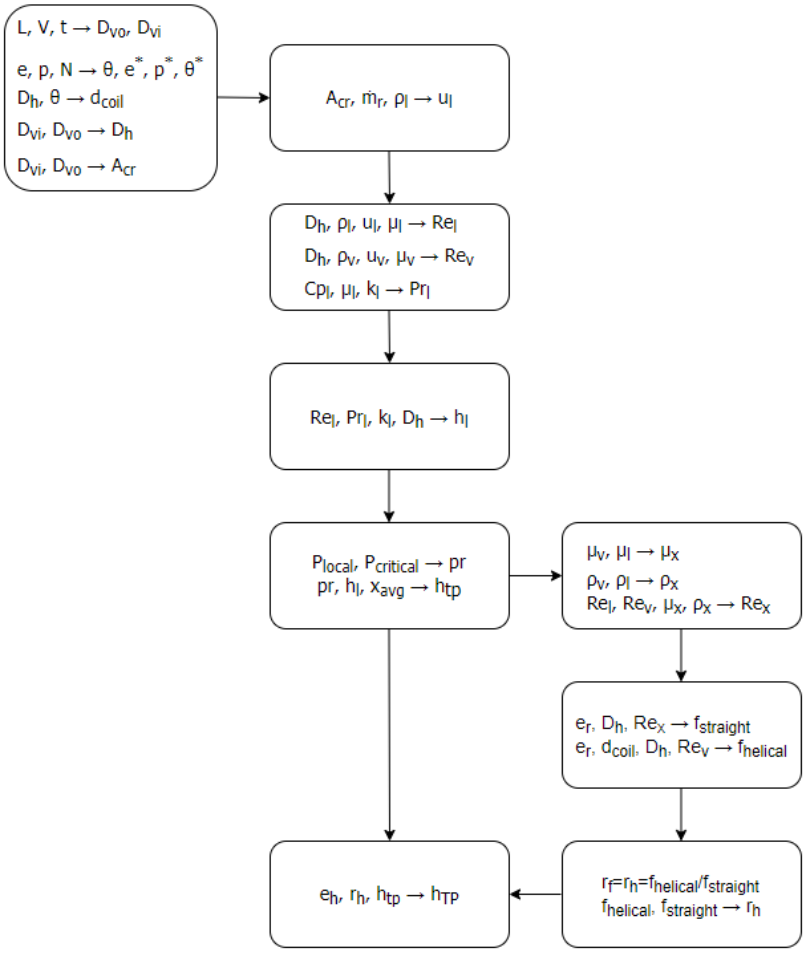

Figure 3-8: Flow chart of the R-407C two-phase convection heat transfer coefficient simulation routine.

As mentioned earlier, there exists a two-phase region in a section of the annulus in the coaxial condenser. This section of the annulus is divided into five, constant quality, increments as seen in Figure 3-5. The two-phase refrigerant convection heat transfer coefficient for a straight concentric tube heat exchanger (h_{tp}) can be calculated by employing Equation (3.41), the technique used by Shah (1979:548).

This technique requires the computation of the convective liquid refrigerant heat transfer coefficient (h_l) and the ratio of the refrigerant local static pressure to the refrigerant critical pressure (pr). These parameters was computed by employing Equation (3.40) and Equation (3.42) respectively. By knowing the average quality of the two-phase refrigerant in the section of the annulus being analysed, the two-phase refrigerant convection heat transfer coefficient for a straight concentric tube

heat exchanger of similar size to the coaxial condenser was computed by employing Equation (3.41).

Equation (3.43) will be employed to convert the two-phase refrigerant convection heat transfer coefficient from the straight concentric tube heat exchanger to the coaxial condenser. This Equation (3.43) includes the use of the heat transfer enhancement factor (e_h) and ratio (r_h). The e_h value remains unchanged in the single- and two-phase convection heat transfer coefficient simulation calculations. However, the r_h value differs from the single- and two-phase simulation calculations.

The determination of r_h in the two-phase region is accomplished by employing Equation (3.34) as used in the single-phase region. However, the computation of $f_{straight}$ and $f_{helical}$ is computed differently for the two-phase region.

The two-phase straight concentric tube friction factor, $f_{straight}$, is a function of e_r, D_h and the two-phase refrigerant Reynolds number (Re_x). Re_x is computed by employing Equation (3.49) after the computation of the two-phase refrigerant viscosity and density ratios by using Equations (3.46) and (3.47) respectively. By applying the computed parameters of e_r, D_h and Re_x the parameter $f_{straight}$ was computed by employing Equation (3.48).

The two-phase helical coil friction factor, $f_{helical}$, is a function of e_r, D_h, the vapour refrigerant Reynolds number (Re_v) and d_{coil}. By applying the mentioned computed parameters, $f_{helical}$ was calculated by employing Equation (3.50).

After the computation of the heat transfer enhancement factor (e_h) and ratio (r_h), the two-phase refrigerant convection heat transfer coefficient for the coaxial condenser (h_{TP}) was computed by employing Equation (3.43).

3.6.3 Coaxial condenser heat transfer simulation

This section discusses the simulation routine to predict the heat transfer of the coaxial condenser.

The total heat transfer of the coaxial condenser was predicted by employing Equation (3.15) which includes the overall heat transfer coefficient (UA) and the log mean temperature difference (LMTD). The UA for the coaxial condenser was computed by employing Equation (3.54) while the LMTD for the counter-flow configuration was determined by using Equation (3.17).

The total heat transfer of the water (q_w) was calculated by using Equation (3.4) by knowing the water mass flow rate and the water inlet and outlet enthalpy of each section of the coaxial tube.

By computing all the refrigerant thermodynamic properties over the length of the annulus for each increment, the refrigerant heat transfer was computed by using Equation (3.4). The refrigerant heat transfer is equal to the heat transfer of the water side which is the same as the total heat transfer of the coaxial condenser indicated by the energy balance equation mentioned earlier.

3.6.4 Water pressure drop simulation

This section describes the simulation routine to predict the total water pressure drop flowing inside the coaxial tube.

The total pressure drop of the water can be computed by employing Equation (3.33), which is a correlation used by Christensen et al. (1993:11). This water pressure drop correlation uses a friction factor as a parameter along with the coaxial condenser length, volume-based inside diameter, water density and velocity.

This friction factor is a function of the water Reynolds number and the non-dimensional geometric parameters namely e^*, p^* and θ^*. By using the computed water Reynolds number from section 3.6.1 and the known non-dimensional geometric parameters, the friction factor was computed by employing either

Equation (3.32 a) or (3.32 b) depending on the magnitude of the water Reynolds number.

By employing Equation (3.33), the total water pressure drop across the coaxial tube was computed by adding an additional parameter to the correlation known as the water friction enhancement factor (e_{f_w}). The computation method of this enhancement factor and the reason for adding this factor to the water pressure drop correlation were discussed in section 3.5.1.3.1.

3.6.5 R-407C pressure drop simulation

3.6.5.1 Single-phase pressure drop

This section describes the simulation routine to predict the single-phase refrigerant pressure drop flowing inside the annulus of the coaxial condenser.

To calculate the single-phase refrigerant pressure drop inside the annulus of the coaxial condenser, the pressure drop must first be determined for a straight concentric tube heat exchanger of similar size as explained earlier. To compute this pressure drop, Equation (3.38) must be used, a correlation used by Christensen et al. (1993:15). In Equation (3.38), the pressure drop is a function of ρ_{R_S}, u_{R_S}, $f_{straight}$, L and D_h. By applying the mentioned computed parameters, the single-phase refrigerant pressure drop for a straight concentric tube heat exchanger ($\Delta P_{straight}$) was calculated by employing Equation (3.38).

By using the computed friction enhancement factor (e_f), the single-phase friction enhancement ratio (r_f) from section 3.6.2.1 and $\Delta P_{straight}$, the single-phase refrigerant pressure drop inside the annulus of the coaxial condenser was computed by employing Equation (3.39). The computation method of e_f was discussed in section 3.5.1.3.2.

3.6.5.2 Two-phase pressure drop

This section describes the simulation routine to predict the two-phase refrigerant pressure drop flowing inside the annulus of the coaxial condenser.

The same approach from the single-phase pressure drop calculation is followed in the computation of the two-phase refrigerant pressure drop. The two-phase refrigerant pressure drop for a straight concentric tube heat exchanger ($\Delta P_{straight}$) is calculated with Equation (3.44), a correlation used by Traviss et al. (1971:13). This correlation indicates that the two-phase pressure drop is subject to the quality of the refrigerant (x) in the section of the annulus being analysed, the refrigerant mass flux (G_{R407C}), Re_v, μ_x, ρ_x, ρ_v and D_h. The refrigerant mass flux was computed by employing Equation (3.53). Using the known refrigerant quality and the computed parameters from the previous sections, $\Delta P_{straight}$ was calculated by employing Equation (3.44).

To convert the two-phase pressure drop from $\Delta P_{straight}$ to ΔP_{TP} (the two-phase pressure drop inside the annulus of the coaxial condenser) requires the implementation of e_f and the two-phase r_f. The two-phase parameter, r_f, was calculated by using Equation (3.34). However, $f_{straight}$ and $f_{helical}$ were computed by employing Equations (3.48) and (3.50) respectively, as discussed in section 3.6.2.2.

By applying the computed parameters of e_f, r_f and $\Delta P_{straight}$ the two-phase pressure drop for the coaxial condenser was computed by employing Equation (3.51).

3.6.5.3 Total refrigerant pressure drop simulation

The total pressure drop of the refrigerant in the annuls of the coaxial condenser, ΔP_r, was computed by simply adding the computed single- and two-phase refrigerant pressure drops together by employing Equation (3.52).

3.7 Uncertainty analysis

An uncertainty analysis will be conducted on the experimental heat transfer of the water obtained in the test set-up (Chapter 4). This uncertainty analysis is based on the method stipulated by JCGM (2018:18-20). The accuracy of all the measuring equipment used in the test set-up will be applied to determine the absolute uncertainty of the experimental water heat transfer.

The experimental heat transfer of the water is calculated with equation (3.4). The experimental measurements used for this calculation is:

- Water mass flow rate ($\dot{m}_w$) [kg/s].
- Inlet water temperature (T_{w_i}) [°C].
- Inlet water pressure (P_{w_i}) [kPa].
- Outlet water temperature (T_{w_o}) [°C].
- Outlet water pressure (P_{w_o}) [kPa].
- Inlet water enthalpy (h_{w_i}) which is a function of the inlet water temperature and pressure: $h_{w_i} = f(T_{w_i}; P_{w_i})$ [J/kg].
- Outlet water enthalpy (h_{w_o}) which is a function of the outlet water temperature and pressure: $h_{w_o} = f(T_{w_o}; P_{w_o})$ [J/kg].

The uncertainty calculation of the experimental heat transfer of the water is as follows:

$$u(q_w) = \sqrt{\left(u(\dot{m}_w).\frac{\partial Q_w}{\partial \dot{m}_w}\right)^2 + \left(u(h_{w_o}).\frac{\partial Q_w}{\partial h_{w_o}}\right)^2 + \left(u(h_{w_i}).\frac{\partial Q_w}{\partial h_{w_i}}\right)^2} \tag{3.55}$$

With the percentage error of the experimental water heat transfer ($W_{w_{error}}$) calculated as:

$$W_{w_{error}} = \left(\frac{u(q_w)}{Q_w} \right) \tag{3.56}$$

3.8 Percentage error

This section will discuss the calculation of the percentage error between an experimental and theoretical data point. In this study, the percentage error between the total experimental and theoretical heat transfers, pressure drops and LMTD needs to be determined. Equation (3.57) is used to determine the percentage error as follows:

$$Error = abs(\frac{(e-t)}{e}) \tag{3.57}$$

where

e = the experimental value.

t = the theoretical value.

3.9 Summary

In this chapter, the theoretical background of a straight concentric and coaxial heat exchanger was explained in detail. The aim of this chapter was to review the complex geometry and applicable heat transfer and pressure drop correlations, found in literature, to formulate a thermal-fluid simulation model of a coaxial heat exchanger. A comprehensive simulation routine, comprising the correlations found in literature, to predict the heat transfer and pressure drop of a refrigerant-to-water titanium coaxial condenser were discussed. An uncertainty analysis and percentage error method between theoretical and experimental data were also described.

The following chapter will describe the test set-up of the titanium coaxial condenser. The test set-up is used to obtain experimental data on the titanium coaxial condenser over a wide variety of operating conditions.

CHAPTER 4

EXPERIMENTAL SET-UP

4.1 Introduction

In the previous chapter, the geometry as well as heat transfer and pressure drop correlations, found in literature, of a concentric tube and coaxial coil heat exchanger was discussed. A simulation routine for a titanium coaxial condenser was formulated using these correlations as well as measured geometry from the coil used in the test set-up.

In this chapter the test set-up of the titanium coaxial condenser will be described along with the measuring equipment of the test set-up. An uncertainty analysis is also conducted followed by the calibration of the measuring equipment. The purpose of the test set-up is to obtain experimental data of the titanium coaxial condenser. This experimental data will be used to verify the simulation model of the titanium coaxial condenser by comparing the experimental data with the simulated results.

4.2 Test set-up layout

A test set-up was constructed by fitting a titanium coaxial condenser into a water heating heat pump of similar capacity as seen in Figures 4-1 and 4-2.

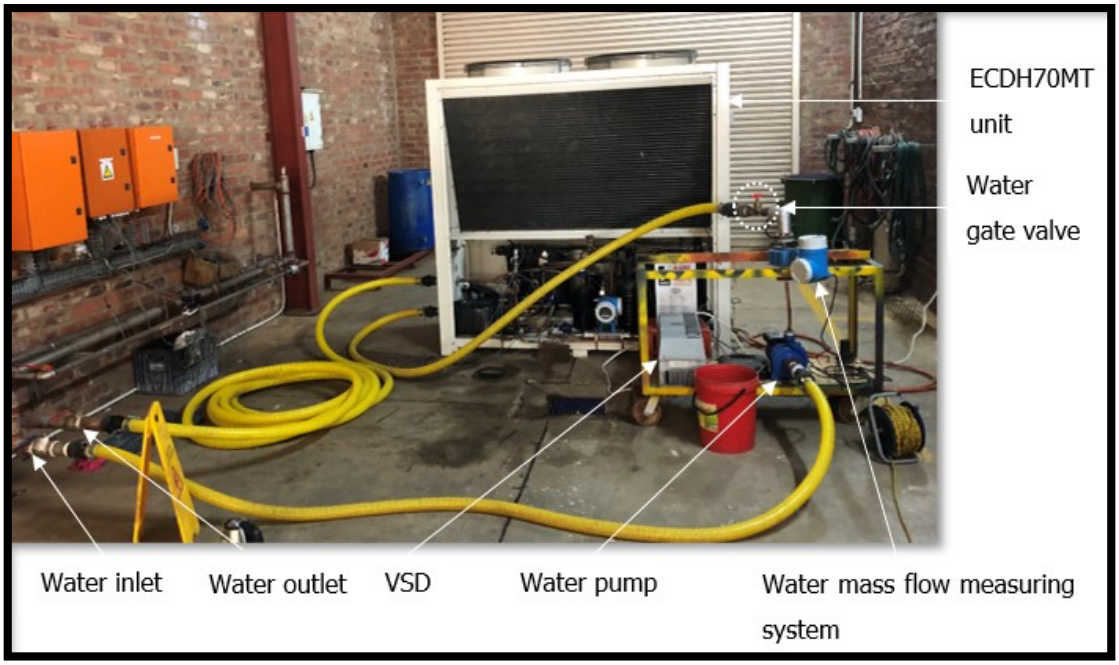

Figure 4-1: Test set-up of the titanium coaxial coil.

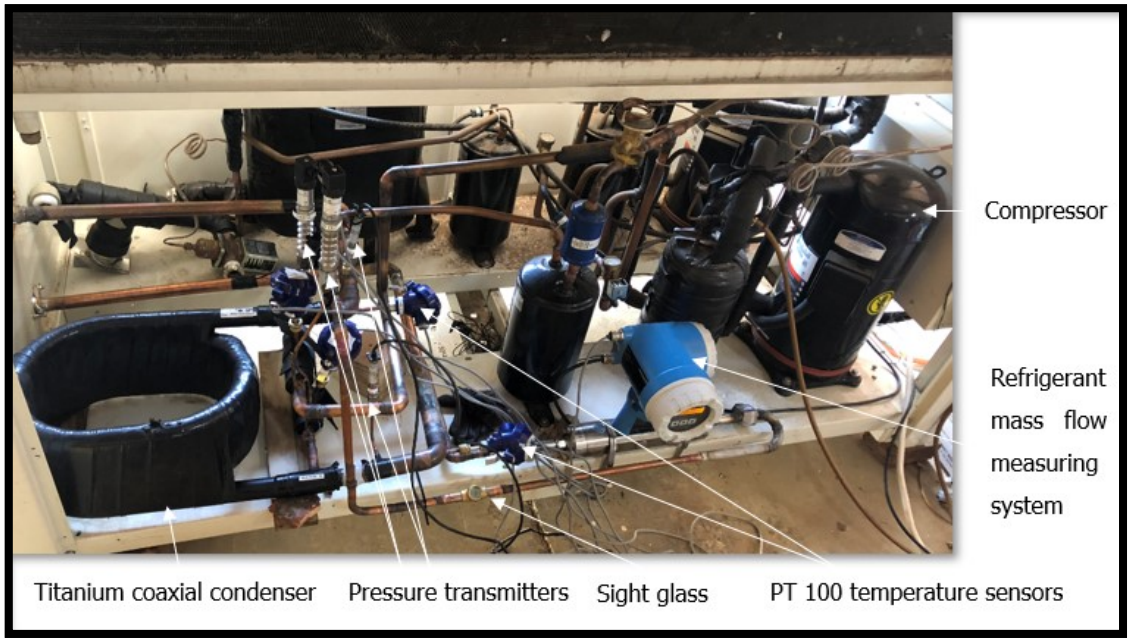

Figure 4-2: Titanium coaxial condenser fitted into a water heating heat pump.

The titanium coaxial coil used for testing is the model ET020ST which is manufactured by Extek (Extek, 2015). The specifications of this coil are summarised in Table 3-1.

According to the manufacturers the coil has a rated capacity of 20 kW at the following conditions:

- Inlet water temperature = 30°C.
- Outlet water temperature = 35°C.
- Condensing temperature = 40°C, with 3°C sub-cooling.
- Refrigerant used = R-410A.

Sub-cool implies that the sub-cooled liquid of the fluid is cooled below the fluid saturation temperature, thus the R-410A sub-cooled liquid is 3°C cooler than the R-410A saturation temperature in the above statement.

The manufactures did not provide extensive performance data of this condensing heat exchanger and conducted the test using the refrigerant, R-410A, opposed to R-407C as used in this study. Thus, the decision was made to construct a test set-up using the titanium coaxial coil in a water heating heat pump as a condenser implementing the refrigerant, R-407C. The test set-up will yield valuable experimental data to be used in this study.

The water heating heat pump used in the test set-up is the ECDH70MT unit provided by M-Tech Industrial. The ECDH70MT unit has two parallel circuits where each circuit consist of a separate vapour compression cycle. The titanium coaxial condenser is installed in the first circuit of the ECDH70MT unit while the compressor of the second circuit is disconnected. Only the first circuit of the ECDH70MT unit will be used for the test set-up.

Each of the two installed compressors (Copeland VR125) of the ECDH70MT unit is rated to deliver 40 kW of heat with the refrigerant, R-407C, evaporating at 10°C and condensing at 50°C. This is much higher than the rated 20 kW heat capacity of the ET020ST condenser coil. To account for this change in capacity, a variable speed drive (VSD) is connected to the compressor to control the heating capacity of the compressor to the desired point.

To obtain the experimental data needed for the heat transfer calculations discussed in Chapter 3, a layout of the test set-up, as illustrated in Figure 4-3, is chosen.

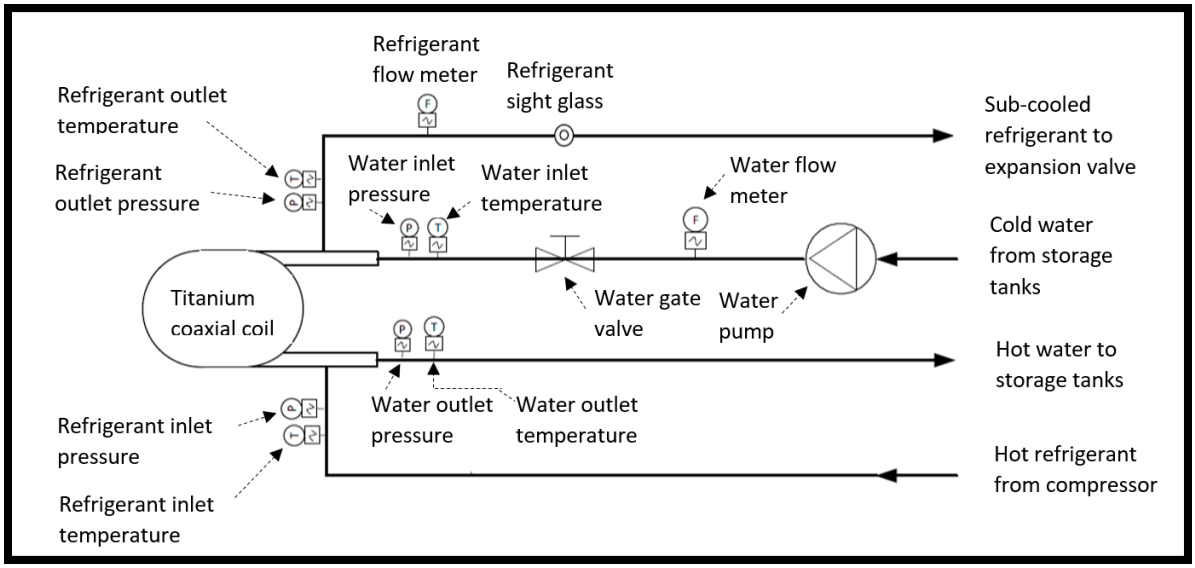

Figure 4-3: Schematic of test set-up layout.

For the water side, a pressure transmitter, temperature sensor and a water flow meter are fitted at the water inlet to the titanium coaxial coil. Another pressure transmitter and temperature sensor are fitted to the water outlet of the coil. The same is done for the refrigerant side. However, the refrigerant flow meter is fitted at the refrigerant outlet of the titanium coaxial coil to only measures the R-407C sub-cooled liquid. Measuring the volume flow rate of a liquid is far more accurate opposed to gauging a gas volume flow rate.

The pressure transmitters and temperature sensors are placed as close as possible to the water and refrigerant inlets and outlets to measure the temperatures and pressures just before entering and after exiting the coaxial coil. This is done to obtain an accurate inlet and outlet value opposed to the measuring devices being installed further away from the inlets and outlets.

4.3 Testing of the titanium coaxial coil

To characterise the titanium coaxial condenser coil, three properties needs to be varied and the performance logged. The three properties are the refrigerant condensing pressure, the compressor power supply frequency which will result in a varied refrigerant flow rate, and the water inlet temperatures. The testing ranges of these properties are described below.

The condensing pressure will be adjusted to and logged in close proximity of 1650, 1882, 2134 and 2408 kPa. The condensing pressure of the refrigerant is chosen as constant variable instead of the condensing temperature, this is due to the temperature glide of the zeotropic refrigerant, R-407C. Thus, the condensing temperature is harder to obtain in the test set-up than the condensing pressure. The above-mentioned condensing pressures comprise temperatures of 45°C, 50°C, 55°C and 60°C respectively at the dew point of the refrigerant.

To obtain the above-mentioned condensing pressures within the system, a water gate valve is installed on the inlet water side between the inlet water temperature sensor and the water flow meter as illustrated on Figure 4-3. The refrigerant condensing pressure is a function of the condenser heat sink's average temperature, i.e. the water flowing through the coaxial coil. To adjust the refrigerant condensing pressure, the water gate vale is either opened or nearly closed to choke the water flow, this will increase or decrease the water temperature throughout the condenser. To obtain a lower refrigerant condensing pressure, the water gate valve needs to be opened to decrease the water temperature through the condenser and vice versa to obtain a high refrigerant condensing pressure.

As per the Copeland VR125 original equipment manufacturer (OEM), the frequency supplied to the compressor can be safely varied between 45 – 60 Hz. Thus, the power supply frequency to the compressor will be set and logged at 45, 50, 55 and 60 Hz. The inlet water temperatures will be controlled in the approximation of 15, 20, 25, 35 and 40°C.

The inlet water is supplied form a 10 000-litre tank which is linked to a pre-cooler. The pre-cooler controls the water temperature of the tank to ensure a constant inlet water temperature is maintained during testing. Prevision was made for the inlet water temperature to fluctuate between ±0.5°C while the test was conducted. The hot outlet water of the ECDH70MT unit is pumped into the top of the same 10 000-litre tank where the pre-cooler cools the water down to the desired inlet water temperature. The test set-up has two existing water pumps installed in the pipelines

of the 10 000-litre tank. A third 1.33 kW water pump is added in the layout, as illustrated in Figure 4-3, to enhance the water flow rate capacity.

The testing of the titanium coaxial coil is done on the following bases as seen in the logical test flow diagram in Figure 4-4. Firstly, the desired water inlet temperature is set at a specified test value. Secondly, the desired power supply frequency is set on the VSD at a specified test value followed by the lowest refrigerant condensing pressure specified above. The lowest refrigerant condensing pressure is chosen as starting point as this will produce the largest water mass flow rate. Once the water inlet temperature and the power supply frequency of the compressor is set at a specified point, all the refrigerant condensing pressure values is tested at the above-mentioned condensing pressure values from the lowest to highest value.

Once all the condensing pressure values are tested and performances logged at the specified inlet water temperature and VSD power supply frequency, the power supply frequency is adjusted to a new value as mentioned above and the test cycle is repeated. After all the condensing pressure values at all the power supply values are tested and performances logged, the water inlet temperature is adjusted to a new testing value and the test cycle is repeated.

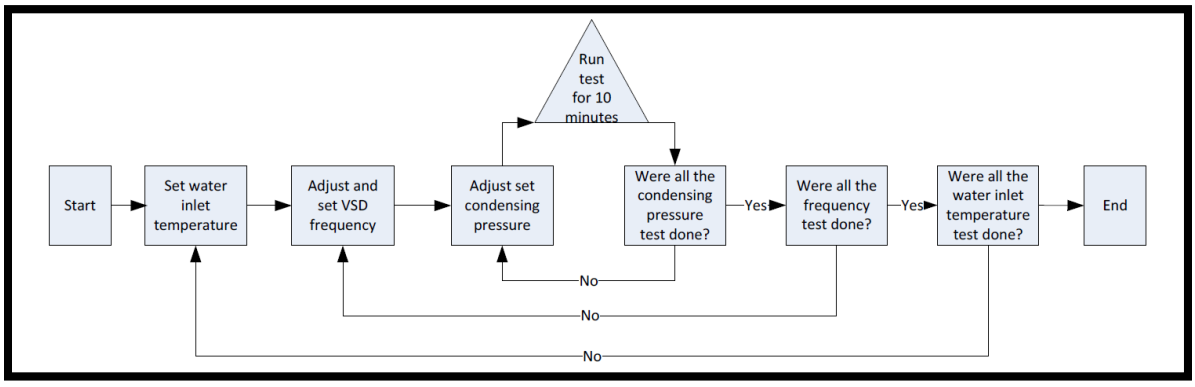

Figure 4-4: Logical test flow diagram.

When the inlet water temperature, power supply frequency and condensing pressure values are set, the ECDH70MT unit is left to operate for ten minutes to allow the heat pump unit to stabilise. Due to the temperature glide of the refrigerant R-407C, the condensing pressure is not entirely stable, thus it is decided that a

specified condensing pressure may stay in a range of ±40 kPa. Once the unit has stabilised and the condensing pressure is within range the test is conducted for ten minutes with the data being logged every 5 seconds.

The test matrixes used in the test set-up is illustrated in Appendix G. Some of the conditions stipulated by the test matrix is not possible to obtain due to a limited achievable water mass flow rate. The three water pumps along with the piping configurations made it possible to obtain a maximum water mass flow rate of 1.324 kg/s.

During testing, the health of the system must be kept in save working ranges. These ranges consist of a maximum refrigerant gas inlet temperature of 90°C, a maximum working pressure of 2800 kPa and at least 4°C of sub-cooling. These ranges may also contribute to unachievable conditions while testing.

4.4 Measurement, control and data acquisition system

The output data of the measuring equipment used as described in the test set-up layout on Figure 4-3 is logged on the Memograph M RSG40, an electronic acquisitioning system manufactured by Endress and Hauser. This section will provide information on the measuring and control equipment as well as the electronic acquisitioning system used in the testing set-up of the titanium coaxial coil.

4.4.1 Measuring equipment

4.4.1.1 Pressure measurement

The four pressure transmitters used in the test set-up are located at the inlet and outlet of both the refrigerant and water sides as seen in Figure 4-3. Two types of pressure transmitters were used to obtain experimental data on the refrigerant and water side. The two pressure transmitters used at the inlet and outlet of the refrigerant side are both WIKA S-10 pressure transmitters as seen on Figure 4-5. The pressure transmitter has a measuring range of 0 – 0.1 to 0 – 1000 bar with a

relative uncertainty of 0.2%. The WIKA S-10 generates an analogue output signal of 4 – 20 mA.

Figure 4-5: WIKA S-10 pressure transmitter (Wika, 2019).

Two Ashcroft K1 pressure transmitters is used at the inlet and outlet of the water side. The Ashcroft K1 pressure transmitter at the inlet of the water side has a measuring range of 150 psig while the measuring range of the transmitter at the outlet side is 100 psig. Both transmitters generates an output voltage of 1 – 5 Vdc and has a relative uncertainty of 1%. The Ashcroft K1 pressure transmitter is illustrated in Figure 4-6.

Figure 4-6: Ashcroft K1 pressure transmitter (Ashcroft, 2014).

4.4.1.2 Temperature measurement

The locations of the four temperature sensors used in the test set-up is illustrated in Figure 4-3. The temperature sensors used in the test set-up is the grade A three-wire PT 100 sensors (Figure 4-7). The sensor is protected inside a die-cast aluminium thermowell probe (NEMA type 4x) and has a measuring range of -50°C to 300°C with an uncertainty of ±[0.15+0.002(t)]°C.

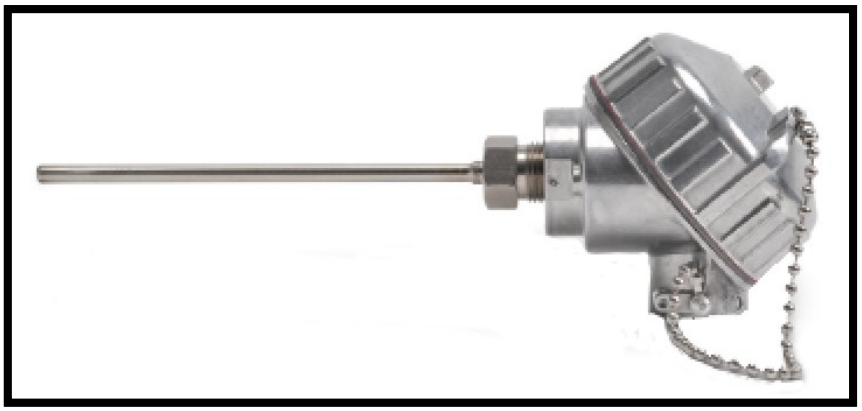

Figure 4-7: Three-wire PT 100 temperature sensor.

4.4.1.3 Mass flow measurement

4.4.1.3.1 Water mass flow

The water mass flow sensor is installed at the inlet water side as illustrated on Figure 4-3. The Coriolis electromagnet flow measuring system from Endress and Hauser is used as the water mass flow measuring system with the Promag 50 transmitter and Promag P sensor as seen on Figure 4-8. The Coriolis electromagnet flow measuring system has an analogue output signal of 0/4 – 20 mA.

The water flows within a pipe through Coriolis electromagnet flow measuring system with a nominal diameter of 15 mm, thus the recommended flow range of this flow measuring system due to the pipe diameter is rated at 0.0667 – 1.667 kg/s. The maximum measured uncertainty is 0.5% of the measured flow.

The recommended flow range of the Coriolis electromagnet flow measuring system (0.0667 – 1.667 kg/s) is ideal for the water mass flow rate of the titanium coaxial condenser experienced during testing. The minimum water flow encountered in the test set-up was 0.164 kg/s with the maximum water flow as 1.324 kg/s.

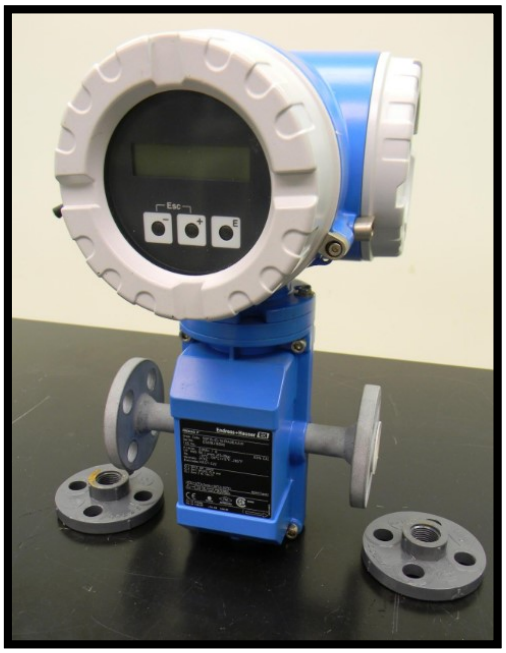

Figure 4-8: Endress and Hauser Promag 50 transmitter with Promag P sensor.

4.4.1.3.2 Refrigerant mass flow

The refrigerant flow meter is installed at the outlet of the refrigerant side as seen on Figure 4-3. The Coriolis mass flow measuring system from Endress and Hauser model Promass 80M is used as the refrigerant mass flow measuring system illustrated in Figure 4-9. The Promass 80M has an analogue output signal of 0/4 – 20 mA.

The refrigerant flows within a pipe in the Coriolis mass flow measuring system with a nominal diameter of 8 mm, thus the recommended flow range for the refrigerant fluid of this flow measuring system due to the pipe diameter is rated at 0 – 0.556 kg/s. The maximum measured error for the refrigerant liquid is $\pm 0.15\% \pm \left[\left(\frac{\text{zero-point stability}}{\text{measured value}}\right).100\right]\%$. The zero-point stability is 0.1 kg/h (2.778×10^{-5} kg/s) at the maximum flow rate of 0.556 kg/s as defined by the Endress and Hauser technical information sheet for an 8mm nominal diameter pipe.

The recommended flow range of the Promass 80M Coriolis mass flow measuring system (0 – 0.556 kg/s) is ideal for the refrigerant mass flow rate of the titanium coaxial condenser experienced during testing. The minimum liquid refrigerant flow encountered during testing was 0.1537 kg/s with a maximum flow of 0.2465 kg/s.

Figure 4-9: Endress and Hauser Promass 80M (Endress and Hauser, 2019).

4.4.2 Control equipment

4.4.2.1 Variable speed drive (VSD)

The VSD or VFD (variable frequency drive) used in the testing set-up is the Danfoss ADAP-KOOL AKD LonWorks drive as illustrated in Figure 4-10. A three-phase supply voltage of 3 x 200-240 V gives an output power range of 0.25 – 45 kW with a supply frequency of 50/60 Hz.

Figure 4-10: Danfoss ADAP-KOOL AKD LonWorks VSD.

4.4.3 Acquisitioning system

4.4.3.1 Memograph M RSG40

The Memograph M RSG40 from Endress and Hauser (Figure 4-11) is used as the data manager and logger of the experimental data from the test set-up. The refrigerant and water mass flow measuring systems along with the four pressure transmitters and temperature sensors are all connected to the Memograph M RSG40. The 4 – 20 mA analogue output signals and 1 – 5 V output voltages generated by the measuring equipment is converted to usable data with the software ReadWin. This measured usable data is stored on the on-board memory of the data logger.

The on-board memory of the data logger is copied to a USB drive and loaded on to a personal computer. The data is received as a CSV file where it is opened in a Microsoft Excel spread sheet to further inspect the experimental data.

The Memograph M RSG40 has a maximum measured error of ±0.1% oMR (of measured reading) for both mass flow measuring systems and the pressure transmitters. The maximum measured error for the temperature sensors are ±0.1% oMR + 0.8 K.

Figure 4-11: Endress and Hauser Memograph M RSG40 (Endress and Hauser, 2019).

4.5 Uncertainty analysis

The uncertainty analysis of the experimental data is based on the method stipulated by JCGM (2018:18-20). An uncertainty analysis was conducted on the experimental heat transfer of the water. All the uncertainties of the measuring equipment (Table 4-1) is used to determine the absolute heat transfer uncertainty of the coaxial condenser. The pressure sensors and mass flow measuring systems were calibrated by the manufacturers and the temperature sensors were calibrated using a temperature bath described in section 4.6. The uncertainty calculations on the experimental heat transfer of the water is illustrated in Appendix D.

Table 4-1: Uncertainty of the measuring equipment.

Device	**Device purpose**	**Uncertainty**
Promag P	Water mass flow measuring system	0.5%
Ashcroft K1 Pressure transmitter	Water pressure transmitter	1%
Three-wire PT 100	Water temperature sensor	±[0.15+0.002(t)] °C

The uncertainty calculation of the experimental water heat transfer is determined with Equations (3.55) and (3.56). A random data point was chosen to illustrate how the calculation was performed. This data point consists of the following properties summarised in Table 4-2:

Table 4-2: Uncertainty analysis data point properties

Variable	**Value**
Frequency	60 Hz
Condensing pressure	1882 kPa
$\dot{m}_w$	0.615 kg/s
T_{w_o}	36.02 °C
T_{w_i}	19.82 °C
P_{w_o}	36.54 kPa
P_{w_i}	55.43 kPa
Q_w	41683 W

Using Equation (3.55), the partial differential equations are calculated separately as follows:

$$\frac{\partial Q_w}{\partial \dot{m}_w} = (h_{w_o} - h_{w_i})$$

$$\frac{\partial Q_w}{\partial h_{w_o}} = \dot{m}_w$$

$$\frac{\partial Q_w}{\partial h_{w_i}} = -\dot{m}_w$$

Inserting the uncertainties of the measuring equipment used on the waterside (Table 4-1) and the calculated partial differential equations into Equation (3.55), the experimental water heat transfer uncertainty was determined as:

$$u(q_w) = \sqrt{\left((0.005).(67750)\right)^2 + \left((0.01616).(0.615)\right)^2 + \left((0.01957).(-0.615)\right)^2}$$

$u(q_w)$ = 338.75 W

Equation (3.56) is used to determine the percentage error as follows:

$$W_{w_{error}} = \left(\frac{338.75}{41683}\right)$$

$W_{w_{error}}$ = 0.813%

The maximum uncertainty of the water heat transfer is 3.05% with an average uncertainty of 1.025%.

Further detail on the uncertainty analysis of the water experimental heat transfer is available in Appendix D.

4.6 Calibration

4.6.1 Three-wire PT 100 sensors

To obtain reliable and accurate experimental temperature data, the four three-wire PT 100 sensors were calibrated with one another in a temperature bath. The four temperature sensors were submerged in an ice bath to obtain the same temperature for each individual sensor as illustrated in Figures 4-12 and 4-13.

Figure 4-12: Four three-wire PT 100 sensors submerged in an ice bath.

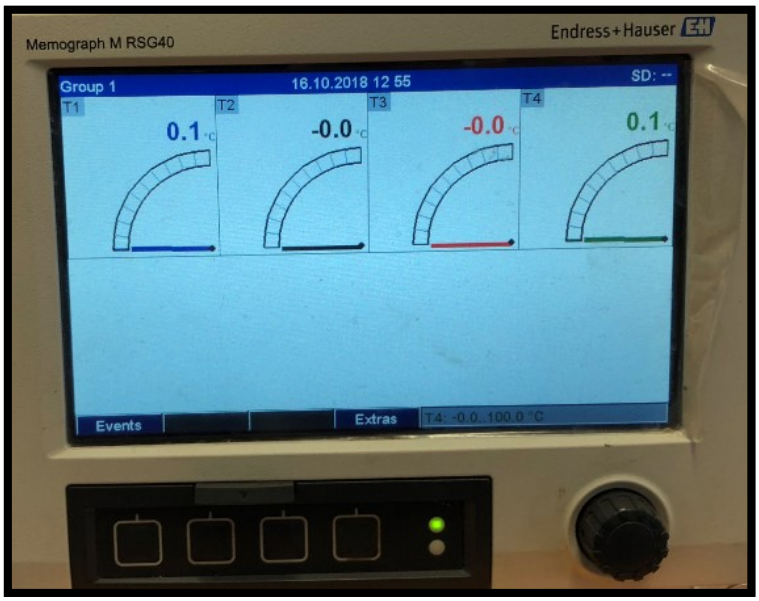

Figure 4-13: Four three-wire PT 100 sensors obtaining the same temperature.

The four temperature sensors were moved to a warm water bath with an initial water temperature of 85°C. While the temperature sensors stayed in the bath, two predetermined temperature stages as well as a random temperature stage were logged as the water cooled. This is done to ensure each temperature sensor reflects the same temperature value than one another at each temperature stage.

The two predetermined temperature stages are 75°C and 50°C with the random temperature stage at 56.7°C. The results of this process are summarised in Table 4-3.

Table 4-3: Three-wire PT 100 sensor calibration

Temperature stage [°C]	**Temperature sensor**	**Value [°C]**
75	T1	75.1
	T2	75.0
	T3	75.0
	T4	75.0
56.7	T1	56.7
	T2	56.7
	T3	56.7
	T4	56.7
50	T1	50.0
	T2	49.9
	T3	50.0
	T4	50.0

As seen from the results in Table 4-3, the temperature sensors reflected the same temperature value as one another at each temperature stage. The experimental

temperature data recorded by the four three-wire PT 100 temperature sensors can be used with certainty.

4.7 Summary

In this chapter the layout of the test set-up along with the testing method of the titanium coaxial condenser were explained. The measuring devices and the acquisitioning system used in the test set-up was also described. An uncertainty analysis was conducted on the resulting experimental data to represent the validity of the data used to characterise the titanium coaxial condenser. The results of the uncertainty analysis yielded an average water heat transfer uncertainty of 1.025%.

The next chapter will discuss and interpret the results produced by the titanium coaxial condenser simulation model.

CHAPTER 5

SIMULATION RESULTS AND VERIFICATION

5.1 Introduction

In the previous chapter, the test set-up and method of testing the titanium coaxial condenser were discussed. The measuring equipment used in the test set-up along with an uncertainty analysis were also analysed.

In this chapter the simulation results and the accuracy thereof will be discussed. The accuracy of the simulation model is determined by comparing the theoretical data to the experimental data and calculating the percentage error between the two values with equation (3.57). The aim of this chapter is to determine if the simulation model produces a true representation of the heat transfer and pressure drop occurring inside the titanium coaxial condenser operating over a wide variety of operating conditions.

5.2 Correlation accuracy

In this section the theoretical results compared to the experimental data will be discussed. The predicted heat transfer, water and refrigerant pressure drop as well as the LMTD from the simulation model are compared to the experimental data. A sample calculation, listed in Appendix B, was made to ensure that the heat transfer and pressure drop correlations were implemented correctly in the simulation model.

Firstly, the results of the simulation model without implementing enhancement factors will be compared to the experimental data. The aim of comparing the theoretical data to the experimental data without the use of enhancement factors is to indicate why enhancement factors are needed in the simulation model.

Secondly, the results of the simulation model implementing the heat transfer and refrigerant pressure drop enhancement factors from Rousseau et al. (2003:237),

found in literature, will be compared to the experimental data. The enhancement factors from Rousseau et al. (2003:237) will be labelled as the Rousseau heat transfer- and pressure drop factor, respectively. The objective here is to test if the Rousseau-factor produces acceptable heat transfer and pressure drop prediction values when implemented in the simulation model.

It is expected that the simulation model implementing the Rousseau-factor will deliver inaccurate heat transfer and pressure drop prediction values. This is anticipated as Rousseau et al. (2003) based their research on a copper coaxial heat exchanger with different geometry parameters than the titanium coaxial condenser used in this study. The authors also implemented the refrigerant, R22, opposed to R-407C.

Finally, due to the expected inaccurate prediction values from implementing the Rousseau-factor in the simulation model, it was concluded that average enhancement factors, calculated from the experimental data obtained from the test set-up, will be assigned to the heat transfer and pressure drop correlations in the simulation model. The theoretical results from the simulation model will be compared to the experimental data to determine the accuracy of the simulation model implementing these average enhancement factors.

The experimental data gathered from the test set-up is displayed in Appendix C – Part 1 along with the theoretical data obtained through the simulation model using the average enhancement factors (Table 5-2) displayed in Appendix C – Part 2.

During the testing phase, the inlet water temperature, supply frequency and the refrigerant condensing pressure were varied as described in Chapter 4. The exact conditions, represented by the test matrixes (Appendix G), were impossible to obtain with the inlet water temperature and refrigerant condensing pressure drifting slightly during the ten-minute testing period for each data point. The resulting data points gathered from the test set-up is labelled under the specific refrigerant condensing pressure they were tested for.

Four groups of experimental data were gathered with each group representing the refrigerant condensing pressure they were tested for. The average condensing pressure for the data points in each group was determined and is labelled as such. The four experimental data groups with their average condensing pressures are as follows:

- Group 1 with an average condensing pressure of 1648.88 kPa ranging between 1618 – 1680 kPa.
- Group 2 with an average condensing pressure of 1882.00 kPa ranging between 1860 – 1897 kPa.
- Group 3 with an average condensing pressure of 2144.31 kPa ranging between 2103 – 2182 kPa.
- Group 4 with an average condensing pressure of 2417.53 kPa ranging between 2392 – 2458 kPa.

The four condensing pressure data groups are displayed on graphs were the theoretical data is compared to the experimental data. The four groups are represented on the graphs as follows:

- Group 1 – Condensing pressure of 1648.88 kPa = Blue dots (●).
- Group 2 – Condensing pressure of 1882.00 kPa = Maroon cubes (■).
- Group 3 – Condensing pressure of 2144.31 kPa = Green diamonds (◆).
- Group 4 – Condensing pressure of 2417.53 kPa = Purple triangles (▲).

5.2.1 Simulation model results: No enhancement factor

The results of the simulation model with no enhancement factor, displayed in the graphs to follow, indicates why an enhancement factor is needed. The enhancement factor accommodates for any differences in the coaxial tube and helical coil annulus as well as original assumptions made in the friction-heat transfer analogy (Rousseau et al. 2003).

5.2.1.1 Heat transfer results

No heat transfer enhancement factor is used in the heat transfer correlation of the simulation model and the results are displayed in Figure 5-1. The average percentage error between the experimental data and simulated results are 5.23% with a maximum percentage error of 20.02%.

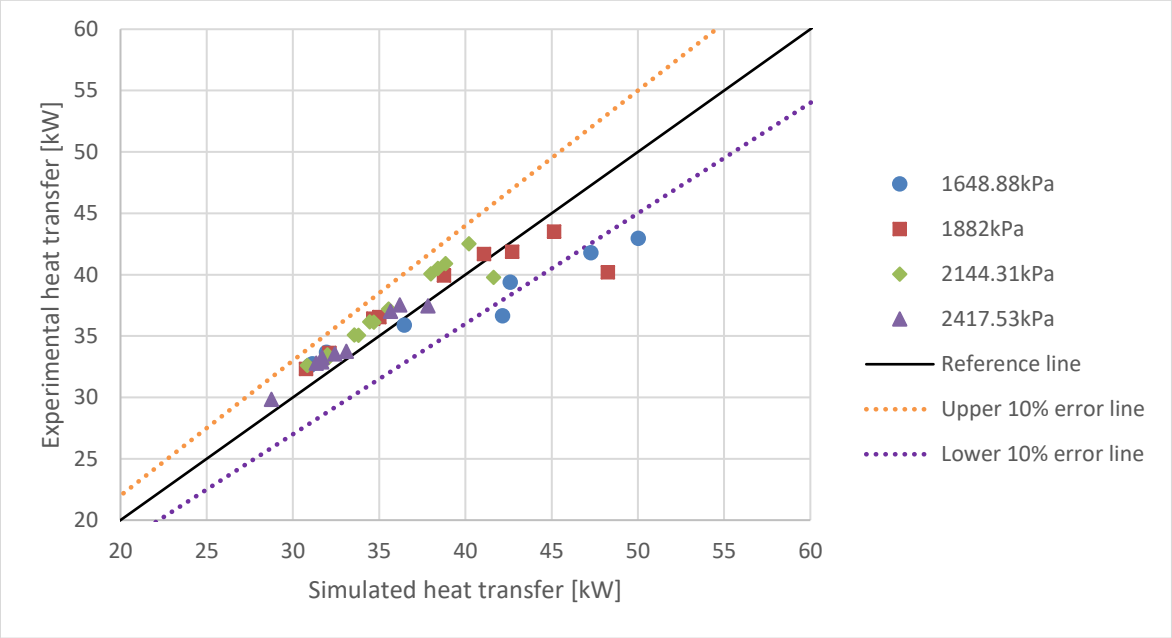

Figure 5-1: Heat transfer simulation with no enhancement factor.

In general, it can be seen on Figure 5-1 that 8.51% of the simulation results are outside a 10% error from the experimental values. The simulation model, with no enhancement factor, under predicts the data points in groups 3 to 4 and over predicts the data points in group 1.

5.2.1.2 Pressure drop results

5.2.1.2.1 Water pressure drop

No water friction enhancement factor was used to predict the water pressure drop. The average percentage error between the experimental values and the simulation values are 19.54% with a maximum percentage error of 75.54%. The comparison between the experimental and simulation values are seen on Figure 5-2.

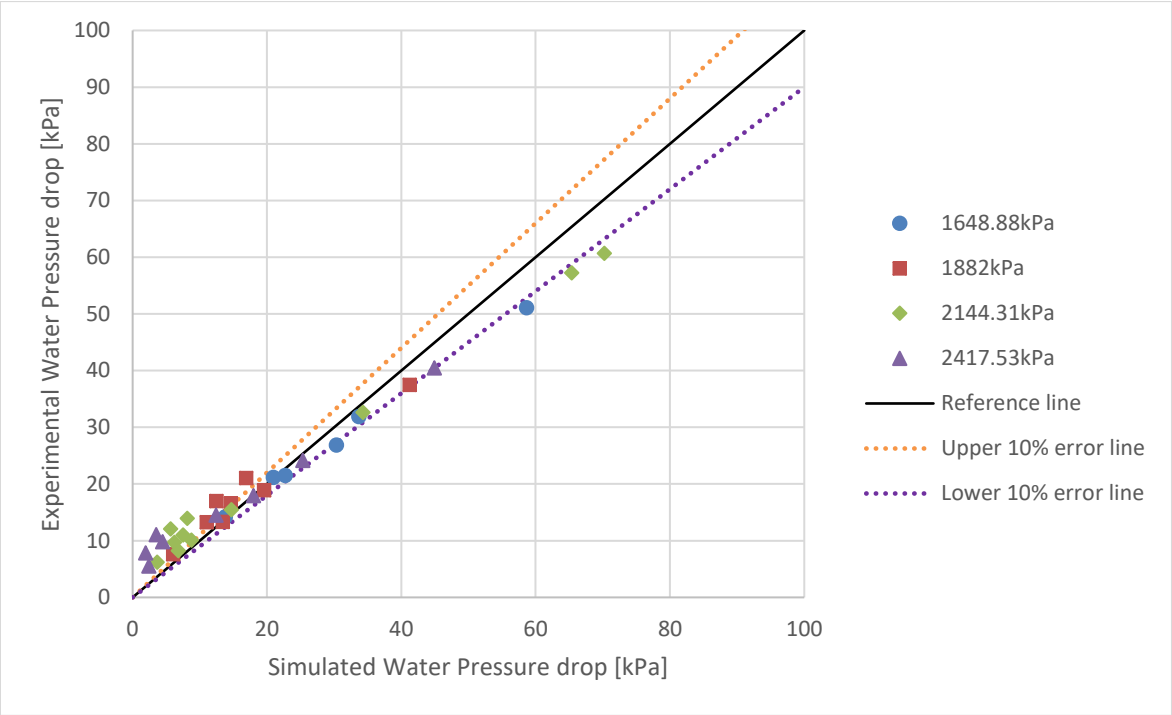

Figure 5-2: Water pressure drop simulation with no enhancement factor.

From the results seen in Figure 5-2, 25.53% of the simulated values are within a 10% error from the experimental water pressure drop values using no water friction enhancement factor. The simulation model initially under predicts the water pressure drop at small pressure drop values but increasingly over predicts the water pressure drop values as the pressure drop increases.

5.2.1.2.2 R-407C pressure drop

No refrigerant pressure drop enhancement factor was used to predict the R-407C pressure drop. The average percentage error between the experimental values and the simulation values are 90.42% with a maximum percentage error of 93.39%. The comparison between the experimental and simulation values are seen on Figure 5-3.

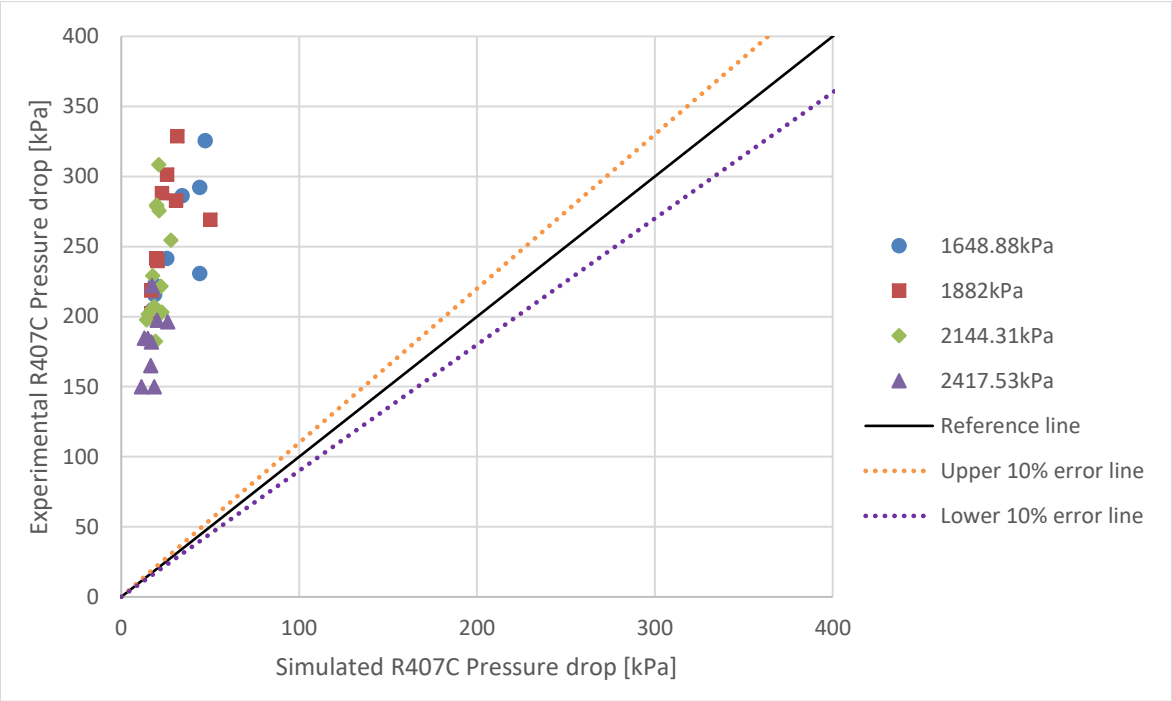

Figure 5-3: R-407C pressure drop simulation with no enhancement factor.

From the results seen on Figure 5-3, no simulated values are within a 10% error from the experimental values. This under predicting behaviour could be due to the simulation model using no enhancement factor. Thus, no differences between helical coil and coaxial tube heat exchangers are introduced in the simulation model causing a smaller pressure drop to be simulated.

5.2.1.3 LMTD results

No enhancement factor was used in the simulation model to predict the LMTD values of the titanium coaxial condenser. Figure 5-4 illustrates the results with the average percentage error of 11.57% between the experimental and simulation values. The maximum percentage error is 18.93%.

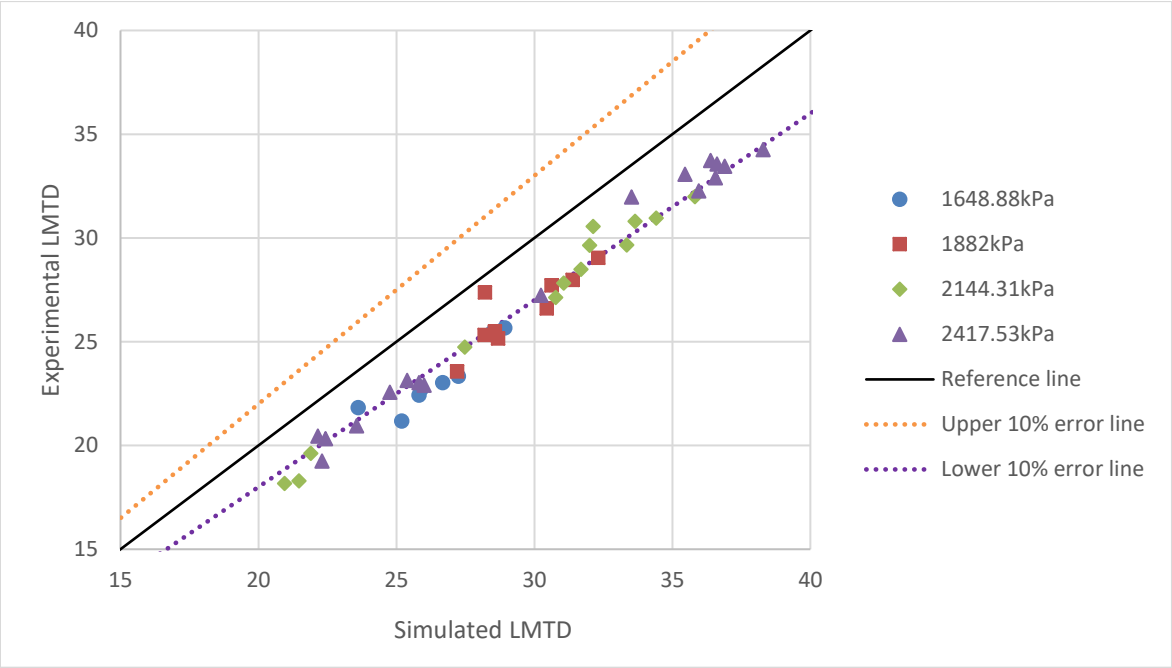

Figure 5-4: LMTD simulation with no enhancement factor.

The results show that 25.53% of the simulated results are within a 10% error from the experimental values.

5.2.2 Simulation model results: Rousseau-factor

The results of the simulation model while implementing the Rousseau-factor in the heat transfer and pressure drop correlations are displayed in this section. A comprehensive list of the percentage error between the experimental and theoretical data for each data point, with the Rousseau-factor used in the simulation model, is displayed in Appendix F – Part 1.

Note that Rousseau et al. (2003) did not study the water pressure drop of a coaxial heat exchanger, thus the authers did not include a water friction enhancement factor to be added to the water pressure drop correlation. The water pressure drop results are not included in this section.

The Rousseau heat transfer and pressure drop factors are summarised in Table 5-1.

Table 5-1: Rousseau-factors

Rousseau heat transfer factor ($e_{h,Rousseau}$)	Rousseau pressure drop factor ($e_{f,Rousseau}$)
0.867	4.409

5.2.2.1 Heat transfer results

The Rousseau heat transfer factor is used in the heat transfer correlation of the simulation model and the results are displayed in Figure 5-5. The average percentage error between the experimental data and simulated results are 8.32% with a maximum percentage error of 22.18%.

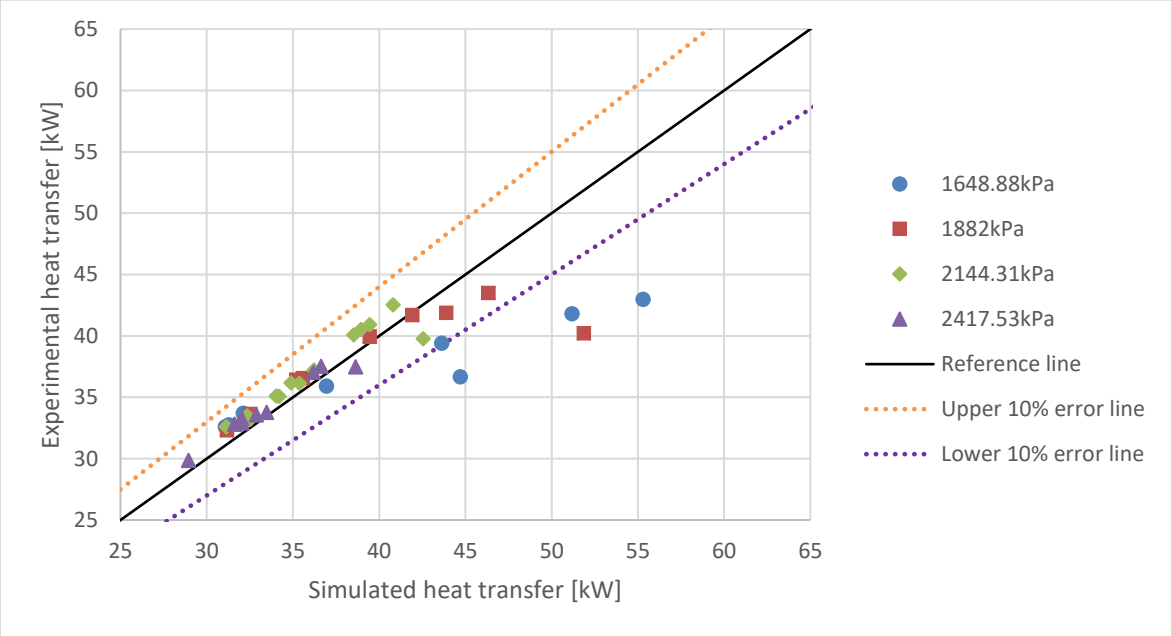

Figure 5-5: Heat transfer simulation with Rousseau-factor.

The results from Figure 5-5 indicates that the simulation model generally under predicts the total heat transfer of the coaxial condenser.

5.2.2.2 Pressure drop results

5.2.2.2.1 R-407C pressure drop

The Rousseau pressure drop factor was used to predict the R-407C pressure drop. The average percentage error between the experimental values and the simulation values are 52.87% with a maximum percentage error of 79.23%. The comparison between the experimental and simulation values are seen on Figure 5-6.

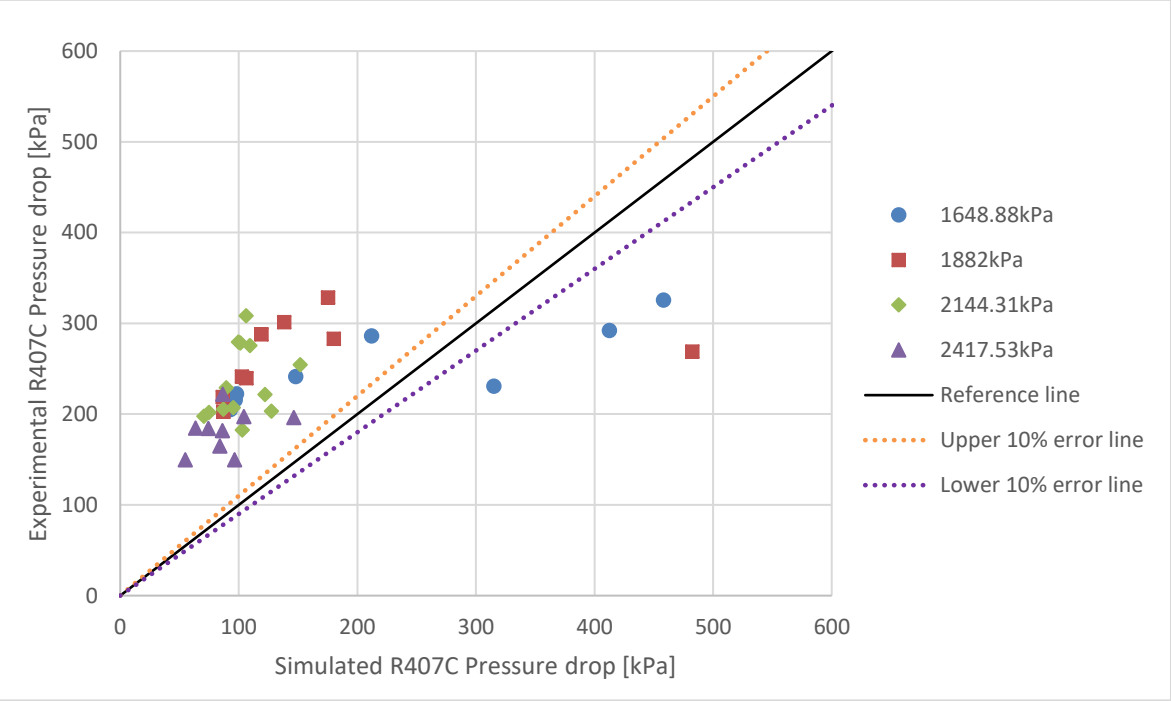

Figure 5-6: R-407C pressure drop simulation with Rousseau-factor.

From the results seen on Figure 5-6, the simulation model with the implementation of the Rousseau pressure drop factor generally under predicts the refrigerant pressure drop.

5.2.2.3 LMTD results

The Rousseau heat transfer factor was used in the simulation model to predict the LMTD values of the titanium coaxial condenser. Figure 5-7 illustrates the results with the average percentage error of 8.32% between the experimental and simulation values. The maximum percentage error was computed as 22.18%.

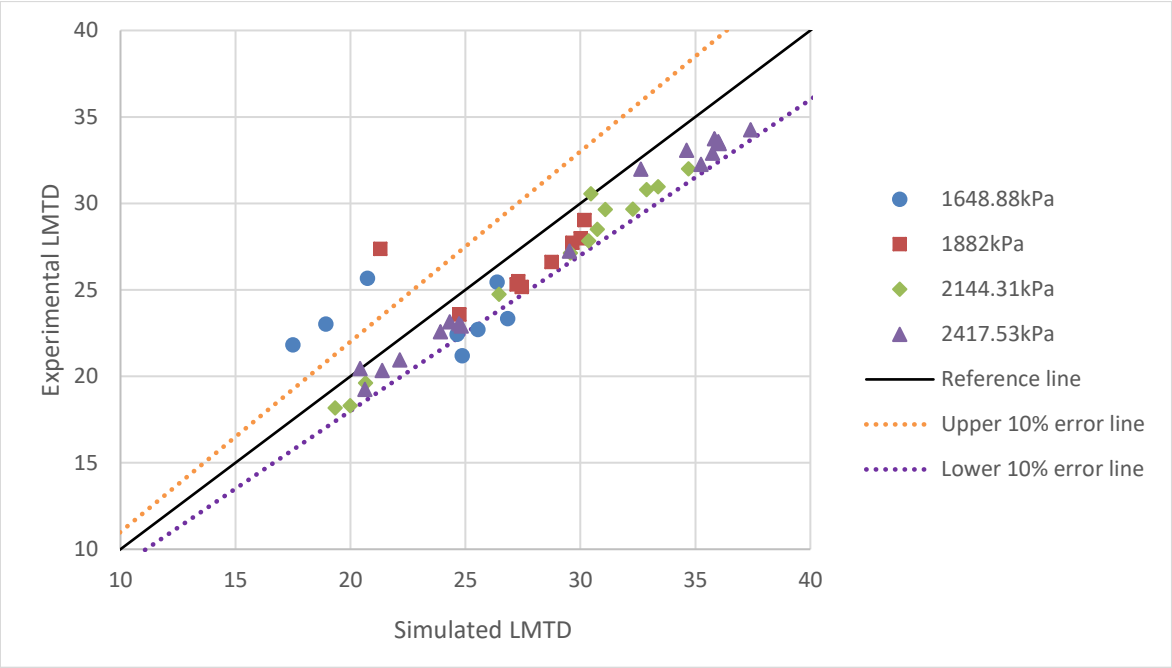

Figure 5-7: LMTD simulation with Rousseau-factor.

Figure 5-7 illustrates that the simulation model with the Rousseau-factor generally over predicts the simulated LMTD values when compared to the experimental values.

5.2.3 Simulation model results: Average enhancement factor

A routine was formulated and linked to the simulation model where it was used to obtain three values resulting in the best fit between the simulated and experimental heat transfer and pressure drop, respectively. These three values are known as the heat transfer-, friction-, and water friction enhancement factors.

The computed average enhancement factors are summarised in Table 5-2 along with the average sub-cool value used in the simulation model. The average sub-cool was computed by employing the same method as used for the computation of the average enhancement factors.

Table 5-2: Average enhancement factors.

Heat transfer enhancement factor (e_h)	R-407C friction enhancement factor (e_f)	Water friction enhancement factor (e_{f_w})	Sub-cool [°C]
0.5288	5.1534	1.2711	2.3243

These average enhancement factors were used to predict the heat transfer, water and refrigerant pressure drops as well as the LMTD values. The results of the percentage error between the experimental and theoretical data, with the implementation of the average enhancement factors (Table 5-2) in the simulation model, are displayed in Appendix F – Part 2.

5.2.3.1 Heat transfer results

The average heat transfer enhancement factor of $e_h = 0.5288$ (Table 5-2) was used in the simulation model to predict the heat transfer of the titanium coaxial condenser. An average percentage error of 5.79% between the experimental and simulation values was determined. The maximum percentage error was determined as 42.88%. To put this in perspective, the titanium coaxial condenser was on average in the region of 5.79% either too large or too small. The results are displayed in Figure 5-8.

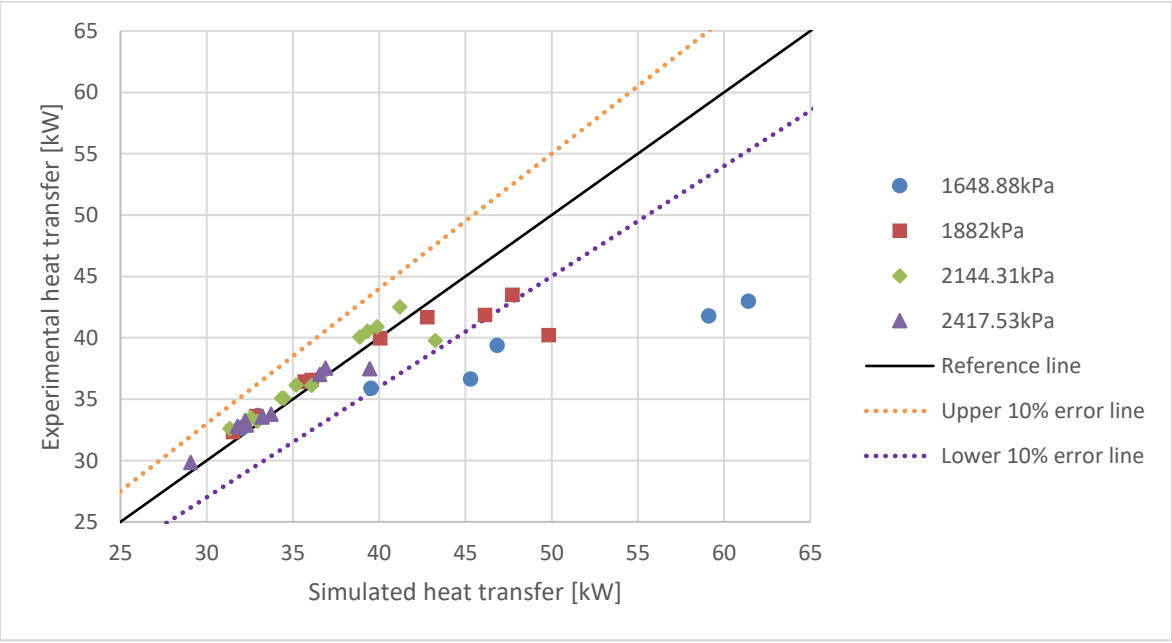

Figure 5-8: Heat transfer simulation with average enhancement factor, e_h = 0.5288.

Figure 5-8 indicates that 85.11% of the simulated data are within a 10% error from the experimental data..

5.2.3.2 Pressure drop results

5.2.3.2.1 Water pressure drop

The water pressure drop was predicted using the average water friction enhancement factor of $e_{f_w} = 1.2711$ (Table 5-2) in the simulation model. An average percentage error of 28.29% was obtained between the experimental and simulated values. The maximum percentage error was determined as 68.92%. The results is illustrated in Figure 5-9.

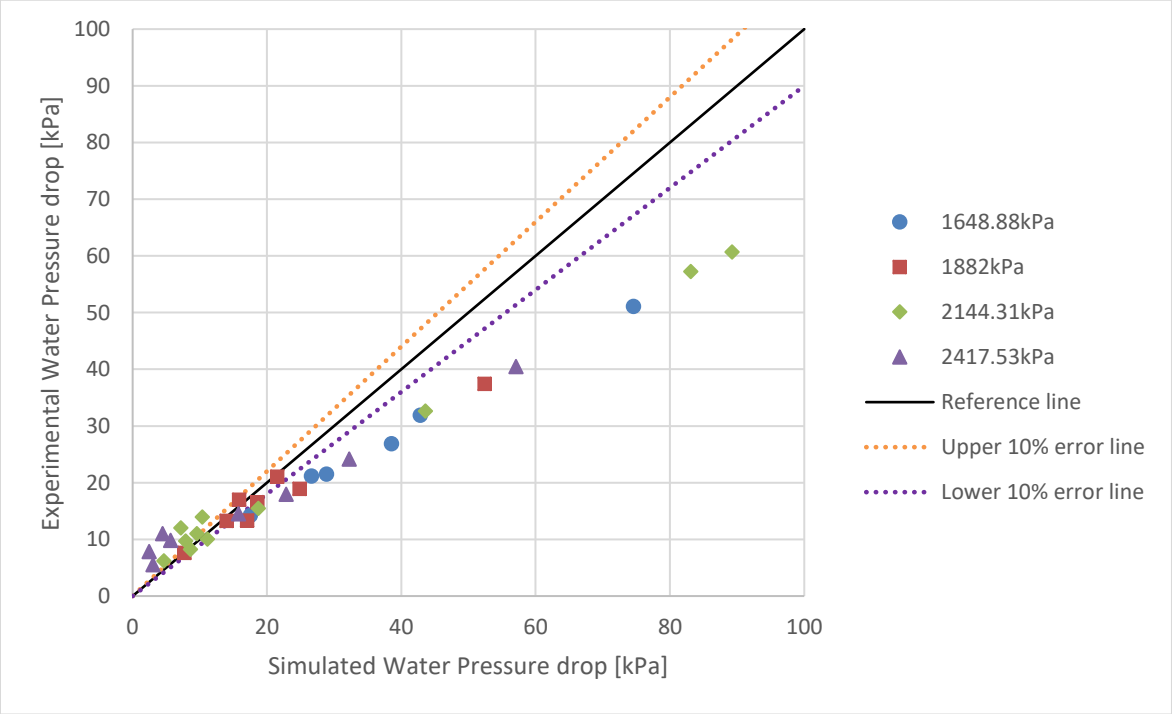

Figure 5-9: Water pressure drop simulation with average enhancement factor, $e_{f,w}$ = 1.2711.

Only 12.77% of the simulated values are within a 10% error of the experimental values. The average enhancement factor causes the simulation model to under predict for low water pressure drop values and progressively over predicts the simulated values as the water pressure increases. The results from Figure 5-9 suggests that the average water friction enhancement factor is ineffective and

cannot be used in the simulation water pressure drop correlation. An alternative solution to the water pressure drop prediction will be discussed later in this chapter.

5.2.3.2.2 R-407C pressure drop

The average friction enhancement factor of $e_f = 5.1534$ (Table 5-2) was used to predict the refrigerant pressure drop. The average percentage error between the experimental and simulated values are 32.62% with the maximum percentage error of 55.92%. Figure 5-6 displays the results.

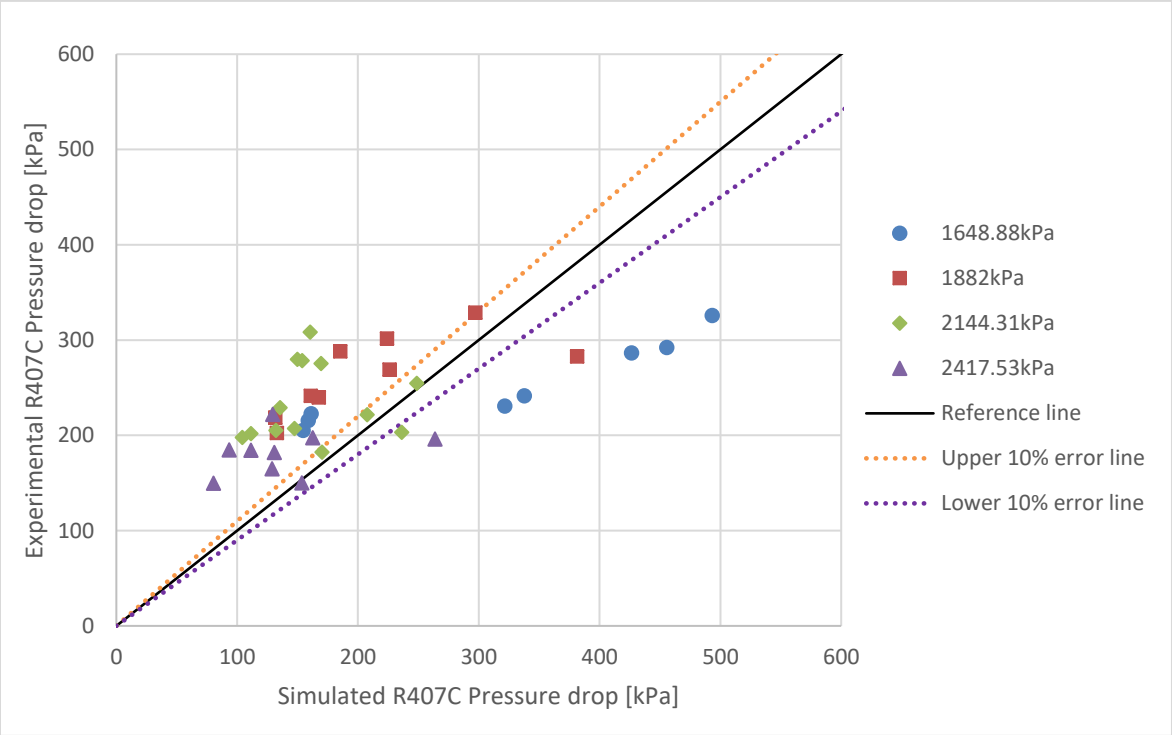

Figure 5-10: R-407C pressure drop simulation with average enhancement factor, e_f = 5.1534.

A total of 12.77% of the simulated values are within a 10% error of the experimental values. The simulation model with the average friction enhancement factor generally under predicts the pressure drop while only 19.15% of the data points are over predicted.

5.2.3.3 LMTD results

The LMTD was predicted with the simulation model using the average heat transfer enhancement factor of $e_h = 0.5288$ (Table 5-2). An average percentage error

between the experimental and simulated values were determined as 6.83%. The maximum percentage error was determined as 37.45%. Figure 5-11 illustrates the results.

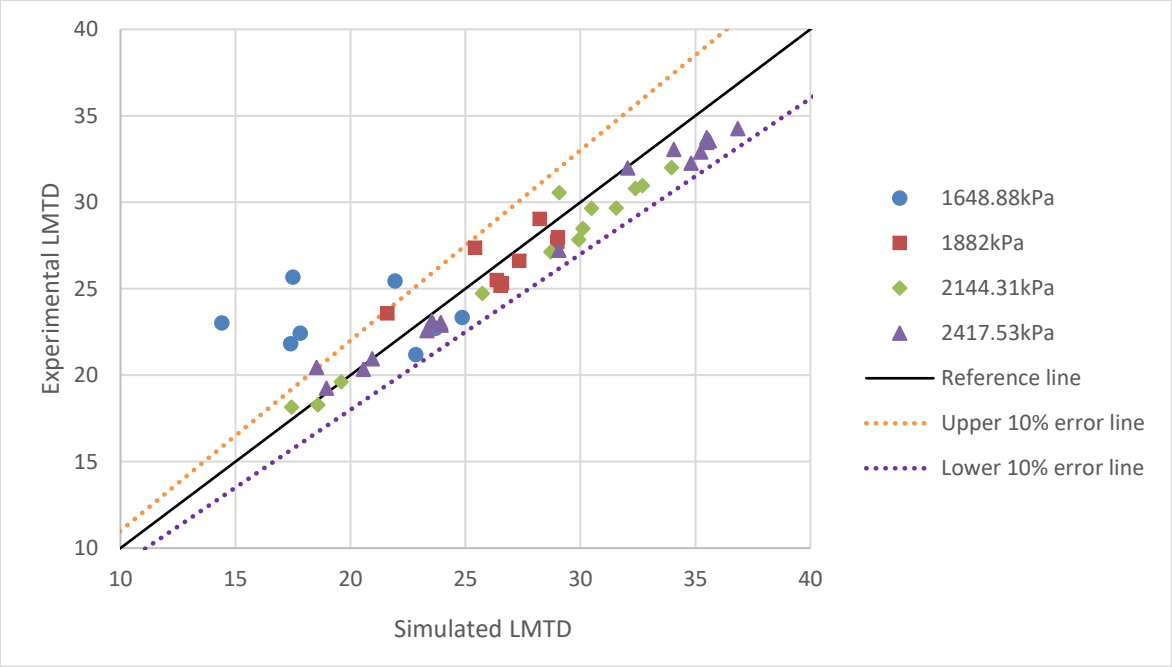

Figure 5-11: LMTD simulation with average enhancement factor, e_h = 0.5288.

Figure 5-11 shows that 89.36% of the simulated values are within a 10% error of the experimental values.

5.2.4 Prediction of the water pressure drop

Figure 5-2 indicates that the simulation model over predicts the water pressure drop as the water mass flow rate increases when no water friction enhancement factor is used. In Figure 5-9, the simulation model over predicts the water pressure drop even further when the average water friction enhancement factor is used. In both Figures 5-2 and 5-9, the average slope of the data is increased from using no water friction enhancement to using the average water friction enhancement factor.

To correct the water pressure drop prediction, the trendline of each data group in Figure 5-2 was used to determine an average trendline equation for the water pressure drop data with no enhancement factor. A trendline is an equation that describes the relationship between two variables, in this case the trendline equation

describes the experimental water pressure drop in relation with the simulation water pressure drop. The trendline equation is used for the water pressure drop to correct the average slope of the data to better fit the reference line as seen on Figure 5-13. Figure 5-12 displays the trendline of each data group from Figure 5-2.

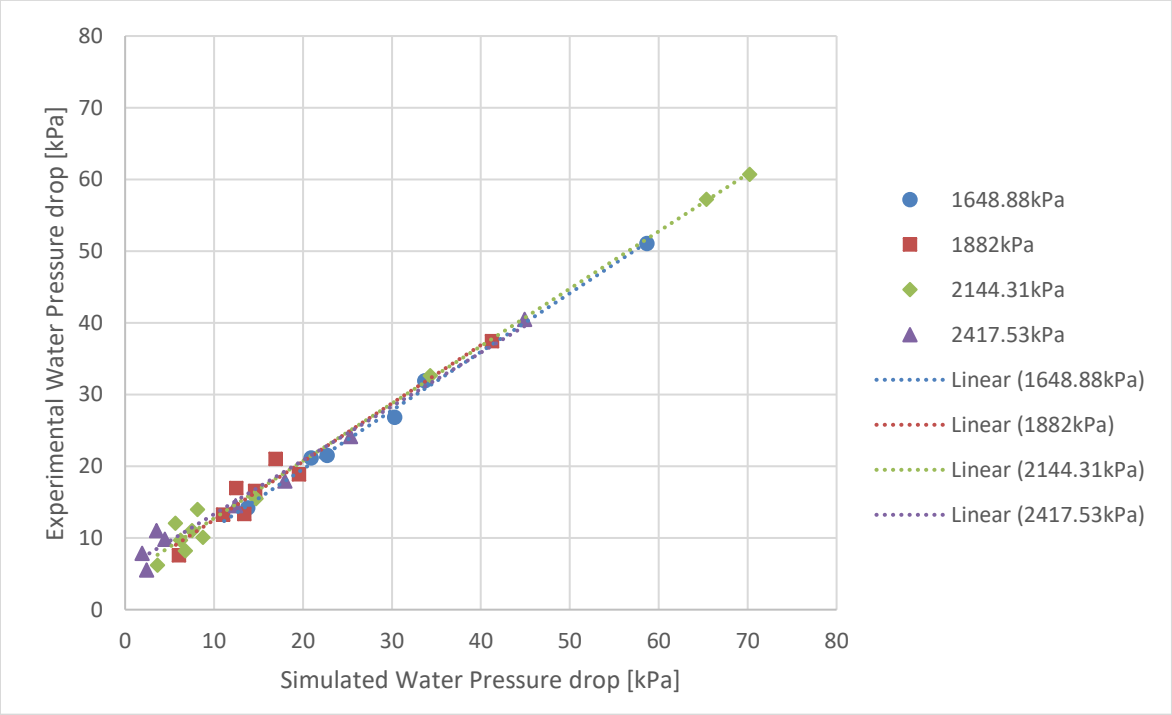

Figure 5-12: Water pressure drop trendlines with no enhancement factor.

The trendline equations for each data group are as follows:

- Group 1 trendline equation: $y = 0.8175x + 3.25$.
- Group 2 trendline equation: $y = 0.812x + 4.4131$.
- Group 3 trendline equation: $y = 0.8004x + 4.7337$.
- Group 4 trendline equation: $y = 0.7512x + 5.8062$.

The average trendline for the four data groups are as follows:

$$y = 0.7953x + 4.55$$

The water pressure drop correlation is adjusted with the average trendline as follows:

$$\Delta P_{Trendline} = 0.7953(\Delta P_w) + 4.55 \quad (6.1)$$

With the water pressure drop (ΔP_w) calculated with Equation (3.33). The water pressure drop correlation with the average trendline, Equation (6.1), is implemented into the simulation model and used to compute new simulated water pressure drop values. The average percentage error between the experimental and simulated water pressure drop values are 8.41% with a maximum percentage error of 34.11%. Figure 5-13 illustrates the results.

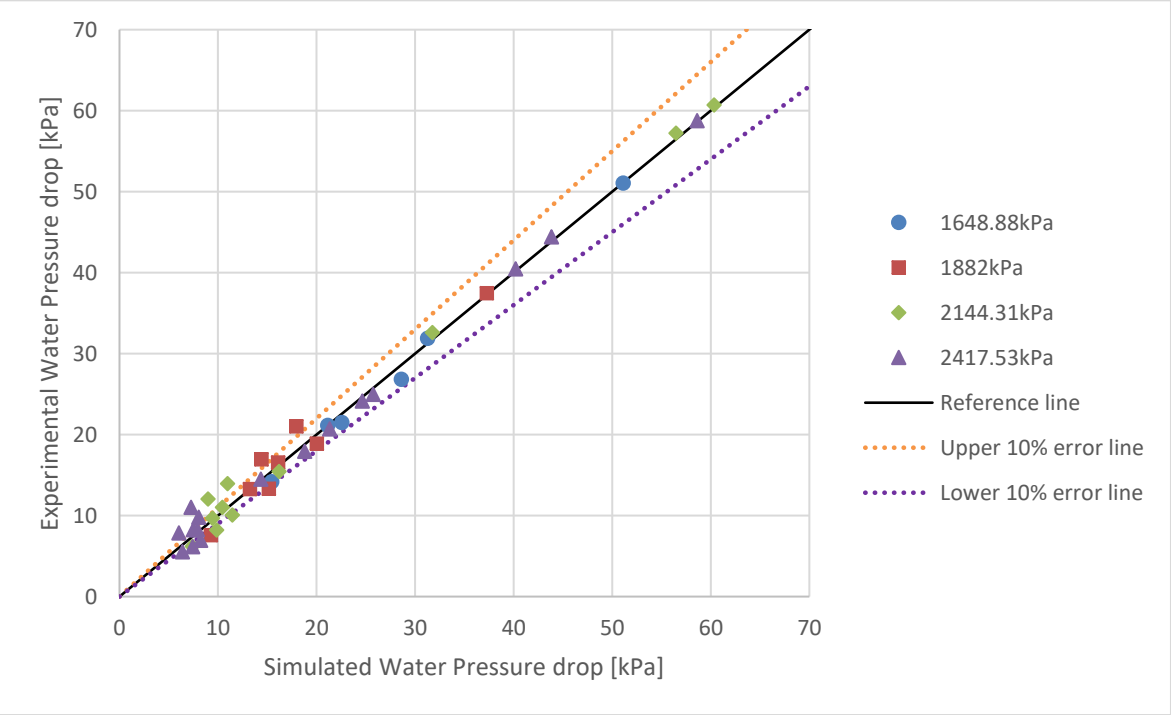

Figure 5-13: Water pressure drop with trendline equation.

Figure 5-13 shows that 55.32% of the simulated values are within a 10% error of the experimental results. Enhancing the average slope of the water pressure drop data resulted in a decrease in the average percentage error between the experimental and simulated water pressure drop values compared to implementing an average water friction enhancement factor.

5.3 Results summary

All the results of the simulation model implementing the Rousseau-factor, average enhancement and new average enhancement factors are summarised in Table 5-3.

Table 5-3: Summary of simulation model results.

Enhancement category	**Heat transfer**		**Water pressure drop**		**R-407C pressure drop**		**LMTD**	
	Avg. error [%]	Max error [%]	Avg. error [%]	Max error [%]	Avg. error [%]	Max error [%]	Avg. error [%]	Max error [%]
No enhancement	5.23	20.02	19.54	75.54	90.42	93.39	11.57	18.93
Rousseau-factor	5.36	29.0	-	-	52.87	79.23	8.32	22.18
Average enhancement	5.79	42.88	28.29	68.92	32.62	52.92	6.83	37.45

The simulation model using the average enhancement factors yielded an overall smaller average percentage error between the theoretical and experimental data for the refrigerant pressure drop and LMTD value compared to the simulation model results implementing the Rousseau-factor.

The prediction of the water pressure drop with an average water friction enhancement factor was ineffective. The simulation model produced a smaller average percentage error between the theoretical and simulation data for the water pressure drop when applying the average trendline of the experimental and simulation comparison plot (Figure 5-12) into the water pressure drop correlation. This resulted in an average difference between the experimental and theoretical water pressure drop of 8.41% compared to the 28.29% average percentage error when using the average water friction enhancement factor ($e_{f_w} = 1.2711$) in the simulation model.

5.4 Summary

In this chapter, the results of the coaxial condenser simulation model implementing different enhancement factors were explored and interpreted. In the next chapter, the conclusion as well as recommendations for further research concerning this study will be discussed.

CHAPTER 6

CONCLUSION AND RECOMMENDATIONS

6.1 Introduction

In the previous chapter, the simulation model results were discussed with the simulation model implementing no, Rousseau-factor and average enhancement factors.

In this chapter, the summary of the study with the conclusion of the simulation results (Chapter 5) will be discussed. Recommendations for further work on this study will also be mentioned following the conclusion.

6.2 Summary of study

Chapter 1 focused on a mobile refrigeration plant, specifically the ACU MKII, with a stainless-steel tube-in-tube condenser pack heat exchanger currently installed in the unit. The rapid corrosion of this stainless-steel condenser pack heat exchanger due to inadequate mine supply water used as heat sink made the titanium coaxial coil a suitable replacement candidate. The titanium coaxial coil was developed in recent times which means no extensive performance data exists for the heat exchanger. A thermal-fluid simulation model of the titanium coaxial coil heat exchanger needed to be developed to accurately predict the heat transfer and pressure drop of the coil used as a condenser.

Chapter 2 consists of an extensive literature review on pervious work conducted on passive heat exchangers and coaxial coils. The focus of the literature review was on finding correlations and existing simulation models to predict the heat transfer and pressure drop for coaxial coil heat exchangers. The simulation model developed by Rousseau et al. (2003:232) proved to be an adequate model to accurately predict the heat transfer and pressure drop characteristics of a coaxial coil.

Chapter 3 discussed the basic theory as well as correlations used to determine the heat transfer and pressure drop of heat exchangers, particularly for a coaxial coil heat exchanger. This chapter also discussed a simulation routine, implementing correlations found in literature, to accurately predict the heat transfer and pressure drop of a titanium coaxial condenser. A method to determine the uncertainty of the experimental heat transfer and pressure drop as well as the percentage error between theoretical and experimental data was discussed.

Chapter 4 consists of the test set-up layout and the testing method of the titanium coaxial condenser. The measuring equipment used in the test set-up was discussed with an uncertainty analysis conducted on the experimental data. The focus of Chapter 4 was to obtain experimental data on the titanium coaxial condenser operating over a wide range of conditions. The experimental data was used to determine average enhancement factors for the titanium coaxial condenser as well as to verify and test the applicability of the correlations used in the simulation model.

Chapter 5 consists of the results of the simulation model implementing no enhancement factors, the Rousseau-factor, and average enhancement factors. The average water friction enhancement factor was found to be ineffective in predicting the water pressure drop over the coaxial coil. A water trendline equation was implemented and delivered acceptable simulation results. The results of the simulation model implementing the above-mentioned enhancement factors along with the water trendline equation were discussed.

6.3 Conclusion

In Chapter 5 the experimental data (Appendix C – Part 1) were used to obtain individual enhancement factors (Appendix E). Average enhancement factors (Table 5-2) were derived from these individual enhancement factors. The average enhancement factors were used in the heat transfer and pressure drop correlations of the titanium coaxial condenser simulation model.

The results of the simulation model implementing these average enhancement factors were compared to the experimental data for the heat transfer, water and

refrigerant pressure drop as well as the LMTD values. The average percentage error between the experimental and theoretical values for the heat transfer were 5.79% with a maximum error of 42.88%.

The prediction of the water pressure drop proved to be ineffective when a water friction enhancement factor was used in the simulation model. The simulation model produced a smaller average percentage error between the experimental and theoretical data for the water pressure drop when applying the average trendline of the experimental and simulation comparison plot (Figure 5-12) into the water pressure drop correlation. The average difference between the experimental and theoretical water pressure drop with the average trendline in the water pressure drop correlation are 8.41% with a maximum error of 34.11%.

The refrigerant pressure drop displayed an average difference between the experimental and theoretical refrigerant pressure drop of 32.62% with a maximum difference of 55.92%. The LMTD values displays an average difference of 6.83% with a maximum difference of 37.45%.

In conclusion, the average enhancement factors listed in Table 5-2 produced an acceptable prediction of the heat transfer, refrigerant pressure drop and LMTD for the titanium coaxial condenser.

6.4 Recommendations

During the duration of this study, some limitations were identified. The following recommendations could be useful for future work concerning this study:

- Incremental measurement of the refrigerant temperature and pressure inside the coaxial coil annulus. This incremental data will be valuable in identifying the locations of the sub-cool, two-phase and superheat regions inside the annulus. This will also allow the calculation of the incremental Nusselt number values, leading to the computation of the incremental convection heat transfer coefficient values producing a true representation of the heat distribution throughout the coaxial annuls.

It is noted that this incremental measurement of the temperature and pressure inside the annulus will be extremely difficult to achieve concerning the high degree of complexity associated with the coaxial coil geometry as illustrated in Chapter 3.

- A wider range of experimental data on a titanium coaxial condenser would be beneficial. This data will be valuable in the pursuit to formulate accurate and precise simulation models for this type of heat exchanger.

REFERENCES

Anderson, R. & De Souza, E., 2017. Heat stress management in underground mines. *International Journal of Mining Science and Technology,* pp. 651-655.

Ashcroft, 2014. *K1 Pressure transducer/transmitter.* [Online] Available at: http://www.ashcroft.com/products/transducers_and_transmitters/transmitter/k1-pressure-transducer.cfm

Bergman, T. L., Lavine, A. S., Incropera, F. P. & Dewitt, D. P., 2011. *Fundamentals of heat and mass transfer; 7th edition.* 7th ed. Hoboken, NJ: John Wiley & Sons.

BP group, 2006. *GP 44-80: Guidance on practice for relief disposal systems.* [Online] Available at: https://www.scribd.com/document/338299125/GP-44-80-Design-Guidelines-for-Relief-Disposal-Systems [Accessed 2 November 2019].

Christensen, R., Arnold, J. & Garimella, S., 1993. *Fluted tube heat exchanger design manual*.

Christensen, R. & Garimella, S., 1990. *Spirally-fluted and enhanced tubes in confined crossflow; Part II: Fluted tube annuli.* Columbus: The Ohio State University, engineering experiment station.

Christensen, R. & Srinivasan, V., 1990. *Spirally-fluted tubes and enhanced tubes in confined crossflow; Part I: Flow inside fluted tubes.* Columbus: The Ohio State University, engineering experiment station.

Das, S., 1993. Water flow through helical coils in turbulent condition. *The Canadian Journal of Chemical Engineering,* pp. 971-973.

Endress and Hauser, 2019. *Memograph M RSG40.* [Online] Available at: https://www.us.endress.com/en/field-instruments-overview/system-components-recorder-data-manager/Memograph-M-RSG40-Advanced-Graphic-Data-Manager

Endress and Hauser, 2019. *Promass 80M.* [Online] Available at: https://www.endress.com/en/field-instruments-overview/80M#

Extek, 2015. *Coaxial Type Titanium Heat Exchanger.* [Online] Available at: http://www.extek.com.cn/en/products.asp [Accessed 21 May 2018].

Helmenstine, A. M., 2019. *Specific heat definition.* [Online] Available at: https://www.thoughtco.com/definition-of-specific-heat-605673 [Accessed 03 February 2020].

Howes, M., 2011. *Ventilation and Cooling in Underground Mines.* [Online] Available at: http://www.iloencyclopaedia.org/part-xi-36283/mining-and-quarrying/123-74-mining-and-quarrying/ventilation-and-cooling-in-underground-mines [Accessed 11 April 2018].

Huang, L., Aute, V. & Radermacher, R., 2014. A finite volume coaxial heat exchanger model with moving boundaries and modifications to correlations for two-phase flow in fluted annuli. *International journal of refrigeration,* Volume 40, pp. 11-23.

JCGM, 2018. *Evaluation of measurement data — Guide to the expression of uncertainty in measurement,* JCGM.

Kroemer Elbert, E. K., Kroemer, B. H. & Kroemer Hoffman, D. A., 2018. Chapter 6 - How the body interacts with the environment. *Ergonomics ,* Volume Third edition, pp. 253-321.

MacBain, S., Bergles, A. & Raina, S., 1997. Heat transfer and pressure drop chracteristics of flow in a horizontal deep spirally fluted tube. *HVAC&R research,* 3(Part I), pp. 65-80.

M-Tech Industrial, 2015. *Mine air cooling unit.* [Online] Available at: https://mtechindustrial.com/products/acu-air-cooling-units [Accessed 21 May 2018].

Ndiaye, D., 2017. Transient model of a refrigerant-to-water helically coiled tube-in-tube. *Applied Thermal Engineering,* Volume 112, pp. 413-423.

Potgieter, R., van Antwerpen, H., Nel, B. & van Eldik, M., 2015. *Solving localised cooling problems: Operational experience with Air Cooling Units at Beatrix mine.* Potchefstroom.

Potgieter, R. & van Eldik, M., 2017. *Operational advantages of mobile refrigeration using a closed loop heat rejection configuration.* Potchefstroom.

Rankin, R. & van Eldik, M., 2011. *The application of localized vapour compression technology in deep mine cooling: Presenting the underground air cooling unit (ACU)*.

Rousseau, P., van Eldik, M. & Greyvenstein, G., 2003. Detailed simulation of fluted tube water heating condensers. *International Journal of Heat and Mass Transver,* Volume 26, pp. 232 - 239.

Sahdev, M., 2010. *Pinch technology: Basics for beginners.* [Online] Available at: http://www.cheresources.com/content/articles/heat-transfer/pinch-technology-basics-for-beginners?pg=1 [Accessed 21 November 2019].

Sami, S. & Schnolate, J., 1992. Comparative study of two phase flow boiling of refrigerant mixtures and pure refrigerant inside enhanced surface tubing. *International communications in heat and mass transfer,* Volume 19, pp. 137-148.

Sami, S., Tulej, P. & Song, B., 1994. Heat transfer characteristics of ternary blends inside enhanced surface tubing. *International communications in heat and mass transfer,* Volume 21, pp. 489-498.

Shah, M., 1979. A general correlation for heat transfer during film condensation inside pipes. *International journal of heat and mass transfer,* 22(4), pp. 547-556.

Shah, M., 1981. Heat transfer during film condensation in tubes and annuli: A review of the literature. *ASHRAE Transactions,* 87(1), pp. 1086-1105.

Srinivasan, V. & Christensen, R., 1992. Experimental investigation of heat transfer and pressure drop characteristics of flow through spirally fluted tubes. *Experimental Thermal and Fluid Science, Volume 5, Issue 6,* pp. 820 - 827.

Srinivasan, V. & Christensen, R., 1992. Experimental investigation of heat transfer and pressure drop characteristics of flow through spirally fluted tubes. *Experimental Thermal and Fluid Science,* 5(6), pp. 820 - 827.

Swamee, P. & Jain, A., 1976. Explicit equations for pipe-flow problems. *J hydraulic Div Proc,* pp. 657-664.

Thulukkanam, K., 2013. In: L. L. Faulkner, ed. *Heat exchanger design handbook.* 2nd ed. Boca Raton: CRC Press, pp. 54-56.

Traviss, D. P., Baron, A. B. & Rohsenow, W. M., 1971. *Forced convection condensation inside tubes,* Massachusetts: ASHRAE.

van Eldik, M., 1998. *Simulation of a Micro Heat Pump Cycle.* Potchefstroom: Potchefstroom University of Christian Higher Education. (Dissertation - M.Eng.).

van Eldik, M. & Wessels, G., 2013. The applicability of an existing fluted tube condenser model when used with refrigerant R-407C. *International journal of refrigeration,* 36(8), pp. 2379-2386.

Vijayaragham, S., Kambiz, V. & Christensen, R., 1994. Analysis of heat transfer and fluid through a spirally fluted tube using a porous substrate approach. *Journal of Heat Transfer,* Volume 116, pp. 543-551.

Wang, L. et al., 2000. Heat transfer characteristics of carbon steel spirally fluted tube for high pressure preheaters. *Energy conversion and management,* 41(10), pp. 993-1005.

Wessels, G., 2007. *The applicability of an existing tube condenser model when used with refrigerant R-407C.* Potchefstroom: North-West University. (Dissertation - M.Eng.).

Wika, 2019. *High-quality pressure transmitter.* [Online] Available at: https://en.wika.com/s_10_en_co.WIKA#

APPENDIX A – EES CODE

Appendix A consists of the EES code formulated for this study.

```
Function pressuredropwaterside(Re_water_volume_based; Dv_i_actual; e_star; p_star; theta_star;
L_coaxial_pipe_input; rho_water_avg; mu_water_avg; u_water; e_f_water)

If Re_water_volume_based<=1500 Then
                f_friction = 0,554 * ((64,0)/(Re_water_volume_based - 45,0)) * (e_star)^(0,384) *
(p_star)^(-1,454+2,083*e_star) * (theta_star)^(-2,426)
Else
                f_friction = 1,209 * (Re_water_volume_based)^(-0,261) * (e_star)^(1,26-0,05*p_star)
* (p_star)^(-1,66+2,033*e_star) * (theta_star)^(-2,699+3,67*e_star)
Endif

pressuredropwaterside = e_f_water *
(0,5*rho_water_avg*(u_water^2)*(f_friction*L_coaxial_pipe_input/Dv_i_actual))/1000
End

Function
watersideheattransfer(Re_water_volume_based;rho_water_avg;mu_water_avg;k_water_avg;Cp_w
ater;Dv_i_actual; e_star; p_star; theta_star)

Pr_water = (Cp_water*1000) * mu_water_avg / k_water_avg
If Re_water_volume_based<=5000 Then
                Nusselt_water = 0,014*(Re_water_volume_based^(0,842))*(e_star^(-
0,067))*(p_star^(-0,293))*(theta_star^(-0,705))*(Pr_water^(0,4))
Else
                Nusselt_water = 0,064*(Re_water_volume_based^(0,773))*(e_star^(-
0,242))*(p_star^(-0,108))*(theta_star^(0,599))*(Pr_water^(0,4))
Endif
    watersideheattransfer = Nusselt_water*k_water_avg/Dv_i_actual
End

Function singlephasepressuredrop(m_dot_R407C;A_cr_R407C;d_coil;
D_ho;L_sec;rho_R407C_in;rho_R407C_out;mu_R407C_in;mu_R407C_out;theta_star;p_star;e_sta
r;e_r;e_f)
mu_R407C_avg = (mu_R407C_in+mu_R407C_out)/2
rho_R407C_avg = (rho_R407C_in+rho_R407C_out)/2
G_R407C = m_dot_R407C/A_cr_R407C
u_R407C = G_R407C/rho_R407C_avg
Re_R407C = G_R407C*D_ho/mu_R407C_avg
f_helical = 4*(0,079*Re_R407C^(-0,25)+0,0075*(D_ho/d_coil)^(0,5)+17,5782*Re_R407C^(-
0,3137)*(D_ho/d_coil)^(0,3621)*(e_r/D_ho)^(0,6885))
f_straight = 0,25/((log10(e_r/(3,7*D_ho)+(5,74/Re_R407C^(0,9))))^(2))
r_f = f_helical/f_straight
singlephasepressuredrop = e_f * r_f * f_straight * L_sec * rho_R407C_avg * u_R407C^(2)/(2 *
D_ho)/1000
End

Function singlephaseheattransfer(m_dot_R407C;A_cr_R407C;d_coil;
D_ho;rho_R407C_in;rho_R407C_out;mu_R407C_in;mu_R407C_out;k_R407C_in;k_R407C_out;C
p_R407C;theta_star;p_star;e_star;e_r;e_h)
mu_R407C_avg = (mu_R407C_in+mu_R407C_out)/2
k_R407C_avg = (k_R407C_in+k_R407C_out)/2
rho_R407C_avg = (rho_R407C_in+rho_R407C_out)/2
G_R407C = m_dot_R407C/A_cr_R407C
```

```
u_R407C = G_R407C/rho_R407C_avg
Pr_R407C = Cp_R407C*mu_R407C_avg/k_R407C_avg *1000
Re_R407C = G_R407C*D_ho/mu_R407C_avg
Nusselt_R407C = 0,023*Re_R407C^(0,8)*Pr_R407C^(0,3)
f_helical = 4 * (0,079*Re_R407C^(-0,25) + 0,0075 * (D_ho/d_coil)^(0,5) + 17,5782 * Re_R407C^(-
0,3137) * (D_ho/d_coil)^(0,3621) * (e_r/D_ho)^(0,6885))
f_straight = 0,25/(((log10(e_r/(3,7*D_ho)+(5,74/Re_R407C^(0,9)))))^(2))
r_f =f_helical/f_straight
singlephaseheattransfer = e_h * r_f * Nusselt_R407C * k_R407C_avg/D_ho
End

Function
twophasepressuredrop(m_dot_R407C;A_cr_R407C;d_coil;D_ho;L_sec;x_R407C_in;x_R407C_out;
rho_REF_l;rho_REF_v;mu_REF_l;mu_REF_v;e_f;e_r)
x_R407C_avg = (x_R407C_in+x_R407C_out)/2
mu_R407C_x = mu_REF_v/mu_REF_l
rho_R407C_x = rho_REF_v/rho_REF_l
G_R407C = m_dot_R407C/A_cr_R407C
Re_R407C_liquid = G_R407C*D_ho/mu_REF_l
Re_R407C_vapour = G_R407C*D_ho/mu_REF_v
Re_R407C_x = Re_R407C_liquid+mu_R407C_x*((1/rho_R407C_x)^(0,5))*Re_R407C_vapour
P_R407C_Traviss = 0,09 * Re_R407C_vapour^(-
0,2)*x_R407C_avg^(1,8)*(1+2,85*(mu_R407C_x^(-0,1)*((1-
x_R407C_avg)/x_R407C_avg)^(0,9)*rho_R407C_x^(0,5))^(0,523))^(2)*G_R407C^2/(rho_REF_v*D
_ho)*L_sec
f_helical = 4 * (0,079*Re_R407C_vapour^(-0,25) + 0,0075 * (D_ho/d_coil)^(0,5) + 17,5782 *
Re_R407C_vapour^(-0,3137) * (D_ho/d_coil)^(0,3621) * (e_r/D_ho)^(0,6885))
f_straight = 0,25/((log10(e_r/(3,7*D_ho)+(5,74/Re_R407C_x^(0,9))))^(2))
r_f = f_helical/f_straight
twophasepressuredrop = e_f * r_f * P_R407C_Traviss/1000
End

Function
twophaseheattransfer(m_dot_R407C;A_cr_R407C;d_coil;D_ho;P_REF_in;p_REF_out;x_R407C_in
;x_R407C_out;rho_REF_l;rho_REF_v;mu_REF_l;mu_REF_v;k_R407C_liquid_avg;Cp_R407C_liqu
id;e_h;e_r)
x_R407C_avg = (x_R407C_in+x_R407C_out)/2
mu_R407C_x = mu_REF_v/mu_REF_l
rho_R407C_x = rho_REF_v/rho_REF_l
G_R407C = m_dot_R407C/A_cr_R407C
Re_R407C_liquid = G_R407C * D_ho/mu_REF_l
Re_R407C_vapour = G_R407C*D_ho/mu_REF_v
Re_R407C_x = Re_R407C_liquid+mu_R407C_x*((1/rho_R407C_x)^(0,5))*Re_R407C_vapour
P_REF_ave = (P_REF_in+p_REF_out)/2
Pr_R407C_liquid = Cp_R407C_liquid*mu_REF_l/k_R407C_liquid_avg*1000
P_critical_R407C = 4632 [kPa]
Pressure_Ratio = P_REF_ave/P_critical_R407C
TwoPhaseHeatTransfer_liquid =
0,023*Re_R407C_liquid^(0,8)*Pr_R407C_liquid^(0,4)*k_R407C_liquid_avg/D_ho
TwoPhaseHeatTransfer_Shah = TwoPhaseHeatTransfer_liquid*((1-
x_R407C_avg)^(0,8)+3,8*x_R407C_avg^(0,76)*(1-x_R407C_avg)^(0,04)/Pressure_Ratio^(0,38))
f_helical = 4 * (0,079*Re_R407C_vapour^(-0,25) + 0,0075 * (D_ho/d_coil)^(0,5) + 17,5782 *
Re_R407C_vapour^(-0,3137) * (D_ho/d_coil)^(0,3621) * (e_r/D_ho)^(0,6885))
f_straight = 0,25/((log10(e_r/(3,7*D_ho)+(5,74/Re_R407C_x^(0,9))))^(2))
r_f = f_helical/f_straight
twophaseheattransfer = e_h * r_f * TwoPhaseHeatTransfer_Shah
End

"\\\\\\\\\\\\\\\\\\\\\\\\\\\\\\\\\\\\\\\\\\\\\\\\\\\\\\\\UNCERTAINTY\\\\\\\\\\\\\\\\\\\\\\\\\\\\\\\\\\\\\\\\\\\\\\\\\\\\\\\\"
```

```
"ONLY FOR PARAMETRIC TABLE USE"
"Uncertainty inputs - Water side"
{u_m_dot_water = 0.005
u_Tw_in_Celcius = 0.15 + 0.002*(T_water_in_exp)
u_Tw_out_Celcius = 0.15 + 0.002*(T_water_out_exp)
u_Tw_in = u_Tw_in_Celcius/T_water_in_exp
u_Tw_out = u_Tw_out_Celcius/T_water_out_exp
u_Pw_in = 0.01
u_Pw_out = 0.01
u_hw_in = u_Tw_in + u_Pw_in
u_hw_out = u_Tw_out + u_Pw_out
h_water_out_exp = enthalpy(Water,T=T_water_out_exp,P=P_water_out_exp) * 1000
h_water_in_exp = enthalpy(Water,T=T_water_in_exp,P=P_w_in_exp) * 1000

Q_w_exp = m_dot_water_exp * (h_water_out_exp - h_water_in_exp)"<----- Main formula"

Q_w_m = (h_water_out_exp - h_water_in_exp)
Q_w_hw_out = m_dot_water_exp
Q_w_hw_in = - m_dot_water_exp

q_u_water = sqrt(((u_m_dot_water)*Q_w_m)^2 + ((u_hw_out)*Q_w_hw_out)^2 +
((u_hw_in)*Q_w_hw_in)^2)

W_error_water = (q_u_water/Q_w) * 100}

"Uncertainty inputs - Refrigerant side"
{u_m_dot_R407C = 0.0015 + (((1/36000)/m_dot_R407C_exp)*100)
u_T_R407C_in = 0.15 + 0.002*(T_R407C_in_exp)
u_P_R407C_in = 0.002
u_T_REF_out = 0.15 + 0.002*(T_REF_out_exp)
u_P_R407C_out = 0.002

u_h_REF_in = u_T_R407C_in + u_P_R407C_in
u_h_REF_out = u_T_REF_out + u_P_R407C_out

Q_R407C = m_dot_R407C_exp * (h_REF_in_exp - h_REF_out_exp)"<----- Main formula"

Q_R407C_m = (h_REF_in_exp - h_REF_out_exp)
Q_R407C_h_in = m_dot_R407C_exp
Q_R407C_h_out = -m_dot_R407C_exp

q_u_R407C = sqrt(((u_m_dot_R407C)*Q_R407C_m)^2 + ((u_h_REF_in)*Q_R407C_h_in)^2 +
((u_h_REF_out)*Q_R407C_h_out)^2)

W_error_R407C = (q_u_R407C/Q_R407C) * 100}

Duplicate i = 1;15
T_water_in_uncertainty[i] = 0,15 + 0,002 * (T_w_in[i])      "<--- Absolute uncertainty"
T_water_out_uncertainty[i] = 0,15 + 0,002 * (T_w_out[i]) "<--- Absolute uncertainty"
T_R407C_in_uncertainty[i] =0,15+0,002*T_REF_in[i]      "<--- Absolute uncertainty"
T_R407C_out_uncertainty[i] = 0,15 + 0,002 * (T_REF_out[i])"<--- Absolute uncertainty"
P_R407C_uncertainty[i] = 0,002                                  "<--- Relative uncertainty"
End

m_dot_w_uncertainty = 0,005                                     "<--- Relative uncertainty"
m_dot_R407C_uncertainty = (0,0015 + (((1/36000)/m_dot_R407C)*100) + 0,0015 -
(((1/36000)/m_dot_R407C)*100))/2                                "<--- Relative uncertainty"

"Average water uncertainty"
W_water_1650_avg = avgparametric('1650 - Uncertainty (water)';'W_error_water')
```

```
W_water_1882_avg = avgparametric('1882 - Uncertainty (water)';'W_error_water')
W_water_2134_avg = avgparametric('2134 - Uncertainty (water)';'W_error_water')
W_water_2408_avg = avgparametric('2408 - Uncertainty (water)';'W_error_water')
W_water_Total_avg = (W_water_1650_avg + W_water_1882_avg + W_water_2134_avg +
W_water_2408_avg)/4

"Max water uncertainty"
W_water_1650_Max = maxparametric('1650 - Uncertainty (water)';'W_error_water')
W_water_1882_Max = maxparametric('1882 - Uncertainty (water)';'W_error_water')
W_water_2134_Max = maxparametric('2134 - Uncertainty (water)';'W_error_water')
W_water_2408_Max = maxparametric('2408 - Uncertainty (water)';'W_error_water')
W_water_Overall_Max =
max(W_water_1650_Max;W_water_1882_Max;W_water_2134_Max;W_water_2408_Max)

"Average refrigerant uncertainty"
W_REF_1650_avg = avgparametric('1650 - Uncertainty (R407C)';'W_error_R407C')
W_REF_1882_avg = avgparametric('1882 - Uncertainty (R407C)';'W_error_R407C')
W_REF_2134_avg = avgparametric('2134 - Uncertainty (R407C)';'W_error_R407C')
W_REF_2408_avg = avgparametric('2408 - Uncertainty (R407C)';'W_error_R407C')
W_REF_Total_avg = (W_REF_1650_avg + W_REF_1882_avg + W_REF_2134_avg +
W_REF_2408_avg)/4

"Max refrigerant uncertainty"
W_REF_1650_Max = maxparametric('1650 - Uncertainty (R407C)';'W_error_R407C')
W_REF_1882_Max = maxparametric('1882 - Uncertainty (R407C)';'W_error_R407C')
W_REF_2134_Max = maxparametric('2134 - Uncertainty (R407C)';'W_error_R407C')
W_REF_2408_Max = maxparametric('2408 - Uncertainty (R407C)';'W_error_R407C')
W_REF_Overall_Max =
max(W_REF_1650_Max;W_REF_1882_Max;W_REF_2134_Max;W_REF_2408_Max)

"\\\\\\\\\\\\\\\\\\\\\\\\\\\\\\\\\\\\\\\\\\\\\\\\\\\\\\\\\\\\\\\\\\\\\\INPUTS\\\\\\\\\\\\\\\\\\\\\\\\\\\\\\\\\\\\\\\\\\\\\\\\\\\\\\\\\\\\\\\\\\\\\\\\\"

"Average heat transfer enhancement factor"
e_h = 0,5288

“Average friction enhancement factor”
e_f = 5,1534

“Average water friction enhancement factor – equal to 1 for trendline equation”
e_f_water = 1

“Water pressure drop – Trendline equation”
DELTAP_water_Trendline = 0,79525 * (DELTAP_water_TOTAL) + 4,547225

“Average sub cool “
DELTAT_sub_cool = 2,3243

"Absolute surface roughness value for titanium (mm)"
e_r = 0,0457/1000 [m]

"Coaxial pipe inputs"
VOLUME_coaxial_coil = 0,00218952 [m^3]
L_coaxial_pipe_input = 5,0689 [m]
t = 0,0007 [m]

"Volume based inside diameter"
Dv_i_actual = sqrt((4*VOLUME_coaxial_coil)/(PI*L_coaxial_pipe_input))

"Volume based outside diameter"
Dv_o_actual = Dv_i_actual + 2*t
```

```
A_water = PI*(Dv_i_actual/2)^2

D_ht_I = 0,13194 [m]
D_ht_o = 0,13634 [m]

"Pitch (p)"
p = 0,013334 [m]
p_star = p/Dv_i_actual

"Flute depth (e)"
e = 0,005058333 [m]
e_star = e/Dv_i_actual

"Flute starts"
N_flute_starts = 6

"Helix angle (theta)"
theta  = arctan((PI*Dv_o_actual)/(N_flute_starts*p))
theta_star = theta/(PI/2)

D_oi = 0,0333175 [m]
D_ho = D_oi - Dv_o_actual
d_coil = D_ho/(sin(theta))
A_cr_R407C = PI*(D_oi/2)^2 - PI*(Dv_o_actual/2)^2

"TOTALS"
Q_TOTAL = -sum(Q[i];i = 1;15)
DELTAP_R407C = P_REF_in[1] -   P_REF_out[15]
DELTAP_water = P_w_in[15] - P_w_out[1]
L_sec_TOTAL  = sum(L_sec[i];i = 1;15)
UA_TOTAL = sum(UA[i]; i = 1;15)
LMTD = ((T_REF_out[15] - T_w_in[15]) - (T_REF_in[1] - T_w_out[1]))/(ln((T_REF_out[15] -
T_w_in[15])/(T_REF_in[1] - T_w_out[1])))
k_Titanium_avg = sum(k_Titanium[i]; i = 1;15)/15
mu_water_avg = sum(mu_water_avg[i]; i = 1;15)/15
rho_water_avg = sum(rho_water_avg[i]; i = 1;15)/15
u_water = sum(u_water[i]; i = 1;15)/15
Re_water_volume_based = sum(Re_water_volume_based[i]; i = 1;15)/15
DELTAP_water_TOTAL = pressuredropwaterside(Re_water_volume_based; Dv_i_actual; e_star;
p_star; theta_star; L_coaxial_pipe_input; rho_water_avg; mu_water_avg; u_water; e_f_water)

"\\\\\\\\\\\\\\\\\\\\\\\\\\\\\\\\\\\\\\\\\\\\\\\\\\\\\\\\\\\\\\\\\\\\\\\\\\\\\\\\\\\\\\\\\\\\\\\\\\\\\\\\\\\\\\\\\\\\\\\\\\\\\\\\\\\\\\\\\\\\\\\\\\\\\\\\\\\\\\\\INLET\\\\\\\\\\\\\\\\\\\\\\\\\\\\\\\\\\\\\\\\\\\\\\\\\\\\\\\\\\\\\\\\\\\\\\\\\\\\\\\\\\\\\\\\\\\\\\\\\\\\\\\\\\\\\\\\\\\\\\\\\\\\\\\\\\\\\\\\\\\\\\\\\\\\\\\\\\\\\\\\"

"Sub-cooled temperature of the refrigerant on startup"
DELTAT_sub_cool = T_REF_out[13] - T_REF_out[15]    "Obtain T_REF_out[15]"

"Refrigerant used in this study"
R1$ = 'R407C'

"R407C critical pressure"
P_critical = P_crit(R1$)

"_________________PLOT___________________"

"Average value plot"
Duplicate i =1;15
s_Plot_avg[16-i] = s_R407C_avg[i]
T_REF_avg[i] = (T_REF_in[i] + T_REF_out[i])/2
T_water_avg[i] = (T_w_in[i] + T_w_out[i])/2
```

```
"Inlet value plot"
s_Plot_inlet[16-i] = s_R407C_in[i]

"Outlet value plot"
s_Plot_out[16-i] = s_R407C_out[i]
End

"\\\\\\\\\\\\\\\\\\\\\\\\\\\\\\\\\\\\\\\\\\\\\\\\\\\\\\\\\\\\\\\\SUPERHEAT_3_INCREMENTS\\\\\\\\\\\\\\\\\\\\\\\\\\\\\\\\\\\\\\\\\\\\\\\\\\\\\\\\\\\\\\\\"

Q_R407C_superheat = m_dot_R407C*(h_REF_out_superheat - h_REF_in[1])

"Initial refrigerant enthalpy"
h_REF_in[1] = enthalpy(R1$;T=T_REF_in[1];P=P_REF_in[1])
h_REF_out_superheat = enthalpy(R1$;x=1;P=P_REF_out[3])

Duplicate i = 1;3
T_REF_out[i] = temperature(R1$;P=P_REF_out[i];h=h_REF_out[i])
T_REF_in[i+1] = T_REF_out[i]

Q[i] = Q_R407C_superheat/3
Q[i] = m_dot_R407C*(h_REF_out[i] - h_REF_in[i])
h_REF_in[i+1] = h_REF_out[i]

u_R407C_in[i] = m_dot_R407C/(rho_R407C_in[i]*A_cr_R407C)

Cp_water[i] = cp(Water;T=T_w_in[i];P=P_w_in[i])

Q[i+1] = m_dot_w*Cp_water[i]*(-T_w_out[i] + T_w_in[i])

T_w_out[i] = T_w_in[i-1]

DELTAT_max[i] = T_REF_in[i] - T_w_in[i]

"Water conductivity properties"
k_water_avg[i] = (k_water_in[i]+k_water_out[i])/2
k_water_in[i] = conductivity(Water;T=T_w_in[i];P=P_w_in[i])
k_water_out[i] = conductivity(Water;T=T_w_out[i];P=P_w_out[i])

"Water viscosity properties"
mu_water_avg[i] = (mu_water_in[i]+mu_water_out[i])/2
mu_water_in[i] = viscosity(Water;T=T_w_in[i];P=P_w_in[i])
mu_water_out[i] = viscosity(Water;T=T_w_out[i];P=P_w_out[i])

"Water density properties"
rho_water_avg[i] = (rho_water_in[i]+rho_water_out[i])/2
rho_water_in[i] = density(Water;T=T_w_in[i];P=P_w_in[i])

rho_water_out[i] = density(Water;T=T_w_out[i];P=P_w_out[i])

"Water velocity properties"
u_water[i] = m_dot_w/(rho_water_avg[i]*A_water)
u_water_in[i] = m_dot_w/(rho_water_in[i]*A_water)
u_water_out[i] = m_dot_w/(rho_water_out[i]*A_water)

"Water Reynolds number"
Re_water_volume_based[i] = (rho_water_avg[i]*u_water[i]*Dv_i_actual)/mu_water_avg[i]
Re_water_in[i] = (rho_water_in[i]*u_water_in[i]*Dv_i_actual)/mu_water_in[i]
Re_water_out[i] = (rho_water_out[i]*u_water_out[i]*Dv_i_actual)/mu_water_out[i]
```

```
"Water pressure"
P_w_out[i] = P_w_in[i]
P_w_out[i] = P_w_in[i-1]

C_water[i] = m_dot_w * Cp_water[i]
C_REF[i] = m_dot_R407C * C_R407C_avg[i]

C_min[i] = min(C_water[i];C_REF[i])
C_max[i] = max(C_water[i];C_REF[i])

C_R[i] = C_min[i] / C_max[i]

q_max[i] = C_min[i]*DELTAT_max[i]
epsilon[i] = -Q[i]/q_max[i]

NTU[i] = 1/(C_R[i]-1)*ln((epsilon[i]-1)/(epsilon[i]*C_R[i]-1))
NTU[i] = UA[i]/C_min[i]

"Heat transfer of the water"
h_w[i] = watersideheattransfer(Re_water_volume_based[i];rho_water_avg[i];mu_water_avg[i];
k_water_avg[i];Cp_water[i];Dv_i_actual; e_star; p_star; theta_star)
End

Duplicate i = 1;2
"Refrigerant conductivity"
k_R407C_in[i] = conductivity(R1$;T=T_REF_in[i]; P=P_REF_in[i])
k_R407C_out[i] = conductivity(R1$;T=T_REF_out[i]; P=P_REF_out[i])

"Refrigerant viscosity"
mu_R407C_in[i] = viscosity(R1$;T=T_REF_in[i]; P=P_REF_in[i])
mu_R407C_out[i] = viscosity(R1$;T=T_REF_out[i]; P=P_REF_out[i])

"Refrigerant density"
rho_R407C_in[i] = density(R1$;T=T_REF_in[i]; P=P_REF_in[i])
rho_R407C_out[i] = density(R1$;T=T_REF_out[i]; P=P_REF_out[i])

"Refrigerant specific heat"
Cp_R407C_in[i] = cp(R1$;T=T_REF_in[i]; P=P_REF_in[i])
Cp_R407C_out[i] = cp(R1$;T=T_REF_out[i]; P=P_REF_out[i])

"Refrigerant enthalpy"
s_R407C_in[i] = Entropy(R407C;T=T_REF_in[i];P=P_REF_in[i])
s_R407C_out[i] = Entropy(R407C;T=T_REF_out[i];P=P_REF_out[i])
s_R407C_avg[i] = (s_R407C_in[i] + s_R407C_out[i])/2

C_R407C_avg[i] = (Cp_R407C_in[i] + Cp_R407C_out[i])/2

"Refrigerant pressure drop"
P_R407C_drop[i] = singlephasepressuredrop(m_dot_R407C;A_cr_R407C;d_coil;
D_ho;L_sec[i];rho_R407C_in[i];rho_R407C_out[i];mu_R407C_in[i];mu_R407C_out[i];theta_star;p_s
tar;e_star;e_r;e_f)
P_REF_out[i] = P_REF_in[i] - P_R407C_drop[i]
P_REF_in[i+1] = P_REF_out[i]

"Heat transfer of the refrigerant"
h_REF[i] = singlephaseheattransfer(m_dot_R407C;A_cr_R407C;d_coil;
D_ho;rho_R407C_in[i];rho_R407C_out[i];mu_R407C_in[i];mu_R407C_out[i];k_R407C_in[i];k_R407
C_out[i];C_R407C_avg[i];theta_star;p_star;e_star;e_r;e_h)

"Titanium conductivity"
```

```
k_Titanium[i] = conductivity(Titanium; T=T_w_out[i])

1/(UA[i]*1000) = 1/(h_w[i]*PI*D_ht_i*L_sec[i]) +
(ln(Dv_o_actual/Dv_i_actual)/(2*PI*k_Titanium[i]*L_sec[i])) + 1/(h_REF[i]*PI*D_ht_o*L_sec[i])
End

"Refrigerant properties for the last increment before entering two phase"

"Refrigerant conductivity"
k_R407C_in[3] = conductivity(R1$;T=T_REF_in[3]; P=P_REF_in[3])
k_R407C_out[3] = conductivity(R1$;x=1; P=P_REF_out[3])

"Refrigerant viscosity"
mu_R407C_in[3] = viscosity(R1$;T=T_REF_in[3]; P=P_REF_in[3])
mu_R407C_out[3] = viscosity(R1$;x=1; P=P_REF_out[3])

"Refrigerant density"
rho_R407C_in[3] = density(R1$;T=T_REF_in[3]; P=P_REF_in[3])
rho_R407C_out[3] = density(R1$;x=1; P=P_REF_out[3])

"Refrigerant specific heat"
Cp_R407C_in[3] = cp(R1$;T=T_REF_in[3]; P=P_REF_in[3])
Cp_R407C_out[3] = cp(R1$;x=1; P=P_REF_out[3])

"Refrigerant enthalpy"
s_R407C_in[3] = Entropy(R407C;T=T_REF_in[3];P=P_REF_in[3])
s_R407C_out[3] = Entropy(R407C;T=T_REF_out[3];x=1)
s_R407C_avg[3] = (s_R407C_in[3] + s_R407C_out[3])/2

C_R407C_avg[3] = (Cp_R407C_in[3] + Cp_R407C_out[3])/2

"Refrigerant pressure drop"
P_R407C_drop[3] = singlephasepressuredrop(m_dot_R407C;A_cr_R407C;d_coil;
D_ho;L_sec[3];rho_R407C_in[3];rho_R407C_out[3];mu_R407C_in[3];mu_R407C_out[3];theta_star;
p_star;e_star;e_r;e_f)
P_REF_out[3] = P_REF_in[3] - P_R407C_drop[3]
P_REF_in[4] = P_REF_out[3]

"Heat transfer of the refrigerant"
h_REF[3] = singlephaseheattransfer(m_dot_R407C;A_cr_R407C;d_coil;
D_ho;rho_R407C_in[3];rho_R407C_out[3];mu_R407C_in[3];mu_R407C_out[3];k_R407C_in[3];k_R
407C_out[3];C_R407C_avg[3];theta_star;p_star;e_star;e_r;e_h)

"Titanium conductivity"
k_Titanium[3] = conductivity(Titanium; T=T_w_out[3])

1/(UA[3]*1000) = 1/(h_w[3]* PI*D_ht_i*L_sec[3]) +
(ln(Dv_o_actual/Dv_i_actual)/(2*PI*k_Titanium[3]*L_sec[3])) + 1/(h_REF[3]*PI*D_ht_o*L_sec[3])


"\\\\\\\\\\\\\\\\\\\\\\\\\\\\\\\\\\\\\\\\TWO_PHASE_10_INCREMENTS\\\\\\\\\\\\\\\\\\\\\\\\\\\\\\\\\\\\\\\\"

"Fix quality for the first increment in the two phase region"
x_n_in[4] = 1

"Devide two phase increments into equal quality values"
x_n_out[4] = x_n_in[4] - 1/10

"Refrigerant viscosity - Two phase"
mu_REF_liq[4] = viscosity(R1$;P=P_REF_ave[4]; x = 0)
```

```
mu_REF_vap[4] = viscosity(R1$;P=P_REF_ave[4]; x = 1)

"Refrigerant density - Two phase"
rho_REF_liq[4] = density(R1$; P=P_REF_ave[4]; x = 0)
rho_REF_vap[4] = density(R1$; P=P_REF_ave[4]; x = 1)

"Refrigerant pressure drop - Two phase"
P_R407C_drop[4] =
twophasepressuredrop(m_dot_R407C;A_cr_R407C;d_coil;D_ho;L_sec[4];x_n_in[4];x_n_out[4];rho
_REF_liq[4];rho_REF_vap[4];mu_REF_liq[4];mu_REF_vap[4];e_f;e_r)
P_REF_out[4] = P_REF_in[4] - P_R407C_drop[4]

P_REF_ave[4] = (P_REF_in[4] + P_REF_out[4])/2

T_REF_out[4] = temperature(R1$;P=P_REF_out[4];x=x_n_out[4])

h_REF_out[4] = enthalpy(R1$;P=P_REF_out[4];x=x_n_out[4])
Q[4] = m_dot_R407C*(h_REF_out[4] - h_REF_in[4])
Q[4] = m_dot_w*Cp_water[4]*(-T_w_out[4] + T_w_in[4])

T_w_out[4] = T_w_in[3]

"Water conductivity properties"
k_water_in[4] = conductivity(Water;T=T_w_in[4];P=P_w_in[4])
k_water_out[4] = conductivity(Water;T=T_w_out[4];P=P_w_out[4])
k_water_avg[4] = (k_water_in[4]+k_water_out[4])/2

"Water viscosity properties"
mu_water_in[4] = viscosity(Water;T=T_w_in[4];P=P_w_in[4])
mu_water_out[4] = viscosity(Water;T=T_w_out[4];P=P_w_out[4])
mu_water_avg[4] = (mu_water_in[4]+mu_water_out[4])/2

"Water density properties"
rho_water_in[4] = density(Water;T=T_w_in[4];P=P_w_in[4])
rho_water_out[4] = density(Water;T=T_w_out[4];P=P_w_out[4])
rho_water_avg[4] = (rho_water_in[4]+rho_water_out[4])/2

"Water velocity"
u_water_in[4] = m_dot_w/(rho_water_in[4]*A_water)
u_water_out[4] = m_dot_w/(rho_water_out[4]*A_water)
u_water[4] = m_dot_w/(rho_water_avg[4]*A_water)

"Water Reynolds number"
Re_water_in[4] = (rho_water_in[4]*u_water_in[4]*Dv_i_actual)/mu_water_in[4]
Re_water_out[4] = (rho_water_out[4]*u_water_out[4]*Dv_i_actual)/mu_water_out[4]
Re_water_volume_based[4] = (rho_water_avg[4]*u_water[4]*Dv_i_actual)/mu_water_avg[4]

"Water pressure"
P_w_out[4] = P_w_in[4]
P_w_out[4] = P_w_in[3]

Cp_water[4] = cp(Water;T=T_w_in[4];P=P_w_in[4])

C_water[4] = m_dot_w*Cp_water[4]
C_REF[4] = m_dot_R407C * C_R407C_avg[4]

C_min[4] = min(C_water[4]; C_REF[4])
C_max[4] = max(C_water[4];C_REF[4])

C_R[4] = C_min[4] / C_max[4]
```

```
q_max[4] = C_min[4]*DELTAT_max[4]
epsilon[4] = -Q[4]/q_max[4]

DELTAT_max[4] = T_REF_in[4] - T_w_in[4]

NTU[4] = 1/(C_R[4]-1)*ln((epsilon[4]-1)/(epsilon[4]*C_R[4]-1))
NTU[4] = UA[4]/C_min[4]

"Heat transfer of the water"
h_w[4] = watersideheattransfer(Re_water_volume_based[4];rho_water_avg[4];mu_water_avg[4];
k_water_avg[4];Cp_water[4];Dv_i_actual; e_star; p_star; theta_star)

C_R407C_avg[4] = (Cp_R407C_vap_avg[4]*( x_n_in[4] + x_n_out[4])/2) +
(Cp_R407C_liquid_avg[4] *( 1- (x_n_in[4] + x_n_out[4])/2))

"Refrigerant conductivity - Two phase"
k_R407C_liquid_avg[4] = (conductivity(R1$;x=0; P=P_REF_in[4]) + conductivity(R1$;X=0;
P=P_REF_out[4]))/2
k_R407C_vapour_avg[4] = (conductivity(R1$;x=1; P=P_REF_in[4]) + conductivity(R1$;X=1;
P=P_REF_out[4]))/2

"Refrigerant viscosity - Two phase"
mu_REF_liq_avg[4] = (viscosity(R1$;x=0; P=P_REF_in[4]) + viscosity(R1$;x=0;
P=P_REF_out[4]))/2
mu_REF_vap_avg[4] = (viscosity(R1$;x=1; P=P_REF_in[4]) + viscosity(R1$;x=1;
P=P_REF_out[4]))/2

"Refrigerant density - Two phase"
rho_R407C_liquid_avg[4] = (density(R1$;x=0; P=P_REF_in[4]) + density(R1$;x=0;
P=P_REF_out[4]))/2
rho_R407C_vap_avg[4] = (density(R1$;x=1; P=P_REF_in[4]) + density(R1$;x=1;
P=P_REF_out[4]))/2

"Refrigerant specific heat - Two phase"
Cp_R407C_liquid_avg[4] = (cp(R1$;x=0; P=P_REF_in[4]) + cp(R1$;x=0; P=P_REF_out[4]))/2
Cp_R407C_vap_avg[4] = (cp(R1$;x=1; P=P_REF_in[4]) + cp(R1$;x=1; P=P_REF_out[4]))/2

"Refrigerant enthalpy - Two phase"
s_R407C_in[4] = Entropy(R407C;T=T_REF_in[4];x=1)
s_R407C_out[4] = Entropy(R407C;T=T_REF_out[4];P=P_REF_out[4])
s_R407C_avg[4] = (s_R407C_in[4] + s_R407C_out[4])/2

"Refrigerant heat transfer - Two phase"
h_REF[4] =
twophaseheattransfer(m_dot_R407C;A_cr_R407C;d_coil;D_ho;P_REF_in[4];P_REF_out[4];x_n_in
[4];x_n_out[4];rho_R407C_liquid_avg[4];rho_R407C_vap_avg[4];mu_REF_liq_avg[4];mu_REF_vap
_avg[4];k_R407C_liquid_avg[4];Cp_R407C_liquid_avg[4];e_h;e_r)

"Titanium conductivity"
k_Titanium[4] = conductivity(Titanium; T=T_w_out[4])

1/(UA[4]*1000) = 1/(h_w[4]* PI*D_ht_i*L_sec[4])  +
(ln(Dv_o_actual/Dv_i_actual)/(2*PI*k_Titanium[4]*L_sec[4])) + 1/(h_REF[4]*PI*D_ht_o*L_sec[4])

Duplicate i = 5;12
x_n_in[i] = x_n_out[i-1]

"Devide two phase increments into equal quality values"
x_n_out[i] = x_n_in[i] - 1/10
```

```
h_REF_in[i] = h_REF_out[i-1]
h_REF_out[i] = enthalpy(R1$;P=P_REF_out[i];x=x_n_out[i])
T_REF_in[i] = T_REF_out[i-1]
T_REF_out[i] = temperature(R1$;P=P_REF_out[i];x=x_n_out[i])
Q[i] = m_dot_R407C*(h_REF_out[i] - h_REF_in[i])

Cp_water[i] = cp(Water;T=T_w_in[i];P=P_w_in[i])
Q[i] = m_dot_w*Cp_water[i]*(-T_w_out[i] + T_w_in[i])

T_w_out[i] = T_w_in[i-1]

DELTAT_max[i] = T_REF_in[i] - T_w_in[i]

"Water conductivity properties"
k_water_in[i] = conductivity(Water;T=T_w_in[i];P=P_w_in[i])
k_water_out[i] = conductivity(Water;T=T_w_out[i];P=P_w_out[i])
k_water_avg[i] = (k_water_in[i]+k_water_out[i])/2

"Water viscosity properties"
mu_water_in[i] = viscosity(Water;T=T_w_in[i];P=P_w_in[i])
mu_water_out[i] = viscosity(Water;T=T_w_out[i];P=P_w_out[i])
mu_water_avg[i] = (mu_water_in[i]+mu_water_out[i])/2

"Water density properties"
rho_water_in[i] = density(Water;T=T_w_in[i];P=P_w_in[i])
rho_water_out[i] = density(Water;T=T_w_out[i];P=P_w_out[i])
rho_water_avg[i] = (rho_water_in[i]+rho_water_out[i])/2

"Water velocity"
u_water_in[i] = m_dot_w/(rho_water_in[i]*A_water)
u_water_out[i] = m_dot_w/(rho_water_out[i]*A_water)
u_water[i] = m_dot_w/(rho_water_avg[i]*A_water)

"Water Reynolds number"
Re_water_in[i] = (rho_water_in[i]*u_water_in[i]*Dv_i_actual)/mu_water_in[i]
Re_water_out[i] = (rho_water_out[i]*u_water_out[i]*Dv_i_actual)/mu_water_out[i]
Re_water_volume_based[i] = (rho_water_avg[i]*u_water[i]*Dv_i_actual)/mu_water_avg[i]

"Water pressure"
P_w_out[i] = P_w_in[i]
P_w_out[i] = P_w_in[i-1]

C_water[i] = m_dot_w*Cp_water[i]
C_REF[i] = m_dot_R407C * C_R407C_avg[i]

C_min[i] = min(C_water[i];C_REF[i])
C_max[i] = max(C_water[i];C_REF[i])

C_R[i] = C_min[i] / C_max[i]

q_max[i] = C_min[i]*DELTAT_max[i]
epsilon[i] = -Q[i]/q_max[i]

NTU[i] = 1/(C_R[i]-1)*ln((epsilon[i]-1)/(epsilon[i]*C_R[i]-1))
NTU[i] = UA[i]/C_min[i]

"Heat transfer of the water"
h_w[i] = watersideheattransfer(Re_water_volume_based[i];rho_water_avg[i];mu_water_avg[i];
k_water_avg[i];Cp_water[i];Dv_i_actual; e_star; p_star; theta_star)
```

```
"Refrigerant viscosity"
mu_REF_liquid[i] = viscosity(R1$;P=P_REF_ave[i]; x=0)

mu_REF_vapour[i] = viscosity(R1$;P=P_REF_ave[i]; x=1)

"Refrigerant density"
rho_REF_liq[i] = density(R1$; P=P_REF_ave[i]; x=0)
rho_REF_vap[i] = density(R1$; P=P_REF_ave[i]; x=1)

"Refrigerant pressure drop"
P_R407C_drop[i] =
twophasepressuredrop(m_dot_R407C;A_cr_R407C;d_coil;D_ho;L_sec[i];x_n_in[i];x_n_out[i];rho_R
EF_liq[i];rho_REF_vap[i];mu_REF_liquid[i];mu_REF_vapour[i];e_f;e_r)
P_REF_in[i] = P_REF_out[i-1]
P_REF_out[i] = P_REF_in[i] - P_R407C_drop[i]

P_REF_ave[i] = (P_REF_in[i] + P_REF_out[i])/2

"Refrigerant conductivity - Two phase"
k_R407C_liquid_avg[i] = (conductivity(R1$;x=0; P=P_REF_in[i]) + conductivity(R1$;x=0;
P=P_REF_out[i]))/2
k_R407C_vapour_avg[i] = (conductivity(R1$;x=1; P=P_REF_in[i]) + conductivity(R1$;x=1;
P=P_REF_out[i]))/2

"Refrigerant viscosity - Two phase"
mu_REF_liq_avg[i] = (viscosity(R1$;x=0; P=P_REF_in[i]) + viscosity(R1$;x=0; P=P_REF_out[i]))/2
mu_REF_vap_avg[i] = (viscosity(R1$;x=1; P=P_REF_in[i]) + viscosity(R1$;x=1;
P=P_REF_out[i]))/2

"Refrigerant density - Two phase"
rho_R407C_liquid_avg[i] = (density(R1$;x=0; P=P_REF_in[i]) + density(R1$;x=0;
P=P_REF_out[i]))/2
rho_R407C_vap_avg[i] = (density(R1$;x=1; P=P_REF_in[i]) + density(R1$;x=1;
P=P_REF_out[i]))/2

"Refrigerant specific heat - Two phase"
Cp_R407C_liquid_avg[i] = (cp(R1$;x=0; P=P_REF_in[i]) + cp(R1$;x=0; P=P_REF_out[i]))/2
Cp_R407C_vapour_avg[i] = (cp(R1$;x=1; P=P_REF_in[i]) + cp(R1$;x=1; P=P_REF_out[i]))/2

"Refrigerant enthalpy - Two phase"
s_R407C_in[i] = Entropy(R407C;T=T_REF_in[i];P=P_REF_in[i])
s_R407C_out[i] = Entropy(R407C;T=T_REF_out[i];P=P_REF_out[i])
s_R407C_avg[i] = (s_R407C_in[i] + s_R407C_out[i])/2

C_R407C_avg[i] = (Cp_R407C_vapour_avg[i] * ( x_n_in[i] + x_n_out[i])/2) +
(Cp_R407C_liquid_avg[i] * (1- (x_n_in[i] + x_n_out[i])/2))

"Heat transfer of the refrigerant"
h_REF[i] =
twophaseheattransfer(m_dot_R407C;A_cr_R407C;d_coil;D_ho;P_REF_in[i];P_REF_out[i];x_n_in[i]
;x_n_out[i];rho_R407C_liquid_avg[i];rho_R407C_vap_avg[i];mu_REF_liq_avg[i];mu_REF_vap_avg[
i];k_R407C_liquid_avg[i];Cp_R407C_liquid_avg[i];e_h;e_r)

"Titanium conductivity"
k_Titanium[i] = conductivity(Titanium; T=T_w_out[i])

1/(UA[i]*1000) = 1/(h_w[i]* PI*D_ht_i*L_sec[i]) +
(ln(Dv_o_actual/Dv_i_actual)/(2*PI*k_Titanium[i]*L_sec[i])) + 1/(h_REF[i]*PI*D_ht_o*L_sec[i])
End
```

```
"Determine the last increment in the two phase region before entering sub-cool"
x_n_in[13] = x_n_out[12]
x_n_out[13] = 0

h_REF_in[13] = h_REF_out[12]
h_REF_out[13] = enthalpy(R1$;P=P_REF_out[13];x=x_n_out[13])

T_REF_in[13] = T_REF_out[12]
T_REF_out[13] = temperature(R1$;P=P_REF_out[13];x=x_n_out[13])
Q[13] = m_dot_R407C*(h_REF_out[13] - h_REF_in[13])

Cp_water[13] = cp(Water;T=T_w_in[13];P=P_w_in[13])
Q[13] = m_dot_w*Cp_water[13]*(-T_w_out[13] + T_w_in[13])

T_w_out[13] = T_w_in[12]

DELTAT_max[13] = T_REF_in[13] - T_w_in[13]

"Water conductivity properties"
k_water_in[13] = conductivity(Water;T=T_w_in[13];P=P_w_in[13])
k_water_out[13] = conductivity(Water;T=T_w_out[13];P=P_w_out[13])
k_water_avg[13] = (k_water_in[13]+k_water_out[13])/2

"Water viscosity properties"
mu_water_in[13] = viscosity(Water;T=T_w_in[13];P=P_w_in[13])
mu_water_out[13] = viscosity(Water;T=T_w_out[13];P=P_w_out[13])
mu_water_avg[13] = (mu_water_in[4]+mu_water_out[13])/2

"Water density properties"
rho_water_in[13] = density(Water;T=T_w_in[13];P=P_w_in[13])
rho_water_out[13] = density(Water;T=T_w_out[13];P=P_w_out[13])
rho_water_avg[13] = (rho_water_in[13]+rho_water_out[13])/2

"Water velocity"
u_water_in[13] = m_dot_w/(rho_water_in[13]*A_water)
u_water_out[13] = m_dot_w/(rho_water_out[13]*A_water)
u_water[13] = m_dot_w/(rho_water_avg[13]*A_water)

"Water Reynolds number"
Re_water_in[13] = (rho_water_in[13]*u_water_in[13]*Dv_i_actual)/mu_water_in[13]
Re_water_out[13] = (rho_water_out[13]*u_water_out[13]*Dv_i_actual)/mu_water_out[13]
Re_water_volume_based[13] = (rho_water_avg[13]*u_water[13]*Dv_i_actual)/mu_water_avg[13]

"Water pressure"
P_w_out[13] = P_w_in[13]
P_w_out[13] = P_w_in[12]

C_water[13] = m_dot_w*Cp_water[13]
C_REF[13] = m_dot_R407C * C_R407C_avg[13]

C_min[13] = min(C_water[13];C_REF[13])
C_max[13] = max(C_water[13];C_REF[13])

C_R[13] = C_min[13] / C_max[13]

q_max[13] = C_min[13]*DELTAT_max[13]
epsilon[13] = -Q[13]/q_max[13]

NTU[13] = 1/(C_R[13]-1)*ln((epsilon[13]-1)/(epsilon[13]*C_R[13]-1))
```

```
NTU[13] = UA[13]/C_min[13]

"Heat transfer of the water"
h_w[13] =
watersideheattransfer(Re_water_volume_based[13];rho_water_avg[13];mu_water_avg[13];
k_water_avg[13];Cp_water[13];Dv_i_actual; e_star; p_star; theta_star)

"Refrigerant viscosity"
mu_REF_liq[13] = viscosity(R1$;P=P_REF_ave[13]; x=0)

mu_REF_vap[13] = viscosity(R1$;P=P_REF_ave[13]; x=1)

"Refrigerant density"
rho_REF_liq[13] = density(R1$; P=P_REF_ave[13]; x=0)
rho_REF_vap[13] = density(R1$; P=P_REF_ave[13]; x=1)

"Refrigerant pressure drop - Two phase"
P_R407C_drop[13] =
twophasepressuredrop(m_dot_R407C;A_cr_R407C;d_coil;D_ho;L_sec[13];x_n_in[13];x_n_out[13];
rho_REF_liq[13];rho_REF_vap[13];mu_REF_liq[13];mu_REF_vap[13];e_f;e_r)
P_REF_in[13] = P_REF_out[12]
P_REF_out[13] = P_REF_in[13] - P_R407C_drop[13]

P_REF_ave[13] = (P_REF_in[13] + P_REF_out[13])/2

"Refrigerant conductivity - Two phase"
k_R407C_liquid_avg[13] = (conductivity(R1$;x=0; P=P_REF_in[13]) + conductivity(R1$;X=0;
P=P_REF_out[13]))/2
k_R407C_vapour_avg[13] = (conductivity(R1$;x=1; P=P_REF_in[13]) + conductivity(R1$;X=1;
P=P_REF_out[13]))/2

"Refrigerant viscosity - Two phase"
mu_REF_liq_avg[13] = (viscosity(R1$;x=0; P=P_REF_in[13]) + viscosity(R1$;x=0;
P=P_REF_out[13]))/2
mu_REF_vap_avg[13] = (viscosity(R1$;x=1; P=P_REF_in[13]) + viscosity(R1$;X=1;
P=P_REF_out[13]))/2

"Refrigerant density - Two phase"
rho_R407C_liquid_avg[13] = (density(R1$;x=0; P=P_REF_in[13]) + density(R1$;x=0;
P=P_REF_out[13]))/2
rho_R407C_vap_avg[13] = (density(R1$;x=1; P=P_REF_in[13]) + density(R1$;x=1;
P=P_REF_out[13]))/2

"Refrigerant specific heat - Two phase"
Cp_R407C_liquid_avg[13] = (cp(R1$;x=0; P=P_REF_in[13]) + cp(R1$;x=0; P=P_REF_out[13]))/2
Cp_R407C_vap_avg[13] = (cp(R1$;x=1; P=P_REF_in[13]) + cp(R1$;x=1; P=P_REF_out[13]))/2

"Refrigerant enthalpy - Two phase"
s_R407C_in[13] = Entropy(R407C;T=T_REF_in[13];P=P_REF_in[13])
s_R407C_out[13] = Entropy(R407C;T=T_REF_out[13];P=P_REF_out[13])
s_R407C_avg[13] = (s_R407C_in[13] + s_R407C_out[13])/2

C_R407C_avg[13] = (Cp_R407C_vap_avg[13]*( x_n_in[13] + x_n_out[13])/2) +
(Cp_R407C_liquid_avg[13] * ( 1- (x_n_in[13] + x_n_out[13])/2))

"Heat transfer of the refrigerant - Two phase"
h_REF[13] =
twophaseheattransfer(m_dot_R407C;A_cr_R407C;d_coil;D_ho;P_REF_in[13];P_REF_out[13];x_n
_in[13];x_n_out[13];rho_R407C_liquid_avg[13];rho_R407C_vap_avg[13];mu_REF_liq_avg[13];mu_
REF_vap_avg[13];k_R407C_liquid_avg[13];Cp_R407C_liquid_avg[13];e_h;e_r)
```

```
"Titanium conductivity"
k_Titanium[13] = conductivity(Titanium; T=T_w_out[13])

1/(UA[13] *1000) = 1/(h_w[13]* PI*D_ht_i*L_sec[13]) +
(ln(Dv_o_actual/Dv_i_actual)/(2*PI*k_Titanium[13]*L_sec[13]) ) +
1/(h_REF[13]*PI*D_ht_o*L_sec[13])

"\\\\\\\\\\\\\\\\\\\\\\\\\\\\\\\\\\\\\\\\\\\\\\\\\\\\\\\\\\\\\\\\\\\\SUBCOOL_2_INCREMENTS\\\\\\\\\\\\\\\\\\\\\\\\\\\\\\\\\\\\\\\\\\\\\\\\\\\\\\\\\\\\\\\\\\\\"

Duplicate i = 14;15
T_REF_in[i] = T_REF_out[i-1]
T_REF_out[i] = T_REF_in[i] - DELTAT_sub_cool/2

P_REF_in[i] = P_REF_out[i-1]
P_REF_out[i] = P_REF_in[i] - P_R407C_drop[i]
h_REF_in[i] = h_REF_out[i-1]
h_REF_out[i] = enthalpy(R1$;P=P_REF_out[i];T=T_REF_out[i])

Q[i] = m_dot_R407C*(h_REF_out[i] - h_REF_in[i])

Cp_water[i] = cp(Water;T=T_w_in[i];P=P_w_in[i])
Q[i] = m_dot_w*Cp_water[i]*(-T_w_out[i] + T_w_in[i])

T_w_out[i] = T_w_in[i-1]

DELTAT_max[i] = T_REF_in[i] - T_w_in[i]

"Water conductivity properties"
k_water_in[i] = conductivity(Water;T=T_w_in[i];P=P_w_in[i])
k_water_out[i] = conductivity(Water;T=T_w_out[i];P=P_w_out[i])
k_water_avg[i] = (k_water_in[i]+k_water_out[i])/2

"Water viscosity properties"
mu_water_in[i] = viscosity(Water;T=T_w_in[i];P=P_w_in[i])
mu_water_out[i] = viscosity(Water;T=T_w_out[i];P=P_w_out[i])
mu_water_avg[i] = (mu_water_in[i]+mu_water_out[i])/2

"Water density properties"
rho_water_in[i] = density(Water;T=T_w_in[i];P=P_w_in[i])
rho_water_out[i] = density(Water;T=T_w_out[i];P=P_w_out[i])
rho_water_avg[i] = (rho_water_in[i]+rho_water_out[i])/2

"Water velocity"
u_water_in[i] = m_dot_w/(rho_water_in[i]*A_water)
u_water_out[i] = m_dot_w/(rho_water_out[i]*A_water)
u_water[i] = m_dot_w/(rho_water_avg[i]*A_water)

"Water Reynolds number"
Re_water_in[i] = (rho_water_in[i]*u_water_in[i]*Dv_i_actual)/mu_water_in[i]
Re_water_out[i] = (rho_water_out[i]*u_water_out[i]*Dv_i_actual)/mu_water_out[i]
Re_water_volume_based[i] = (rho_water_avg[i]*u_water[i]*Dv_i_actual)/mu_water_avg[i]

"Water pressure"
P_w_out[i] = P_w_in[i]
P_w_out[i] = P_w_in[i-1]

C_water[i] = m_dot_w*Cp_water[i]
C_REF[i] = m_dot_R407C * C_R407C_avg[i]
```

```
C_min[i] = min(C_water[i];C_REF[i])
C_max[i] = max(C_water[i];C_REF[i])

C_R[i] = C_min[i] / C_max[i]

q_max[i] = C_min[i]*DELTAT_max[i]
epsilon[i] = -Q[i]/q_max[i]

NTU[i] = 1/(C_R[i]-1)*ln((epsilon[i]-1)/(epsilon[i]*C_R[i]-1))
NTU[i] = UA[i]/C_min[i]

"Heat transfer of the water"
h_w[i] = watersideheattransfer(Re_water_volume_based[i];rho_water_avg[i];mu_water_avg[i];
k_water_avg[i];Cp_water[i];Dv_i_actual; e_star; p_star; theta_star)

"Refrigerant conductivity"
k_R407C_in[i] = conductivity(R1$;T=T_REF_in[i]; x=0)
k_R407C_out[i] = conductivity(R1$;T=T_REF_out[i]; x=0)

"Refrigerant viscosity"
mu_R407C_in[i] = viscosity(R1$;T=T_REF_in[i]; x=0)
mu_R407C_out[i] = viscosity(R1$;T=T_REF_out[i];x=0)

"Refrigerant density"
rho_R407C_in[i] = density(R1$;T=T_REF_in[i]; x=0)
rho_R407C_out[i] = density(R1$;T=T_REF_out[i];x=0)

"Refrigerant specific heat"
Cp_R407C_in[i] = cp(R1$;T=T_REF_in[i]; x=0)
Cp_R407C_out[i] = cp(R1$;T=T_REF_out[i]; x=0)

"Refrigerant enthalpy"
s_R407C_in[i] = Entropy(R407C;T=T_REF_in[i];P=P_REF_in[i])
s_R407C_out[i] = Entropy(R407C;T=T_REF_out[i];P=P_REF_out[i])
s_R407C_avg[i] = (s_R407C_in[i] + s_R407C_out[i])/2

"Refrigerant velocity"
u_R407C_in[i] = m_dot_R407C/(rho_R407C_in[i]*A_cr_R407C)
u_R407C_out[i] = m_dot_R407C/(rho_R407C_out[i]*A_cr_R407C)

"Refrigerant pressure drop"
P_R407C_drop[i] = singlephasepressuredrop(m_dot_R407C;A_cr_R407C;d_coil;
D_ho;L_sec[i];rho_R407C_in[i];rho_R407C_out[i];mu_R407C_in[i];mu_R407C_out[i];theta_star;p_s
tar;e_star;e_r;e_f)

C_R407C_avg[i] = (Cp_R407C_in[i] + Cp_R407C_out[i])/2

"Heat transfer of the refrigerant"
h_REF[i] = singlephaseheattransfer(m_dot_R407C;A_cr_R407C;d_coil;
D_ho;rho_R407C_in[i];rho_R407C_out[i];mu_R407C_in[i];mu_R407C_out[i];k_R407C_in[i];k_R407
C_out[i];C_R407C_avg[i];theta_star;p_star;e_star;e_r;e_h)

"Titanium condctivity"
k_Titanium[i] = conductivity(Titanium; T=T_w_out[i])

1/(UA[i]*1000) = 1/(h_w[i]* PI*D_ht_i*L_sec[i]) +
(ln(Dv_o_actual/Dv_i_actual)/(2*PI*k_Titanium[i]*L_sec[i])) + 1/(h_REF[i]*PI*D_ht_o*L_sec[i])
End
```

APPENDIX B - SAMPLE CALCULATION

In this section, a sample calculation implementing the correlations discussed in Chapter 3 is formulated. This sample calculation calculates the heat transfer and pressure drop of a titanium coaxial condenser using the input values of a single data point. This data point consists of the following values:

- $\dot{m}_w$ = 0.235 kg/s
- T_{w_i} = 15.04 °C
- $\dot{m}_r$ = 0.1689 kg/s
- T_{r_i} = 82.34 °C
- P_{r_i} = 2157 kPa
- P_{w_i} = 40.01 kPa
- P_{w_o} = 33.81 kPa

The average enhancement factors are used in the heat transfer and pressure drop correlations of this sample calculation and is listed in Table 5-2 as:

Heat transfer enhancement factor (e_h)	R-407C friction enhancement factor (e_f)	Water friction enhancement factor (e_{f_w})	Sub-cool [°C]
0.5288	5.1534	1.2711	2.3243

Water heat transfer:

The water side conditions are obtained from the water property tables with

$$Cp_w, \mu_w, \rho_w, k_w = f(T_w)$$

The Prandtl number of the water is calculated as

$$\mathrm{Pr}_w = \frac{Cp_w.\mu_w}{k_w} = \frac{(4184)(0.001132)}{0.5774} = 8.202$$

The velocity of the water is given by

$$u_w = \frac{4.\dot{m}_w}{\pi.\rho_w.D_{vi}^{\ 2}} = \frac{4(0.235)}{\pi(999.1)(0.02345)^2} = 0.5446 \text{ m/s}$$

The mass flux of the water is calculated by

$$G_w = u_w.\rho_w = (0.5446)(999.1) = 544.12 \text{ kg/s.m}^2$$

The mass flux is used to determine the water Reynolds number

$$\mathrm{Re}_w = \frac{G_w.D_{vi}}{\mu_w} = \frac{(544.12)(0.02345)}{0.001132} = 11273$$

As seen above, $\mathrm{Re}_w > 5000$, thus the Nusselt number is calculated as

$$Nu_w = 0.064 Re_w^{\ 0.773}.\left(e^*\right)^{-0.242}.\left(p^*\right)^{-0.108}.\left(\theta^*\right)^{-0.599}.Pr_w^{\ 0.4} = 202.9$$

The water convection heat transfer coefficient is calculated as

$$h_w = \frac{Nu_w.k_w}{D_{vi}} = \frac{(202.9)(0.5774)}{0.02345} = 4995 \text{ W/m}^2\text{K}$$

<u>Single-phase R-407C heat transfer:</u>

The refrigerant properties for the single phase are obtained from the R-407C property tables at the average temperature of the refrigerant superheat and sub-cool regions

$$Cp_r, \mu_r, \rho_r, k_r = f(T_r)$$

The refrigerant mass flux is determined as

$$G_r = \frac{\dot{m}_r}{A_{cr}} = \frac{0.1689}{0.0003868} = 436.7 \text{ kg/s.m}^2$$

with the cross-sectional area calculated as

$$A_{cr} = \frac{\pi(D_{oi}^{\ 2} - D_{vo}^{\ 2})}{4} = \frac{\pi((0.033318)^2 - (0.02485)^2)}{4} = 0.0003868 \text{ m}^2$$

The velocity of the refrigerant is given by

$$u_r = \frac{G_r}{\rho_r} = \frac{436.7}{92.16} = 4.738 \text{ m/s}$$

The refrigerant Prandtl number is calculated as

$$\mathrm{Pr}_r = \frac{Cp_r \cdot \mu_r}{k_r} = \frac{(1325)(0.00001566)}{0.01929} = 1.076$$

The refrigerant Reynolds number is given by

$$\mathrm{Re}_r = \frac{G_r . D_h}{\mu_r} = \frac{(436.7)(0.008466)}{0.00001566} = 236085$$

With the annulus hydraulic diameter given by

$$D_h = D_{oi} - D_{vo} = 0.033318 - 0.02485 = 0.008466 \text{ m}$$

The Nusselt number of the refrigerant for a straight pipe heat exchanger is determined as

$$Nu_{straight} = 0.023\,\mathrm{Re}_r^{\ 0.8} . \mathrm{Pr}_r^{\ 0.3} = 0.023(236085)^{0.8}(1.076)^{0.3} = 467.3$$

The single-phase heat transfer enhancement ratio (r_h) is equal to the single-phase friction enhancement ratio (r_f), this is also true for the two-phase enhancement ratios. Thus, the single-phase heat transfer enhancement ratio is given by

$$r_h = \frac{f_{helical}}{f_{straight}}$$

The absolute surface roughness of titanium is used to determine the helical and straight pipe friction factors. The absolute surface roughness of titanium was obtained by BP group (2006) as:

e_r = 0.0000457 m

The single-phase helical friction factor is calculated using the correlation developed by Das (1993):

$$f_{helical} = 4\left[0.079Re_r^{-0.25} + 0.0075\left(\frac{D_h}{d_{coil}}\right)^{0.5} + 17.5782Re_r^{-0.3137}.\left(\frac{D_h}{d_{coil}}\right)^{0.3621}.\left(\frac{e_r}{D_h}\right)^{0.6885}\right]$$

$f_{helical}$ = 0.07438

with

$$d_{coil} = \frac{D_h}{\sin(\theta)} = \frac{0.008466}{\sin(44.3)} = 0.01212 \text{ m}$$

where

$$\theta = \arctan\left(\frac{\pi D_{vo}}{N.p}\right) = \arctan\left(\frac{\pi(0.02485)}{(6)(0.013318)}\right) = 44.3°$$

The single-phase straight concentric tube friction factor is calculated with the use of the correlation determined by Swamee & Jain (1976):

$$f_{straight} = \frac{0.25}{\left\{\log\left[\frac{e_r}{3.7\times D_h} + \left(\frac{5.74}{Re_r^{0.9}}\right)\right]\right\}^2}$$

$f_{straight}$ = 0.03162

Thus, the single-phase heat transfer enhancement ratio is

$$r_h = \frac{0.07438}{0.03162} = 2.352$$

The single-phase refrigerant convection heat transfer coefficient is calculated with the average heat transfer enhancement factor listed in Table 5-1 as

$$h_{SP} = e_h.r_h.Nu_{straight}.\frac{k_r}{D_h} = (0.5288)(2.352)(467.3)(\frac{0.01929}{0.008466})$$

= 1324 W/m^{2}K

Two-phase R-407C heat transfer:

The Reynolds number in the liquid phase is calculated as

$$\mathrm{Re}_l = \frac{G_r.D_h}{\mu_l} = \frac{(436.7)(0.008466)}{0.0001131} = 32687$$

The Reynolds number in the vapour phase is calculated as

$$\mathrm{Re}_v = \frac{G_r.D_h}{\mu_v} = \frac{(436.7)(0.008466)}{0.00001526} = 242216$$

The heat transfer occurring in the liquid phase of the refrigerant in a straight pipe heat exchanger is given by

$$h_l = 0.023\,\mathrm{Re}_l^{0.8}.\mathrm{Pr}_l^{0.3}.\frac{k_l}{D_h} = 0.023(32687)^{0.8}.(2.687)^{0.3}\left(\frac{0.07382}{0.008466}\right) = 1217 \text{W/m}^2\text{K}$$

The two-phase heat transfer occurring in the liquid phase of the refrigerant in a straight pipe heat exchanger is calculated using the method of Shah (1979:548):

$$h_{tp} = h_l\left[\left(1-x_{avg}\right)^{0.8} + \frac{3.8x_{avg}^{0.76}\left(1-x_{avg}\right)^{0.04}}{pr^{0.38}}\right] = 5333 \text{ W/m}^2\text{K}$$

with

$x_{avg} = 0.5$

$$pr = \frac{P_{Local}}{P_{Critical}} = \frac{2157}{4632} = 0.4657$$

The heat transfer enhancement ratio for the two-phase region is calculated as

$$r_h = \frac{f_{helical}}{f_{straight}}$$

The two-phase helical friction factor is calculated using the correlation developed by Das (1993):

$$f_{helical} = 4\left[0.079Re_v^{-0.25} + 0.0075\left(\frac{D_h}{d_{coil}}\right)^{0.5} + 17.5782Re_v^{-0.3137}.\left(\frac{D_h}{d_{coil}}\right)^{0.3621}.\left(\frac{e_r}{D_h}\right)^{0.6885}\right]$$

$= 0.07401$

The viscosity relation, at the average refrigerant temperature, is determined as

$$\mu_{r_x} = \frac{\mu_v}{\mu_l} = \frac{0.00001526}{0.0001131} = 0.1349$$

The density relation, at the average refrigerant temperature, is calculated as

$$\rho_{r_x} = \frac{\rho_v}{\rho_l} = \frac{99.25}{1025} = 0.09685$$

The Reynolds number in the two-phase region is used to determine the friction factor in a straight pipe heat exchanger. The two-phase Reynolds number is given by

$$\mathrm{Re}_{r_x} = \mathrm{Re}_l + \mu_{r_x}\left(\frac{1}{\rho_{r_x}}\right)^{0.5}.\mathrm{Re}_v = 32687 + 0.1349\left(\frac{1}{0.09685}\right)^{0.5}(242216)$$

$= 137721$

The two-phase friction factor in a straight concentric tube heat exchanger is calculated with the use of the correlation determined by Swamee & Jain (1976):

$$f_{straight} = \frac{0.25}{\left\{\log\left[\frac{e_r}{3.7 \times D_h} + \left(\frac{5.74}{Re_{r_x}^{0.9}}\right)\right]\right\}^2} = 0.03195$$

Thus, the two-phase heat transfer enhancement ratio is

$$r_h = \frac{0.07401}{0.03195} = 2.316$$

The average heat transfer enhancement factor listed in Table 5-1 is used to calculate the two-phase convection heat transfer coefficient of the coaxial condenser as

$$h_{TP} = e_h.r_h.h_{tp} = 6545 \text{ W/m}^2\text{K}$$

Heat transfer output values of simulation model:

The overall heat transfer coefficient is determined with the above calculated heat transfer coefficients as

$$\frac{1}{UA} = \frac{1}{h_w.\pi.D_{vi}.L} + \frac{\ln\left(D_{vo}/D_{vi}\right)}{2\pi.k_{Ti}.L} + \frac{1}{(h_r).\pi.D_{vo}.L}$$

$UA = 1943$ W/K

With the thermal conductivity of titanium obtained from the titanium property tables at the average water temperature as

$$k_{Ti} = f(T_{w_{avg}}) = f(31.93) = 21.86 \text{ W/m.K}$$

The log mean temperature difference (LMTD) is calculated as

$$\Delta T_{lm} = \frac{\Delta T_1 - \Delta T_2}{\ln\left(\frac{\Delta T_1}{\Delta T_2}\right)} = \frac{(T_{r_i} - T_{w_o}) - (T_{r_o} - T_{w_i})}{\ln\left(\frac{(T_{r_i} - T_{w_o})}{(T_{r_o} - T_{w_i})}\right)}$$

The refrigerant outlet temperature (T_{r_o}) is obtained by dividing the coaxial coil into ten increments as discussed in Chapter 3 (Figure 3-5). The bubble and dew point temperatures are calculated at the respective increments with the refrigerant pressure as

$$T_{r_{BUBBLE}} = f(P_r; x) = f(2157; 1) = 53.357°C$$

$$T_{r_{DEW}} = f(P_r; x) = f(2157; 0) = 48.831°C$$

The refrigerant outlet temperature is equal to the dew point temperature minus the specified degree of sub-cool (Table 5-2)

$$T_{r_o} = T_{r_{DEW}} - T_{sub-cool} = 48.83 - 2.324 = 46.5°C$$

An estimated value of 45°C is assigned to the water outlet temperature (T_{w_o}). The LMTD is calculated as

$$\Delta T_{lm} = \frac{(82.34 - 45) - (46.5 - 15.04)}{\ln\left(\frac{(82.34 - 45)}{(46.5 - 15.04)}\right)} = 34.316°C$$

The estimated heat transfer of the titanium coaxial condenser is calculated as

$$q = UA \cdot \Delta T_{lm} = (1943)(34.316) = 66676.144 \text{ W}$$

The waterside heat transfer is determined as

$$q_w = \dot{m}_w \cdot \left(h_{w_o} - h_{w_i}\right)$$

With the above estimated heat transfer, the water outlet enthalpy (h_{w_o}) is determined as

$$66676.144 = (0.235)(h_{w_o} - 63121)$$

$$\therefore h_{w_o} = 214084.57 \text{ J/kg}$$

A new value for the water outlet temperature (T_{w_o}) is obtained from the calculated outlet water enthalpy as

$$h_{w_o} = f(P_{w_o}; T_{w_o}) = 214084.57 = f(33.81; T_{w_o 1})$$

$$\therefore T_{w_o 1} = 51.13°C$$

The new outlet water temperature value is the first iteration value. This first iteration value replaces the initial estimated outlet water temperature value in the LMTD equation and the calculation process is repeated. This calculation routine is iterated until the outlet water temperature converges producing the following output solutions of the simulation model:

q = 32537.5 W

$$T_{w_o} = 48.5°C$$

The refrigerant inlet enthalpy is obtained from the R-407C property tables with the inlet refrigerant pressure and temperature as

$$h_i = f(T_{r_i}; P_{r_i}) = f(82.34; 2157) = 462.9 \text{ kJ/kg}$$

The heat transfer of the refrigerant is given by

$$q_r = \dot{m}_r.(h_i - h_o)$$

With the calculated heat transfer of the coaxial condenser, the refrigerant outlet enthalpy (h_{r_o}) is calculated as

$$32.5375 = (0.1689)(462.9 - h_{r_o})$$

$$\therefore h_{r_o} = 270.3 \text{ J/kg}$$

<u>Water pressure drop:</u>

The water Reynolds number ($\mathrm{Re}_w = 11273$) calculated in the water heat transfer section of this Appendix, is used to determine the friction factor inside the coaxial tube. With $\mathrm{Re}_w > 1500$, the friction factor is calculated as

$$f = 1.209\left(\mathrm{Re}_w\right)^{-0.261}.\left(e^*\right)^{1.26-0.05p^*}.\left(p^*\right)^{-1.66+2.033e^*}.\left(\theta^*\right)^{-2.699+3.67e^*}$$

= 0.1131

The water pressure drop is calculated with the average water friction enhancement factor (Table 5-2) as

$$\Delta P_w = e_{fw}.\rho.u^2.\frac{f.L}{2D_{vi}} = (1.2711).(9949.1)(0.5446)^2\left(\frac{(0.1131)(5.07)}{2(0.02345)}\right)$$

= 4.623 kPa

As mentioned in Chapter 5, the results showed that the simulation model produces a more realistic prediction for the water pressure drop when the average trendline equation is implemented into the water pressure drop correlation without using a water friction enhancement factor. Thus, it is recommended to determine the water pressure drop as

$$\Delta P_{Trendline} = 0.7953(\Delta P_w) + 4.48 = 0.7953\left(\rho_w.u_w{}^2.\frac{f.L}{2D_{vi}}\right) + 4.55$$

$$= (0.7953)\left((999.1)(0.5446)^2\left(\frac{(0.1131)(5.07)}{2(0.02345)}\right)\right) + 4.55$$

=8.224 kPa

APPENDIX C – PART 1

Part 1 of Appendix C contains the experimental data obtained in the test set-up.

Description	Measurement
Frequency	Supply frequency
$\dot{m}_w$	Water mass flow rate
Tw,i	Inlet water temperature
Tw,o	Outlet water temperature
$\dot{m}_{R407C}$	R-407C mass flow rate
P_{R407C}, i	R-407C condensing pressure
P_{R407C}, o	R-407C outlet pressure
T_{R407C}, i	R-407C inlet temperature
T_{R407C}, o	R-407C outlet temperature
ΔP_{R407C}	R-407C pressure drop
ΔP_w	Water pressure drop
Q	Heat transfer on the water side

Group 1 - 1648.88kPa											
Frequency [Hz]	$\dot{m}_w$ **[kg/s]**	**Tw,i [°C]**	**Tw,o [°C]**	$\dot{m}_{R407C}$ **[kg/s]**	P_{R407C}, i **[kPa]**	P_{R407C}, o **[kPa]**	T_{R407C}, i **[°C]**	T_{R407C}, o **[°C]**	ΔP_{R407C} **[kPa]**	ΔP_w **[kPa]**	**Q [kW]**
45	0.44	15.67	33.43	0.161	1659	1443	64.13	31.91	215.6	-	32.731
45	0.809	20.06	30.89	0.183	1638	1408	66.27	32.33	230.7	-	36.654
50	0.496	15.54	31.78	0.14	1618	1396	66.56	30.27	222.5	14.21	33.68
50	0.668	20.74	32.4	0.137	1680	1475	67.93	32.08	205	21.52	32.586
55	0.631	15.52	30.45	0.198	1654	1368	69.42	31	286.3	21.14	39.389
55	0.787	20.08	30.98	0.182	1655	1413	69.05	31.88	241.5	26.84	35.888
60	0.829	16.03	28.42	0.213	1649	1324	70.66	30.15	325.6	31.91	42.973
60	1.147	19.83	28.54	0.208	1638	1346	70.77	30.6	292.2	51.07	41.795

Group 2 - 1882kPa											
Frequency [Hz]	$\dot{m}_w$ **[kg/s]**	**Tw,i [°C]**	**Tw,o [°C]**	$\dot{m}_{R407C}$ **[kg/s]**	P_{R407C},i **[kPa]**	P_{R407C},o **[kPa]**	T_{R407C},i **[°C]**	T_{R407C},o **[°C]**	ΔP_{R407C} **[kPa]**	ΔP_w **[kPa]**	**Q [kW]**
45	0.302	15.48	41.04	0.157	1877	1675	70.39	37.16	202.5	-	32.312
45	0.477	20.44	38.76	0.189	1892	1653	74.76	37.71	239.6	16.97	36.562
50	0.312	15.17	40.88	0.164	1888	1669	74.64	37.62	218.7	7.6	33.629
50	0.57	20.37	37.23	0.206	1877	1608	77.77	37.79	269.1	21.04	40.208
55	0.44	16.11	37.81	0.205	1897	1609	74.68	36.75	288.1	13.27	39.949
55	0.4961	20.13	37.68	0.18	1860	1618	74.41	36.45	241.5	13.33	36.427
60	0.517	15.78	35.91	0.222	1881	1552	76.45	35.73	328.7	16.56	43.501
60	0.615	19.82	36.02	0.215	1882	1580	76.53	36.14	301.4	18.88	41.683
60	0.953	24.89	35.39	0.217	1884	1601	76.46	36.82	282.9	37.45	41.862

Group 3 - 2144.31kPa											
Frequency [Hz]	$\dot{m}_w$ **[kg/s]**	**Tw,i [°C]**	**Tw,o [°C]**	$\dot{m}_{R407C}$ **[kg/s]**	P_{R407C},i **[kPa]**	P_{R407C},o **[kPa]**	T_{R407C},i **[°C]**	T_{R407C},o **[°C]**	ΔP_{R407C} **[kPa]**	ΔP_w **[kPa]**	**Q [kW]**
45	0.247	16.78	48.31	0.169	2182	1985	77.72	43.08	197.7	-	32.597
45	0.306	20.6	48	0.184	2165	1960	84.2	44.52	205.3	12.04	35.074
45	0.428	25.6	45.19	0.182	2128	1921	78.89	43.11	207.3	-	35.08
45	0.878	34.21	43.25	0.1767	2140	1958	76.72	44.45	182.4	32.62	33.197
50	0.235	15.04	49.07	0.161	2157	1955	82.34	43.49	201.8	6.21	33.483
50	0.377	20.35	45.56	0.21	2146	1892	84.62	43.73	254.6	13.95	39.768
50	1.272	35.23	42.02	0.1931	2136	1933	75.15	43.8	203.2	57.23	36.122
55	0.319	15.74	45.77	0.211	2148	1868	81.57	42.31	279.6	9.68	40.059
55	0.338	19.9	45.46	0.181	2103	1874	81.53	41.96	229.1	8.21	36.148
55	1.324	34.85	41.57	0.208	2153	1932	74.7	43.57	221.7	60.69	37.211
60	0.355	15.59	44.19	0.222	2129	1820	83.2	41.45	308.4	11.02	42.514
60	0.391	19.94	44.71	0.212	2152	1873	83.22	42.23	278.5	10.07	40.524
60	0.531	24.65	43.06	0.219	2137	1862	82.77	42.19	275.5	15.47	40.901

Group 4 – 2417.53kPa											
Frequency [Hz]	$\dot{m}_w$ **[kg/s]**	**Tw,i [°C]**	**Tw,o [°C]**	$\dot{m}_{R407C}$ **[kg/s]**	P_{R407C},i **[kPa]**	P_{R407C},o **[kPa]**	T_{R407C},i **[°C]**	T_{R407C},o **[°C]**	ΔP_{R407C} **[kPa]**	ΔP_w **[kPa]**	**Q [kW]**
45	0.164	14.82	58.35	0.145	2428	2278	90.99	49.66	149.8	7.85	29.846
45	0.234	20.66	55.16	0.175	2392	2210	90.95	49.1	181.9	11.03	33.772
45	0.281	25.43	53.73	0.169	2410	2226	85.93	48.23	184.4	-	33.267
45	0.493	34.35	50.3	0.1751	2397	2232	82.8	49.26	164.9	14.49	32.891
45	0.749	39.37	50.08	0.18	2434	2284	84.1	50.29	149.9	24.15	33.552
50	0.186	14.95	57.01	0.163	2434	2250	90.12	48.96	184.5	5.52	32.792
50	0.268	20.41	53.88	0.202	2409	2187	91.38	49.4	222.1	9.81	37.525
50	0.61	34.72	49.23	0.2042	2403	2206	83.79	49.28	197.5	17.93	37.022
50	1.038	39.3	47.93	0.21	2389	2193	83.3	49.76	196.2	40.47	37.467
55	0.242	15.51	53.87	0.209	2405	2154	88.69	47.64	251.4	8.27	38.909
55	0.241	19.9	55.44	0.182	2458	2246	91.69	48.48	211.5	6.17	35.831
55	0.67	34.78	48.63	0.2137	2421	2196	83.78	48.86	225	20.7	38.814
55	1.098	39.61	48.19	0.22	2440	2219	85.63	49.81	221	44.44	39.403
60	0.26	15.61	53.19	0.215	2414	2140	90.42	47.04	273.5	8.27	40.9
60	0.276	20.3	53.67	0.2	2426	2185	92.47	47.93	241.2	6.94	38.53
60	0.766	35.32	47.96	0.2257	2427	2179	84.27	48.61	248	25	40.498
60	1.318	39.76	47.2	0.23	2411	2187	82.69	48.68	223.8	58.79	41.012

APPENDIX C – PART 2

Part 2 of Appendix C contains the theoretical data obtained through the titanium coaxial condenser simulation model implementing the average enhancement factors listed in Table 5-2.

Group 1 - 1648.88kPa											
Frequency [Hz]	$\dot{m}_w$ **[kg/s]**	**Tw,i [°C]**	**Tw,o [°C]**	$\dot{m}_{R407C}$ **[kg/s]**	P_{R407C},i **[kPa]**	P_{R407C},o **[kPa]**	T_{R407C},i **[°C]**	T_{R407C},o **[°C]**	ΔP_{R407C} **[kPa]**	ΔP_w **[kPa]**	**Q [kW]**
45	0.44	15.67	33.76	0.1607	1659	1500	64.13	33.76	158.7	14.15	32.12
45	0.809	20.06	35.8	0.2125	1638	1317	66.27	28.8	321.4	40.27	45.3
50	0.496	15.54	31.91	0.1607	1618	1457	66.56	32.66	161.2	17.52	32.97
50	0.668	20.74	32.49	0.1572	1680	1525	67.93	34.39	154.6	28.86	31.9
55	0.631	15.52	38.56	0.2122	1654	1228	69.42	27.89	426.4	26.59	46.84
55	0.787	20.08	43.47	0.1824	1655	1317	69.05	26.33	337.72	38.53	39.52
60	0.829	16.03	49.27	0.2465	1649	1156	70.66	22.3	493.3	42.82	61.4
60	1.147	19.83	51.2	0.2323	1638	1182	70.77	21.3	455.6	74.54	59.1

Group 2 - 1882kPa											
Frequency [Hz]	$\dot{m}_w$ **[kg/s]**	**Tw,i [°C]**	**Tw,o [°C]**	$\dot{m}_{R407C}$ **[kg/s]**	P_{R407C},i **[kPa]**	P_{R407C},o **[kPa]**	T_{R407C},i **[°C]**	T_{R407C},o **[°C]**	ΔP_{R407C} **[kPa]**	ΔP_w **[kPa]**	**Q [kW]**
45	0.302	15.48	41.17	0.1625	1877	1744	70.39	39.58	132.9	7.239	31.52
45	0.477	20.44	38.88	0.1806	1892	1725	74.76	39.13	167.5	15.85	36.08
50	0.312	15.17	40.87	0.1657	1888	1756	74.64	39.85	131.6	7.677	32.87
50	0.57	20.37	42.2	0.2423	1877	1650	77.77	37.43	226.2	21.5	49.83
55	0.44	16.11	38.31	0.2002	1897	1712	74.68	38.84	185.4	13.99	40.06
55	0.4961	20.13	37.67	0.1777	1860	1699	74.41	38.55	161	17.03	35.68
60	0.517	15.78	38.12	0.2294	1881	1584	76.45	35.84	297	18.58	47.73
60	0.615	19.82	36.69	0.2089	1882	1658	76.53	37.6	224.1	24.84	42.78
60	0.953	24.89	41	0.2172	1884	1503	76.46	34.7	381.4	52.42	46.12

Group 3 - 2144.31kPa											
Frequency [Hz]	$\dot{m}_w$ **[kg/s]**	**Tw,i [°C]**	**Tw,o [°C]**	$\dot{m}_{R407C}$ **[kg/s]**	P_{R407C}, i **[kPa]**	P_{R407C}, o **[kPa]**	T_{R407C}, i **[°C]**	T_{R407C}, o **[°C]**	ΔP_{R407C} **[kPa]**	ΔP_w **[kPa]**	**Q [kW]**
45	0.247	16.78	47.76	0.1689	2182	2078	77.72	46.67	104.1	5.012	31.33
45	0.306	20.6	47.72	0.1766	2165	2033	84.2	45.77	132	7.19	34.47
45	0.428	25.6	45.13	0.1797	2128	1981	78.89	44.69	147.5	12.75	34.35
45	0.878	34.21	43.38	0.1746	2140	1970	76.72	44.47	170.3	43.6	32.94
50	0.235	15.04	48.5	0.1689	2157	2045	82.34	46.02	111.5	4.623	32.54
50	0.377	20.35	47.96	0.2156	2146	1897	84.62	42.95	248.6	10.35	43.26
50	1.272	35.23	42.19	0.1907	2136	1900	75.15	43.01	236.1	83.09	36.08
55	0.319	15.74	45.23	0.2009	2148	1998	81.57	45.06	149.8	7.896	38.87
55	0.338	19.9	45.07	0.1802	2103	1968	81.53	44.42	135.5	8.61	35.17
55	1.324	34.85	41.68	0.197	2153	1945	74.7	43.97	207.5	89.26	36.79
60	0.355	15.59	43.58	0.2094	2129	1969	83.2	44.45	160.3	9.549	41.2
60	0.391	19.94	44.19	0.2012	2152	1998	83.22	45.06	153.8	11.11	39.31
60	0.531	24.65	42.78	0.2033	2137	1968	82.77	44.43	169.3	18.7	39.87

Group 4 – 2417.53kPa											
Frequency [Hz]	$\dot{m}_w$ **[kg/s]**	**Tw,i [°C]**	**Tw,o [°C]**	$\dot{m}_{R407C}$ **[kg/s]**	P_{R407C},i **[kPa]**	P_{R407C},o **[kPa]**	T_{R407C},i **[°C]**	T_{R407C},o **[°C]**	ΔP_{R407C} **[kPa]**	ΔP_w **[kPa]**	**Q [kW]**
45	0.164	14.82	56.96	0.1537	2428	2348	90.99	51.83	80.33	2.44	29.08
45	0.234	20.66	54.92	0.1726	2392	2198	90.95	49.03	130.8	4.457	33.73
45	0.281	25.43	52.99	0.1744	2410	2299	85.93	50.93	111.3	6.044	32.22
45	0.493	34.35	50.21	0.1775	2397	2268	82.8	50.36	128.9	15.76	32.31
45	0.749	39.37	50.07	0.1818	2434	2281	84.1	50.6	153.4	32.23	33.21
50	0.186	14.95	55.63	0.1688	2434	2341	90.12	51.7	93.35	3.042	31.78
50	0.268	20.41	53.1	0.192	2409	2280	91.38	50.58	129.3	5.66	36.89
50	0.61	34.72	49.19	0.1986	2403	2240	83.79	49.84	162.5	22.85	36.56
50	1.038	39.3	48.49	0.2104	2389	2125	83.3	47.63	263.7	57.07	39.44
55	0.242	15.51	52.69	0.1993	2405	2276	88.69	50.5	129.2	4.823	37.67
55	0.241	19.9	53.91	0.1822	2458	2351	91.69	51.89	107.1	4.705	34.53
55	0.67	34.78	48.51	0.2077	2421	2254	83.78	50.1	167	26.93	38.08
55	1.098	39.61	48.18	0.2105	2440	2237	85.63	49.79	202.5	62.89	39.13
60	0.26	15.61	51.65	0.2063	2414	2281	90.42	50.6	132.8	5.473	39.37
60	0.276	20.3	52.29	0.1936	2426	2303	92.47	51.01	123	5.967	37.26
60	0.766	35.32	47.82	0.2157	2427	2249	84.27	50	178.3	33.99	39.69
60	1.318	39.76	47.26	0.2206	2411	2163	82.69	48.37	247.9	86.53	40.82

APPENDIX D

Appendix D contains the uncertainty analysis data on the water experimental heat transfer.

Description	Measurement
Frequency	Supply frequency
Tw,i	Inlet water temperature
$\dot{m}_w$	Water mass flow rate
P_{R407C}, i	R-407C condensing pressure
Q	Heat transfer on the water side

Group 1 - 1648.88kPa						
Tw,i [°C]	**Frequency [Hz]**	$\dot{m}_w$ **[kg/s]**	P_{R407C}, i **[kPa]**	Q **[kW]**	**Uncertainty [kW]**	**%**
15.67	45	0.44	1659	32.731	-	-
20.06	45	0.809	1638	36.654	-	-
15.54	50	0.496	1618	33.68	0.340	1.01
20.74	50	0.668	1680	32.586	0.244	0.748
15.52	55	0.631	1654	39.389	0.312	0.793
20.08	55	0.787	1655	35.888	0.228	0.635
16.03	60	0.829	1649	42.973	0.259	0.603
19.83	60	1.147	1638	41.795	0.182	0.435

Group 2 - 1882kPa						
Tw,i [°C]	**Frequency [Hz]**	$\dot{m}_w$ **[kg/s]**	P_{R407C}, i **[kPa]**	Q **[kW]**	**Uncertainty [kW]**	**%**
15.48	45	0.302	1877	32.312	-	-
20.44	45	0.477	1892	36.562	0.383	1.048
15.17	50	0.312	1888	33.629	0.538	1.599
20.37	50	0.57	1877	40.208	0.353	0.877
16.11	55	0.44	1897	39.949	0.454	1.136
20.13	55	0.4961	1860	36.427	0.367	1.008
15.78	60	0.517	1881	43.501	0.421	0.968
19.82	60	0.615	1882	41.683	0.339	0.813
24.89	60	0.953	1884	41.862	0.219	0.524

Group 3 – 2144.31kPa						
Tw,i [°C]	**Frequency [Hz]**	**$\dot{m}_w$ [kg/s]**	**P_{R407C}, i [kPa]**	**Q [kW]**	**Uncertainty [kW]**	**%**
16.78	45	0.247	2182	32.597	-	0.903
20.6	45	0.306	2165	35.074	0.573	1.634
25.6	45	0.428	2128	35.08	-	0.521
34.21	45	0.878	2140	33.197	0.189	0.569
15.04	50	0.235	2157	33.483	0.712	2.125
20.35	50	0.377	2146	39.768	0.527	1.326
35.23	50	1.272	2136	36.122	0.142	0.392
15.74	55	0.319	2148	40.059	0.628	1.568
19.9	55	0.338	2103	36.148	0.535	1.479
34.85	55	1.324	2153	37.211	0.140	0.377
15.59	60	0.355	2129	42.514	0.598	1.407
19.94	60	0.391	2152	40.524	0.518	1.278
24.65	60	0.531	2137	40.901	0.385	0.941

Group 4 – 2417.53kPa						
Tw,i [°C]	**Frequency [Hz]**	**$\dot{m}_w$ [kg/s]**	**P_{R407C}, i [kPa]**	**Q [kW]**	**Uncertainty [kW]**	**%**
14.82	45	0.164	2428	29.846	0.910	3.05
20.66	45	0.234	2392	33.772	0.721	2.136
25.43	45	0.281	2410	33.267	-	0.795
34.35	45	0.493	2397	32.891	0.334	1.014
39.37	45	0.749	2434	33.552	0.224	0.667
14.95	50	0.186	2434	32.792	0.880	2.682
20.41	50	0.268	2409	37.525	0.700	1.865
34.72	50	0.61	2403	37.022	0.303	0.819
39.3	50	1.038	2389	37.467	0.180	0.481
15.51	55	0.242	2405	38.909	0.802	2.062
19.9	55	0.241	2458	35.831	0.743	2.074
34.78	55	0.67	2421	38.814	0.290	0.746
39.61	55	1.098	2440	39.403	0.179	0.455
15.61	60	0.26	2414	40.9	0.786	1.922
20.3	60	0.276	2426	38.53	0.698	1.811
35.32	60	0.766	2427	40.498	0.264	0.652
39.76	60	1.318	2411	41.012	0.155	0.379

APPENDIX E

Appendix E contains the individual enhancement factors obtained from the experimental data.

Description	Measurement
$\dot{m}_w$	Water mass flow rate
Tw,i	Inlet water temperature
$\dot{m}_{R407C}$	R-407C mass flow rate
P_{R407C}, i	R-407C condensing pressure
T_{R407C}, i	R-407C inlet temperature
T_{R407C}, o	R-407C outlet temperature
ΔP_{R407C}	R-407C pressure drop
ΔP_w	Water pressure drop
Q	Heat transfer on the water side
e_h	Heat transfer enhancement ratio
e_f	Friction enhancement factor
e_{f_w}	Water friction enhancement factor
Sub-cool	Degree of sub-cool

Group 1 – 1648.88kPa											
Tw,i [°C]	$\dot{m}_{water}$ **[kg/s]**	$\dot{m}_{R407C}$ **[kg/s]**	$P_{R407C,i}$ **[kPa]**	$T_{R407C,o}$ **[°C]**	**Q [kW]**	ΔP_{R407C} **[kPa]**	ΔP_{water} **[kPa]**	e_h	e_f	e_{f_w}	**Sub-cool [°C]**
15.67	0.44	0.161	1659	31.91	32.48	215.6	-	0.4223	5.522	-	2.732
20.06	0.809	0.183	1638	32.33	43.41	230.7	-	1.918	3.804	-	1.362
15.54	0.496	0.14	1618	30.27	33.45	222.5	14.21	0.4485	5.691	1.031	3.123
20.74	0.668	0.137	1680	32.08	32.36	205	21.52	0.514	5.934	0.9481	3.379
15.52	0.631	0.198	1654	31	44.5	286.3	21.14	0.6735	4.607	1.011	1.645
20.08	0.787	0.182	1655	31.88	37.92	241.5	26.84	0.7493	5.401	0.8855	1.982
16.03	0.829	0.213	1649	30.15	52.39	325.6	31.91	1.002	4.195	0.9482	1.291
19.83	1.147	0.208	1638	30.6	49.28	292.2	51.07	1.972	4.625	0.8711	1.453

Group 2 – 1882kPa											
Tw.i [°C]	$\dot{m}_{water}$ **[kg/s]**	$\dot{m}_{R407C}$ **[kg/s]**	$P_{R407C,i}$ **[kPa]**	$T_{R407C,o}$ **[°C]**	**Q [kW]**	ΔP_{R407C} **[kPa]**	ΔP_{water} **[kPa]**	e_h	e_f	e_{f_w}	**Sub-cool [°C]**
15.48	0.302	0.157	1877	37.16	32.07	202.5	-	0.3236	5.31	-	3.15
20.44	0.477	0.189	1892	37.71	36.38	239.6	16.97	0.3748	5.495	1.361	2.081
15.17	0.312	0.164	1888	37.62	33.39	218.7	7.6	0.3043	5.537	1.258	2.567
20.37	0.57	0.206	1877	37.79	49.68	269.1	21.04	0.9912	3.585	1.243	0.9358
16.11	0.44	0.205	1897	36.75	40.6	288.1	13.27	0.3313	5.438	1.206	2.011
20.13	0.4961	0.18	1860	36.45	36.17	241.5	13.33	0.3807	5.681	0.9951	2.542
15.78	0.517	0.222	1881	35.73	47.43	328.7	16.56	0.4153	4.88	1.135	1.656
19.82	0.615	0.215	1882	36.14	43.07	301.4	18.88	0.4178	5.482	0.9669	1.94
24.89	0.953	0.217	1884	36.82	44.52	282.9	37.45	0.6654	5.188	0.9082	1.754

Group 3 – 2144.31kPa											
Tw.i [°C]	P_{R407C}, i **[kPa]**	$\dot{m}_{water}$ **[kg/s]**	$\dot{m}_{R407C}$ **[kg/s]**	T_{R407C}, o **[°C]**	**Q [kW]**	ΔP_{R407C} **[kPa]**	ΔP_{water} **[kPa]**	e_h	e_f	e_{f_w}	**Sub-cool [°C]**
16.78	2182	0.247	0.169	43.08	32.35	197.7	-	0.2396	5.399	-	4.026
20.6	2165	0.306	0.184	44.52	34.84	205.3	12.04	0.2775	5.112	2.126	2.066
25.6	2128	0.428	0.182	43.11	34.82	207.3	-	0.3393	5.198	-	2.663
34.21	2140	0.878	0.1767	44.45	32.94	182.4	32.62	0.5224	5.365	0.9504	2.097
15.04	2157	0.235	0.161	43.49	33.25	201.8	6.21	0.2453	5.328	1.707	3.005
20.35	2146	0.377	0.21	43.73	42.98	254.6	13.95	0.3684	4.45	1.712	1.412
35.23	2136	1.272	0.1931	43.8	35.83	203.2	57.23	0.6962	5.484	0.8752	2.23
15.74	2148	0.319	0.211	42.31	39.78	279.6	9.68	0.2572	5.543	1.559	2.347
19.9	2103	0.338	0.181	41.96	35.91	229.1	8.21	0.2893	5.477	1.212	2.815
34.85	2153	1.324	0.208	43.57	36.92	221.7	60.69	0.609	5.717	0.8641	2.433
15.59	2129	0.355	0.222	41.45	42.23	308.4	11.02	0.2603	5.669	1.469	2.167
19.94	2152	0.391	0.212	42.23	40.26	278.5	10.07	0.2803	5.642	1.153	2.54
24.65	2137	0.531	0.219	42.19	40.63	275.5	15.47	0.331	5.667	1.052	2.321

Group 4 – 2417.53kPa											
Tw.i [°C]	P_{R407C}, i **[kPa]**	$\dot{m}_{water}$ **[kg/s]**	$\dot{m}_{R407C}$ **[kg/s]**	T_{R407C}, o **[°C]**	**Q [kW]**	ΔP_{R407C} **[kPa]**	ΔP_{water} **[kPa]**	e_h	e_f	e_{f_w}	**Sub-cool [°C]**
14.82	2428	0.164	0.145	49.66	29.66	149.8	7.85	0.2055	4.997	4.08	3.215
20.66	2392	0.234	0.175	49.1	33.7	181.9	11.03	0.2772	4.808	3.14	1.262
25.43	2410	0.281	0.169	48.23	33.04	184.4	-	0.2663	5.162	-	3.66
34.35	2397	0.493	0.1751	49.26	32.65	164.9	14.49	0.3229	4.745	1.168	2.752
39.37	2434	0.749	0.18	50.29	33.31	149.9	24.15	0.407	4.383	0.9518	2.703
14.95	2434	0.186	0.163	48.96	32.59	184.5	5.52	0.2109	5.273	2.304	3.379
20.41	2409	0.268	0.202	49.4	37.27	222.1	9.81	0.2353	5.089	2.2	1.739
34.72	2403	0.61	0.2042	49.28	36.75	197.5	17.93	0.3452	4.75	0.9968	2.224
39.3	2389	1.038	0.21	49.76	38.67	196.2	40.47	0.5524	4.516	0.9008	1.495
15.51	2405	0.242	0.209	47.64	38.65	251.4	8.27	0.2262	5.381	2.18	2.862
19.9	2458	0.241	0.182	48.48	35.61	211.5	6.17	0.2283	5.439	1.668	3.809
34.78	2421	0.67	0.2137	48.86	38.52	225	20.7	0.3453	5.103	0.9768	2.468
39.61	2440	1.098	0.22	49.81	39.12	221	44.44	0.4799	5.216	0.8979	1.955
15.61	2414	0.26	0.215	47.04	40.63	273.5	8.27	0.2244	5.548	1.923	3.21
20.3	2426	0.276	0.2	47.93	38.29	241.2	6.94	0.2365	5.53	1.479	3.18
35.32	2427	0.766	0.2257	48.61	40.21	248	25	0.3638	5.352	0.9348	2.393
39.76	2411	1.318	0.23	48.68	40.71	223.8	58.79	0.5612	4.992	0.8635	2.482

APPENDIX F – PART 1

Appendix F – Part 1 displays the percentage error between the experimental and theoretical data while implementing the Rousseau-factor (Table 5-1) in the simulation model.

Description	Measurement
$\boldsymbol{Q_t}$	Theoretical heat transfer
$\boldsymbol{Q_e}$	Experimental heat transfer
$\Delta \boldsymbol{P_{r_t}}$	Theoretical refrigerant pressure drop
$\Delta \boldsymbol{P_{r_e}}$	Experimental refrigerant pressure drop
$\Delta \boldsymbol{P_{w_t}}$	Theoretical water pressure drop
$\Delta \boldsymbol{P_{w_e}}$	Experimental water pressure drop
$LMTD_t$	Theoretical LMTD value
$LMTD_e$	Experimental LMTD value
Error	Percentage error calculated with Equation (3.57)

Group 1 – 1648.88kPa								
Q_t [kW]	Q_e [kW]	Error [%]	ΔP_{r_t} [kPa]	ΔP_{r_e} [kPa]	Error [%]	$LMTD_t$	$LMTD_e$	Error [%]
31.28	32.731	4.43	97.05	215.6	54.99	25.54	22.71	12.46
44.7	36.654	21.95	315.1	230.7	36.58	17.5	21.82	19.80
32.11	33.680	4.66	98.09	222.5	55.91	26.83	23.34	14.95
31.08	32.586	4.62	92.97	205	54.65	24.86	21.18	17.37
43.63	39.389	10.77	212	286.3	25.95	26.37	25.44	3.66
36.95	35.888	2.96	148	241.5	38.72	24.64	22.43	9.85
55.3	42.973	28.69	458.2	325.6	40.72	20.74	25.66	19.17
51.17	41.795	22.43	412.38	292.2	41.13	18.93	23.02	17.77

Group 2 – 1882kPa								
Q_t [kW]	Q_e [kW]	Error [%]	ΔP_{r_t} [kPa]	ΔP_{r_e} [kPa]	Error [%]	$LMTD_t$	$LMTD_e$	Error [%]
31.17	32.312	3.53	86.99	202.5	57.04	27.23	25.32	7.54
35.56	36.562	2.74	106.3	239.6	55.63	27.3	25.5	7.06
32.52	33.629	3.30	86.37	218.7	60.51	29.64	27.72	6.93
51.87	40.208	29.00	482.3	269.1	79.23	21.3	27.37	22.18
39.44	39.949	1.27	119.1	288.1	58.66	30.01	27.97	7.29
35.19	36.427	3.40	102.5	241.5	57.56	27.45	25.16	9.10
46.33	43.501	6.50	175.3	328.7	46.67	30.18	29.04	3.93
41.92	41.683	0.57	138.2	301.4	54.15	28.74	26.61	8.00
43.88	41.862	4.82	180.2	282.9	36.30	24.73	23.57	4.92

Group 3 – 2144.31kPa								
Q_t [kW]	Q_e [kW]	Error [%]	ΔP_{r_t} [kPa]	ΔP_{r_e} [kPa]	Error [%]	$LMTD_t$	$LMTD_e$	Error [%]
31.14	32.597	4.47	70.37	197.7	64.41	30.36	27.83	9.09
34.2	35.074	2.49	86.97	205.3	57.64	31.08	29.64	4.86
34.03	35.080	2.99	95.4	207.3	53.98	26.46	24.73	7.00
32.53	33.197	2.01	102.9	182.4	43.59	20.66	19.61	5.35
32.33	33.483	3.44	74.87	201.8	62.90	32.88	30.8	6.75
42.54	39.768	6.97	151.6	254.6	40.46	30.45	30.55	0.33
35.36	36.122	2.11	127.3	203.2	37.35	19.33	18.17	6.44
38.52	40.059	3.84	99.54	279.6	64.40	33.38	30.96	7.82
34.88	36.148	3.51	89.24	229.1	61.05	30.73	28.49	7.86
36.21	37.211	2.69	121.9	221.7	45.02	19.98	18.29	9.24
40.81	42.514	4.01	106.1	308.4	65.60	34.7	31.99	8.47
38.95	40.524	3.88	101.2	278.5	63.66	32.28	29.66	8.83
39.45	40.901	3.55	109.3	275.5	60.33	29.57	27.13	8.99

Group 4 – 2417.53kPa								
Q_t [kW]	Q_e [kW]	Error [%]	ΔP_{r_t} [kPa]	ΔP_{r_e} [kPa]	Error [%]	$LMTD_t$	$LMTD_e$	Error [%]
28.95	29.846	3.00	54.71	149.8	63.48	35.83	33.73	6.23
33.47	33.772	0.89	86.08	181.9	52.68	32.63	31.97	2.06
32.02	33.267	3.75	74.35	184.4	59.68	29.52	27.23	8.41
32.05	32.891	2.56	83.9	164.9	49.12	23.91	22.57	5.94
32.88	33.552	2.00	96.39	149.9	35.70	21.38	20.33	5.16
31.62	32.792	3.57	63.46	184.5	65.60	35.99	33.56	7.24
36.62	37.525	2.41	86.3	222.1	61.14	34.61	33.06	4.69
36.18	37.022	2.27	104.2	197.5	47.24	24.31	23.14	5.06
38.63	37.467	3.10	146.4	196.2	25.38	20.42	20.45	0.15
37.4	38.909	3.88	87	251.4	65.39	36.03	33.46	7.68
34.33	35.831	4.19	72.19	211.5	65.87	35.24	32.26	9.24
37.68	38.814	2.92	107.4	225	52.27	24.72	23.03	7.34
38.6	39.403	2.04	123.8	221	43.98	22.14	20.95	5.68
39.08	40.900	4.45	89.45	273.5	67.29	37.4	34.25	9.20
37.01	38.530	3.94	82.42	241.2	65.83	35.75	32.9	8.66
39.25	40.498	3.08	114.1	248	53.99	24.81	22.9	8.34
40.08	41.012	2.27	143.9	223.8	35.70	20.62	19.24	7.17

APPENDIX F – PART 2

Appendix F – Part 2 contains the percentage error between the experimental and theoretical data implementing the average enhancement factors (Table 5-2) in the simulation model.

Group 1 – 1648.88kPa											
Q_t [kW]	Q_e [kW]	Error [%]	ΔP_{r_t} [kPa]	ΔP_{r_e} [kPa]	Error [%]	ΔP_{w_t} [kPa]	ΔP_{w_e} [kPa]	Error [%]	$LMTD_t$	$LMTD_e$	Error [%]
32.12	32.731	1.87	158.7	215.6	26.39	14.15	-	-	23.7	22.71	4.36
45.3	36.654	23.59	321.4	230.7	39.32	40.27	-	-	17.4	21.82	20.26
32.97	33.680	2.11	161.2	222.5	27.55	17.52	14.21	30.05	24.86	23.34	6.51
31.9	32.586	2.11	154.6	205	24.59	28.86	21.52	27.79	22.84	21.18	7.84
46.84	39.389	18.92	426.4	286.3	48.93	26.59	21.14	21.57	21.94	25.44	13.76
39.52	35.888	10.12	337.72	241.5	39.84	38.53	26.84	31.11	17.81	22.43	20.60
61.4	42.973	42.88	493.3	325.6	51.50	42.82	31.91	20.97	17.5	25.66	31.80
59.1	41.795	41.40	455.6	292.2	55.92	74.54	51.07	24.99	14.4	23.02	37.45

Group 2 – 1882kPa											
Q_t [kW]	Q_e [kW]	Error [%]	ΔP_{r_t} [kPa]	ΔP_{r_e} [kPa]	Error [%]	ΔP_{w_t} [kPa]	ΔP_{w_e} [kPa]	Error [%]	$LMTD_t$	$LMTD_e$	Error [%]
31.52	32.312	2.45	132.9	202.5	34.37	7.239	-	-	26.58	25.32	4.98
36.08	36.562	1.32	167.5	239.6	30.09	15.85	16.97	1.06	26.36	25.5	3.37
32.87	33.629	2.26	131.6	218.7	39.83	7.677	7.6	40.13	28.99	27.72	4.58
49.83	40.208	23.93	226.2	269.1	15.94	21.5	21.04	2.85	25.42	27.37	7.12
40.06	39.949	0.28	185.4	288.1	35.65	13.99	13.27	18.16	29.02	27.97	3.75
35.68	36.427	2.05	161	241.5	33.33	17.03	13.33	35.71	26.53	25.16	5.45
47.73	43.501	9.72	297	328.7	9.64	18.58	16.56	16.67	28.22	29.04	2.82
42.78	41.683	2.63	224.1	301.4	25.65	24.84	18.88	28.71	27.34	26.61	2.74
46.12	41.862	10.17	381.4	282.9	34.82	52.42	37.45	23.47	21.6	23.57	8.36

Group 3 – 2144.31kPa											
Q_t [kW]	Q_e [kW]	Error [%]	ΔP_{r_t} [kPa]	ΔP_{r_e} [kPa]	Error [%]	ΔP_{w_t} [kPa]	ΔP_{w_e} [kPa]	Error [%]	$LMTD_t$	$LMTD_e$	Error [%]
31.33	32.597	3.89	104.1	197.7	47.34	5.012	-	-	29.93	27.83	7.55
34.47	35.074	1.72	132	205.3	35.70	7.19	12.04	14.70	30.48	29.64	2.83
34.35	35.080	2.08	147.5	207.3	28.85	12.75	-	-	25.73	24.73	4.04
32.94	33.197	0.77	170.3	182.4	6.63	43.6	32.62	20.23	19.59	19.61	0.10
32.54	33.483	2.82	111.5	201.8	44.75	4.623	6.21	32.43	32.39	30.8	5.16
43.26	39.768	8.78	248.6	254.6	2.36	10.35	13.95	8.39	29.07	30.55	4.84
36.08	36.122	0.12	236.1	203.2	16.19	83.09	57.23	23.41	17.44	18.17	3.96
38.87	40.059	2.97	149.8	279.6	46.42	7.896	9.68	11.88	32.7	30.96	5.62
35.17	36.148	2.71	135.5	229.1	40.86	8.61	8.21	38.73	30.1	28.49	5.65
36.79	37.211	1.13	207.5	221.7	6.41	89.26	60.69	24.45	18.58	18.29	1.59
41.2	42.514	3.09	160.3	308.4	48.02	9.549	11.02	10.16	33.96	31.99	6.16
39.31	40.524	3.00	153.8	278.5	44.78	11.11	10.07	32.87	31.56	29.66	6.41
39.87	40.901	2.52	169.3	275.5	38.55	18.7	15.47	25.53	28.71	27.13	5.82

Group 4 – 2417.53kPa											
Q_t [kW]	Q_e [kW]	Error [%]	ΔP_{r_t} [kPa]	ΔP_{r_e} [kPa]	Error [%]	ΔP_{w_t} [kPa]	ΔP_{w_e} [kPa]	Error [%]	$LMTD_t$	$LMTD_e$	Error [%]
29.08	29.846	2.57	80.33	149.8	46.38	2.44	7.85	17.35	35.5	33.73	5.25
33.73	33.772	0.12	130.8	181.9	28.09	4.457	11.03	26.65	32.05	31.97	0.25
32.22	33.267	3.15	111.3	184.4	39.64	6.044	-	-	29.06	27.23	6.72
32.31	32.891	1.77	128.9	164.9	21.83	15.76	14.49	17.87	23.33	22.57	3.37
33.21	33.552	1.02	153.4	149.9	2.33	32.23	24.15	24.97	20.56	20.33	1.13
31.78	32.792	3.09	93.35	184.5	49.40	3.042	5.52	26.21	35.61	33.56	6.11
36.89	37.525	1.69	129.3	222.1	41.78	5.66	9.81	7.77	34.06	33.06	3.02
36.56	37.022	1.25	162.5	197.5	17.72	22.85	17.93	26.72	23.53	23.14	1.69
39.44	37.467	5.27	263.7	196.2	34.40	57.07	40.47	23.38	18.52	20.45	9.44
37.67	38.909	3.18	129.2	251.4	48.61	4.823	8.27	1.35	35.49	33.46	6.07
34.53	35.831	3.63	107.1	211.5	49.36	4.705	6.17	34.34	34.81	32.26	7.90
38.08	38.814	1.89	167	225	25.78	26.93	20.7	25.41	23.93	23.03	3.91
39.13	39.403	0.69	202.5	221	8.37	62.89	44.44	22.77	20.94	20.95	0.05
39.37	40.900	3.74	132.8	273.5	51.44	5.473	8.27	7.62	36.85	34.25	7.59
37.26	38.530	3.30	123	241.2	49.00	5.967	6.94	33.90	35.23	32.9	7.08
39.69	40.498	2.00	178.3	248	28.10	33.99	25	26.32	23.94	22.9	4.54
40.82	41.012	0.47	247.9	223.8	10.77	86.53	58.79	24.78	18.96	19.24	1.46

APPENDIX G

Appendix F contains the test matrixes used during testing in the test set-up. The test set-up was discussed in Chapter 4.

Required setpoint			For info			Data measurements readings											
Water inlet temperature (°C)	Compressor frequency(Hz)	Condensing Pressure (kPa)	Condensing temperature (Dew, °C)	Condensing temperature (Bubble, °C)	Liquid temp (Subcooling Inc.°C)	Time	Condenser inlet temperature (Refrigerant, °C)	Condenser inlet pressure (kPa)	Condenser outlet temperature (Refrigerant, °C)	Condenser outlet pressure (kPa)	Refrigerant flow (Cond outlet)	Evaporating pressure (kPa)	Water inlet temperature (°C)	Water outlet temperature (°C)			
15	45	1 650	45	40.1	30.1												
15	45	1 882	50	45.2	35.2												
15	45	2 134	55	50.5	40.5												
15	45	2 408	60	55.7	45.7												
15	50	1 650	45	40.1	30.1												
15	50	1 882	50	45.2	35.2												
15	50	2 134	55	50.5	40.5												
15	50	2 408	60	55.7	45.7												
15	55	1 650	45	40.1	30.1												
15	55	1 882	50	45.2	35.2												
15	55	2 134	55	50.5	40.5												
15	55	2 408	60	55.7	45.7												
15	60	1 650	45	40.1	30.1												
15	60	1 882	50	45.2	35.2												
15	60	2 134	55	50.5	40.5												
15	60	2 408	60	55.7	45.7												

Required setpoint			For info			Data measurements readings															
Water inlet temperature (°C)	Compressor frequency(Hz)	Condensing Pressure (kPa)	Condensing temperature (Dew, °C)	Condensing temperature (Bubble, °C)	Liquid temp (Subcooling Inc.°C)	Time	Condenser inlet temperature (Refrigerant, °C)	Condenser inlet pressure (kPa)	Condenser outlet temperature (Refrigerant, °C)	Condenser outlet pressure (kPa)	Refrigerant flow (Cond outlet)	Evaporating pressure (kPa)	Water inlet temperature (°C)	Water outlet temperature (°C)							
20	45	1 650	45	40.1	30.1																
20	45	1 882	50	45.2	35.2																
20	45	2 134	55	50.5	40.5																
20	45	2 408	60	55.7	45.7																
20	50	1 650	45	40.1	30.1																
20	50	1 882	50	45.2	35.2																
20	50	2 134	55	50.5	40.5																
20	50	2 408	60	55.7	45.7																
20	55	1 650	45	40.1	30.1																
20	55	1 882	50	45.2	35.2																
20	55	2 134	55	50.5	40.5																
20	55	2 408	60	55.7	45.7																
20	60	1 650	45	40.1	30.1																
20	60	1 882	50	45.2	35.2																
20	60	2 134	55	50.5	40.5																
20	60	2 408	60	55.7	45.7																

Required setpoint			For info			Data measurements readings									
Water inlet temperature (°C)	Compressor frequency(Hz)	Condensing Pressure (kPa)	Condensing temperature (Dew, °C)	Condensing temperature (Bubble, °C)	Liquid temp (Subcooling Inc.°C)	Time	Condenser inlet temperature (Refrigerant, °C)	Condenser inlet pressure (kPa)	Condenser outlet temperature (Refrigerant, °C)	Condenser outlet pressure (kPa)	Refrigerant flow (Cond outlet)	Evaporating pressure (kPa)	Water inlet temperature (°C)	Water outlet temperature (°C)
25	45	1 650	45	40.1	30.1										
25	45	1 882	50	45.2	35.2										
25	45	2 134	55	50.5	40.5										
25	45	2 408	60	55.7	45.7										
25	50	1 650	45	40.1	30.1										
25	50	1 882	50	45.2	35.2										
25	50	2 134	55	50.5	40.5										
25	50	2 408	60	55.7	45.7										
25	55	1 650	45	40.1	30.1										
25	55	1 882	50	45.2	35.2										
25	55	2 134	55	50.5	40.5										
25	55	2 408	60	55.7	45.7										
25	60	1 650	45	40.1	30.1										
25	60	1 882	50	45.2	35.2										
25	60	2 134	55	50.5	40.5										
25	60	2 408	60	55.7	45.7										

Required setpoint			For info			Data measurements readings																
Water inlet temperature (°C)	Compressor frequency(Hz)	Condensing Pressure (kPa)	Condensing temperature (Dew, °C)	Condensing temperature (Bubble, °C)	Liquid temp (Subcooling Inc.°C)	Time	Condenser inlet temperature (Refrigerant, °C)	Condenser inlet pressure (kPa)	Condenser outlet temperature (Refrigerant, °C)	Condenser outlet pressure (kPa)	Refrigerant flow (Cond outlet)	Evaporating pressure (kPa)	Water inlet temperature (°C)	Water outlet temperature (°C)								
35	45	1 650	45	40.1	30.1																	
35	45	1 882	50	45.2	35.2																	
35	45	2 134	55	50.5	40.5																	
35	45	2 408	60	55.7	45.7																	
35	50	1 650	45	40.1	30.1																	
35	50	1 882	50	45.2	35.2																	
35	50	2 134	55	50.5	40.5																	
35	50	2 408	60	55.7	45.7																	
35	55	1 650	45	40.1	30.1																	
35	55	1 882	50	45.2	35.2																	
35	55	2 134	55	50.5	40.5																	
35	55	2 408	60	55.7	45.7																	
35	60	1 650	45	40.1	30.1																	
35	60	1 882	50	45.2	35.2																	
35	60	2 134	55	50.5	40.5																	
35	60	2 408	60	55.7	45.7																	

Required setpoint			For info		Data measurements readings											
Water inlet temperature (°C)	Compressor frequency(Hz)	Condensing Pressure (kPa)	Condensing temperature (Dew, °C)	Condensing temperature (Bubble, °C)	Liquid temp (Subcooling Inc.°C)	Time	Condenser inlet temperature (Refrigerant, °C)	Condenser inlet pressure (kPa)	Condenser outlet temperature (Refrigerant, °C)	Condenser outlet pressure (kPa)	Refrigerant flow (Cond outlet)	Evaporating pressure (kPa)	Water inlet temperature (°C)	Water outlet temperature (°C)
40	45	1 650	45	40.1	30.1											
40	45	1 882	50	45.2	35.2											
40	45	2 134	55	50.5	40.5											
40	45	2 408	60	55.7	45.7											
40	50	1 650	45	40.1	30.1											
40	50	1 882	50	45.2	35.2											
40	50	2 134	55	50.5	40.5											
40	50	2 408	60	55.7	45.7											
40	55	1 650	45	40.1	30.1											
40	55	1 882	50	45.2	35.2											
40	55	2 134	55	50.5	40.5											
40	55	2 408	60	55.7	45.7											
40	60	1 650	45	40.1	30.1											
40	60	1 882	50	45.2	35.2											
40	60	2 134	55	50.5	40.5											
40	60	2 408	60	55.7	45.7											